# Stony Brook University

# Variational Principles in Statistical Mechanics and their application in biology and evolution

A Dissertation presented
by

**Luca Agozzino**

to

The Graduate School
in Partial Fulfillment of the
Requirements
for the Degree of

**Doctor of Philosophy**

in

**Physics**
**(Concentration - Biophysics)**

Stony Brook University

**May 2020**

**Stony Brook University**

The Graduate School

**Luca Agozzino**

We, the dissertation committee for the above candidate for the
Doctor of Philosophy degree, hereby recommend
acceptance of this dissertation

**Ken Dill - Dissertation Advisor**
**Professor, Physics Department**

**Maria Victoria Fernandez Serra - Chairperson of Defense**
**Professor, Physics Department**

**Matthew Dawber**
**Associate Professor, Physics Department**

**Gábor Balázsi - Outside Member**
**Associate Professor, Biomedical Engeneering**

**Helmut Strey - Outside Member**
**Associate Professor, Biomedical Engeneering**

This dissertation is accepted by the Graduate School

Eric Wertheimer

Dean of the Graduate School

Abstract of the Dissertation

**Variational Principles in Statistical Mechanics and their application in biology and evolution**

by
**Luca Agozzino**
**Doctor of Philosophy**
in
**Physics**
**(Concentration - Biophysics)**
Stony Brook University
**2020**

The Maximum Entropy Principle (Max Ent) was introduced by E.T. Jaynes in 1957 as a method to infer the most likely probability distribution given some known partial information about data. Such principle found theoretical grounds in the work of Shore and Johnson in 1980, who showed that its accuracy is due to self-consistency conditions on the laws of probability themselves. This showed how the concept of entropy and its maximization is not limited to equilibrium thermal systems, but it can be extended to non-thermal systems at equilibrium as well as dynamical ones. After a brief overview of the principle itself, and its dynamical form (known as Maximum Caliber principle, or Max Cal) I will discuss some applications of it to systems of physical and biological relevance. In the first part of the dissertation I will show how it is possible to apply Max Ent to the protein's sequence space, in order to determine the features of the time scales of protein evolution, adaptation to different environment and the action of other protein machinery known as chaperones. Making use of the largely accepted idea that proteins physical features are what determines the fitness of a cell, I will show how it is possible to relate the speed of adaptation and evolution to features like a proteins stability and its tendency to aggregate, as well as the concentration of chaperones. In the second part, I will show an application of Max Cal to non-equilibrium, steady state systems, which is of pivotal importance since it represents a class of systems which is among the most studied in the field of non-equilibrium statistical mechanics. I will show how the proper set of constraints resolves some doubts regarding the application of Max Cal to systems which exhibit specific symmetries under space reflection and time reversal. I will conclude the dissertation by showing that Max Cal can be used in a more systematic fashion when some conservation law applies to dynamical quantities, like linear and angular momentum; in such cases the choice of constraints is less arbitrary than in others.

# Contents

# List of Figures

# Publications

The content of this dissertation reproduces either partially or entirely the content of the following publications. All the necessary permissions where obtained in order to reproduce the content.

- Agozzino, L., & Dill, K. A. (2018). Protein evolution speed depends on its stability and abundance and on chaperone concentrations. *Proceedings of the National Academy of Sciences*, *115*(37), 9092-9097
- Ghosh, K., Dixit, P. D., Agozzino, L., & Dill, K. (2020). The Maximum Caliber variational principle for nonequilibria. *Annual review of physical chemistry*, *71*
- Agozzino, L., & Dill, K. (2019). Minimal constraints for maximum caliber analysis of dissipative steady-state systems. *Physical Review E*, *100*(1), 010105.
- Agozzino, L., Balázsi, G., Wang, J., Dill, K. A. (2020). How do cells adapt? Stories told in landscapes. *Annual review of Chemical and Biomolecular Engineering, 11*, in press

# Introduction

# The role of entropy in statistical mechanics and beyond

Among the traditional fields of study of Physics, Statistical Mechanics (SM) can be considered somewhat atypical; while disciplines like Quantum Mechanics or Electrodynamics address very specific problems that are confined within specific regimes (spatial scales, type of interaction, energy scales etc.), Statistical Mechanics is rather a set of tools and methods which can be broadly applied within any other field, whenever it is necessary to describe a system using probabilities instead of dynamical states. This makes such discipline of particular interest not only for the predictions that it allows to make, but also for the fundamental mathematical principles that govern it.

Historically, the methods of SM have been applied to the study of classical microscopical systems of many ($\gtrsim 10^{23}$) particles, and the first successful result was the reproduction of the laws of thermodynamics, leading often to the limiting definition of Statistical Mechanics as a sort of "Microscopic Thermodynamics". This is understandable because Thermodynamics has arguably been the most successful phenomenological theory, being able to describe systems with astronomical numbers of degrees of freedom in terms of average, and hence macroscopical, quantities, therefore, it is appealing to see SM merely as its first-principled theoretical counterpart. However, Statistical Mechanics goes well beyond the explanation of the laws of gases of particles at equilibrium; in fact, its set of tools and its mathematical power can be extended not only to the physics of equilibrium systems, but to non-equilibrium dynamics, as well as to problems which don't necessarily have a physical correspondent,

like traffic patterns, social behavior, or otherwise called *non-thermal systems*.

## 1.1 A statistical ensemble

In Gibbs derivation of equilibrium statistical mechanics [1], an *ensemble* is defined as a collection of *microstates*, hence states of the system which can be microscopically distinguished but with the same identical macroscopic properties, so that any global variable would be the same irrespective of the microscopic configuration. In equilibrium statistical mechanics there are three major ensembles which are taken as examples: *microcanonical*, *canonical* and *grand canonical* ensembles. The difference between each of these examples is the physical conditions that apply to the system: a microcanonical ensemble describes a system which is completely isolated from the external environment, so its energy is conserved; the canonical ensemble describes a system which can exchange energy with a larger system, called *reservoir*, so its energy fluctuates around an average value, but the number of particle is conserved; the grand canonical ensemble describes a system which can exchange both energy and particles with a larger reservoir, the number of particle can fluctuate around an average value, as well.

Each ensemble is characterized by a very well known probability distribution, or the probability to find the system in a particular microstate. For instance, in the case of a microcanonical ensemble, the probability distribution is flat, because each microstate is equally probable; for the canonical ensemble, it is the famous Boltzmann distribution $p_i^* \propto e^{-E_i/k_B T}$, where $E_i$ is the energy of the microstate $i$, $k_B$ the Boltzmann constant and $T$ the temperature.

## 1.2 Entropy and the Boltzmann distribution

In this section we will discuss the general method to infer probability distributions called Maximum Entropy Principle (Max Ent), which can be used, among the other things, to derive Boltzmann probability distribution for canonical ensembles through a variational approach.

The original concept of Entropy was introduced around 1850 by Clausius in the context of the second law of thermodynamics, defined correctly only for reversible processes, hence for any process which involves an infinite succession of equilibrium states, as a differential form $S_{\text{Clausius}} = \int dQ_{rev}/T$. About 20 years later Boltzmann gave a statistical interpretation to this concept. His famous expression $S_{\text{Boltzmann}} = k_B \ln W$ was an assertion that the Clausius macroscopic principle had its roots in the numbers $W$ of possible microscopic arrangements of the system, establishing that Boltzmann's exponential distri-

bution law was the microscopic manifestation of the Second Law variational principle. For now let us keep the two definitions of Entropy as if they were two separate quantities, because it is of core importance for the rest of this discussion.

In more detail, for any probability distribution $\{p_i\} = p_1, p_2, p_3, \ldots$ over options $i = 1, 2, 3, \ldots$, we can define the mathematical entropy of that distribution to be, using Shannon's formula [2]:

$$S_{\text{math}} = -k_B \sum_i p_i \ln p_i \tag{1}$$

This quantity can be computed for any distribution. But this mathematical entropy $S_{\text{math}}$ is not always the same thing as the physical entropy of Clausius, $S_{\text{Clausius}}$. $S_{\text{math}}$ is also not what we need for making theoretical models of physical equilibria; for that, we need $S_{\text{state}}$, which we now describe. First, take the distribution $p_i$ to be over microscopic states of the system. Next, we assert that only the one specific distribution $\{p_i = p_i^*\}$ that maximizes the entropy,

$$S_{\text{state}} = -k_B \sum_{i=\text{states}} p_i^* \ln p_i^* \tag{2}$$

is relevant to Second Law predictions of physical behaviors at equilibrium. $S_{\text{state}}$ is defined for one particular distribution, not for just any mathematical distribution. If the system is isolated there are no information about the measurable quantities, by maximizing the entropy we obtain that each of the states is equally probable: $p_i = 1/W$; therefore in this case $S_{\text{state}} = S_{\text{Boltzmann}} = S_{\text{Clausius}}$.

However, if we assume that the system has some very well defined average energy, controlled by thermal contact to a reservoir, hence the conditions for the canonical ensemble, the prediction procedure is to maximize $S_{\text{math}}$ over $\{p_i\}$, subject to a constraint of average energy

$$\sum_i p_i E_i = \bar{E}, \tag{3}$$

where $E_i$ is the energy of microscopic state $i$, $\bar{E}$ is the average energy of the system, and $k_B T$ are Boltzmann's constant and temperature and that probabilities are normalized quantities $\sum_i p_i = 1$. The result is the Boltzmann-Gibbs distribution,

$$p_i^* = \frac{e^{-E_i/k_B T}}{Q}, \tag{4}$$

where $p_i^*$ are the probabilities that satisfy these conditions, $Q = \sum e^{-E_i/k_BT}$ is the normalization factor, or *partition function*. In this case we can calculate $S_{\text{state}}$:

$$S_{\text{state}} = -k_B \sum_i p_i^* \ln p_i^* = -k_B \sum_i \frac{e^{-E_i/k_BT}}{Q} \ln \frac{e^{-E_i/k_BT}}{Q} = \frac{\bar{E}}{T} + k_B \ln Q \quad (5)$$

It is sufficient to identify $k_BT \ln Q$ with the free energy $G$ to obtain once again $S_{\text{state}} = S_{\text{Clausius}}$. In this case Boltzmann formula $S = k_B \ln W$ is not valid anymore because the hypothesis of equiprobability of the microstates does not hold true: the probability of a microstate is determined by its energy.

This distribution is at the core of equilibrium statistical physics. Eq. 4 predicts the equilibrium populations of all the states $i = 1, 2, 3, \ldots$ in a model.

The lack of care in distinguishing these different meanings of entropy has been a source of confusion. $S_{\text{Clausius}}$ is only a predictor of *macroscopic equilibrium thermodynamics:* that heat tends from hot bodies to cold ones, that particles tend toward places of lower concentrations, and that densities tend to equalize in materials, for example. It does not tell us about the microscale or distribution functions. $S_{\text{state}}$ is a quantity we compute from microscopic physical models of equilibria. To relate an equilibrium model to corresponding macroscopic experiments, we equate $S_{\text{state}} = S_{\text{Clausius}}$. Below, we will describe yet another entropy, which is pertinent to dynamics, namely the path entropy, $S_{\text{path}}$, but first we will discuss the mathematical foundation of this procedure.

## 1.3 The maximum entropy principle

In 1957, E. T. Jaynes showed that informational entropy and thermodynamics entropy are equivalent and that it is possible to infer each of the distributions of Gibbs' ensembles applying a "Maximum Entropy Principle" [3, 4], hence by maximizing $S_{\text{math}}$ enforcing the constraints which correspond to each specific ensemble with the method of the Lagrange multipliers.

The idea behind the principle is the fact that entropy is a measure of how much a system is "biased": the lower the entropy, the more biased a distribution is. And this is a consequence of the choice, or sometimes the necessity, to describe a system using probabilities; in these cases "the maximization of entropy is not an application of a law of physics, but merely a method of reasoning which ensures that no unconscious arbitrary assumptions have been introduced" (quoting from [3]).

This Principle in original Jaynes formulation, however, is sometime interpreted to be arbitrary. On one hand it is reasonable to expect that the actual

probability distribution has to minimize the bias, on the other there seems to be no firm ground to expect that the proper function to maximize is the entropy as defined by Shannon [2], $S_{\text{math}}$. Moreover, often this principle is wrongly expressed as a method of maximizing one's "ignorance" about the system, which naturally doesn't appeal as a learning method.

From this point of view, Jaynes argument falls short to convince skeptics about the validity and the generality of Max Ent, however, this principle can be proved on pure mathematical grounds.

### 1.3.1 The Shore and Johnson argument and the correct expression for the entropy

The process of inferring a probability distribution might seem only a statistical tool, so expecting that a purely mathematical principle like Max Ent might be able to determine some physical outcomes could seem far from reality. However, statistical mechanics is not a discipline entirely determined by the laws of Physics, in that, at least for classical physics (i.e. not quantum) the use of probabilities do describe systems, even when is the best possible method, is still an arbitrary choice. In principle it is mathematically possible to write the equations of motion of each single component of the system, it is just impossible to solve them for any realistic macroscopic system, therefore we prefer to define probability densities and find the equations and the principles that describe how these densities change over time and space. However, if one chooses to describe the system using probabilities, this comes with an important baggage: the description has to satisfy the mathematical laws of probability.

Along this line, Shore and Johnson (SJ) [5] proved that the foundation of the Maximum Entropy principle is a simple self consistency condition of the inferred probability. They start from the assumption that any probability distribution that is inferred by maximizing a functional $H[p]$ needs to satisfy four main axioms (quoting [5]):

- **Uniqueness**: *The result should be unique*;
- **Invariance**: *The choice of coordinate system should not matter*;
- **System Independence**: *It should not matter whether one accounts for independent information about independent systems separately in terms of different densities or together in terms of a joint density*;

- **Subset Independence**: *It should not matter whether one treats an independent subset of system states in terms of a separate conditional density or in terms of the full system density.*

By enforcing these four axioms, whose generality is undisputable, they where able to prove that it always exists a functional of the probability $H[p]$ whose maximum corresponds to the most likely distribution $p^*$. Moreover, they also proved that the Shannon's Entropy functional $H[p] = S_{\text{math}} = -\sum_i p_i \log p_i/q_i$ is such functional, where $q_i$ is a prior for the distribution $p_i$, necessary only when additional information about it is known. Any other functional used to infer probability will either be completely equivalent to $S_{\text{math}}$, with the same maxima and minima, hence inferring the same probability distribution, or it will give a result which violates one of the fundamental axioms of probabability.

An important aspect of SJ derivation is that it never assumes in which space we are dealing with, so as long as a distribution can be correctly defined, these four axioms are satisfied only by a functional like $S_{\text{math}}$. The natural consequence of this is the application to the maximum entropy methodology to non-equilibrium systems.

## 1.4 Maximum Caliber: a variational principle for dynamical systems

In 1979, ET Jaynes introduced the Principle of Maximum Caliber [6–11] (Max Cal), extending his work to non-equilibrium systems. It differs from alternatives in: (1) its basis in particle trajectories, not concentrations, (2) its maximization of *path entropies*, not *state entropies*, (3) its inferences of microscopic models having less confounding logical traps from experimental data restraints, and (4) its axiomatic foundations in probability theory developed by Shore and Johnson [5].

Here is a brief overview. Maximum Caliber is to dynamics what Maximum Entropy is to equilibrium. Where Max Ent focuses on probabilities of *states*, Max Cal focuses on probabilities of *pathways* or *trajectories*.

Let $\{\Gamma\}$ be the set of all possible trajectories of a system that is evolving in time. $\Gamma$ can represent several types of dynamical processes. For example, a system evolving from an initial state at time $T_i$ into a final state at time $T_f$ (see Fig. 1) or trajectories of a system that is at steady state. For the former, the individual trajectories are given by $\Gamma = \{x_{T_i}, x_{T_i+1}, \ldots, x_{T_f}\}$, that the system can take between time points $T_i$ and $T_f$. Other types of trajectories

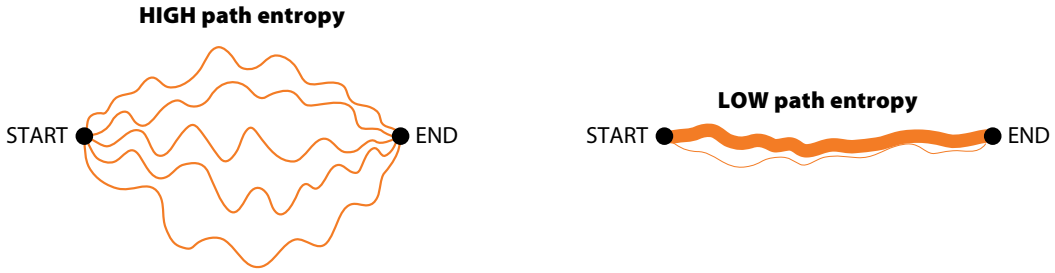


**Figure 1. Path entropy measures the uniformity of the traffic distribution** through different routes. Line thickness indicates the traffic density, i.e. pathway probability.

are discussed below. Let $p_\Gamma$ be the probability distribution defined over the ensemble $\{\Gamma\}$ of paths.

Let $J(\Gamma)$ be a functional defined on the space of paths. Examples of $J$ include the flux of mass/heat carried by the path, or the average dissipation along a path, or an average energy along a path. Suppose we want to infer the distribution $P_\Gamma$ over the paths while constraining the average

$$\langle J \rangle = \sum_\Gamma P_\Gamma J(\Gamma). \tag{6}$$

Here, and in the following of this dissertation, we use the upper case $P$ to specifically indicate probabilities over paths, whereas $p$ is used to indicate generic probabilities and its meaning will be specified when used.

Note that there are potentially infinitely many probability distributions $P_\Gamma$ that are consistent with such constraints. Analogous to the equilibrium situation, we maximize the entropy, but now over all possible paths, not states:

$$S_{\text{path}} = -\sum_\Gamma P_\Gamma \log \frac{P_\Gamma}{q_\Gamma}, \tag{7}$$

subject to constraint in Eq. 6 and normalization; see Fig. 1. $q_\Gamma$ is a reference or prior distribution over paths.

This constrained maximization problem is solved by introducing Lagrange multipliers. We write the unconstrained optimization function, called the Caliber $C$,

$$C = -\sum_\Gamma P_\Gamma \log \frac{P_\Gamma}{q_\Gamma} - \gamma \left( \sum_\Gamma P_\Gamma J(\Gamma) - \langle J \rangle \right) + \alpha \left( \sum_\Gamma P_\Gamma - 1 \right).$$

In Eq. 8, $\gamma$ is a Lagrange multiplier that fixes the ensemble average $\langle J \rangle$ to the given value, and $\alpha$ ensures normalization. After maximization, we find

$$P_\Gamma = \frac{q_\Gamma e^{-\gamma J(\Gamma)}}{Q_d}, \tag{8}$$

where

$$Q_d = \sum_\Gamma q_\Gamma e^{-\gamma J(\Gamma)}, \tag{9}$$

a sum of weights over paths, is the dynamical equivalent of a partition function. A key result of Maximum Caliber is the relationship between measurable average rate quantities and the model dynamical partition function,

$$\langle J \rangle = \sum_\Gamma J(\Gamma) P_\Gamma = -\frac{\partial \log Q_d}{\partial \gamma}. \tag{10}$$

In practice, Max Cal works as follows. First, you assert what trajectories are relevant to the problem at hand. Next, based on relevant constraints, you construct a distribution over the path space (Eq. 9) where you express each trajectory in terms of statistical weights of the steps it takes. Using Eq. 9, you can make predictions analogous to equilibrium statistical mechanics. For example, you can sum all trajectories into a dynamical partition function $Q_d$. Then, you use Eq. 10 to compute all the statistical weights and pathway probabilities that are consistent with the given value of $\langle J \rangle$ and other constraints if relevant.

When a system is far enough from equilibrium, the path entropy is the only meaningful form of entropy, because it becomes impossible to correctly identify a *state*, as in the equilibrium case, as shown in this chapter's appendices. In the appendix we also show how taking the equilibrium limit, the path entropy is completely equivalent to the state entropy, hence maximizing one or the other would lead to the same result, as one requires for self-consistency.

In the next chapter we will show an interesting application of the principle of Maximum Entropy for non-physical systems of biological relevance.

In the successive two chapters we will derive some interesting results from Maximum Caliber for physical systems.

# Chapter 1

What molecular properties determine the rates of cell evolution? Proteins are known to evolve at different rates, partly based on the functions they perform for the cell, but also depending on their physical properties such as folding stabilty and propensity for aggregation [12–19], and also depending on their companion chaperoning [20–27]. While some evolution takes place over thousands to millions of years, other evolution can be much faster. Cancer cells evolve over a human lifetime. And, pathogenic cells can evolve resistance to drugs in just a few years [28–30] or even faster [29]. How do the molecular properties of proteins and chaperones determine the speed of evolution? Here, we develop theory for the rates of protein evolution based on the Maximum Entropy Principle. The distribution of proteins conformations is given by the Boltzmann; in a similar way, Max Ent, combined with protein's physics, can give distribution over *sequence space*, allowing us to obtain results on proteins evolution rates.

## 1.5 The probabilities across sequence space can be derived from a Maximum Entropy approach

The rate at which a protein molecule evolves is given by the dependence on time $t$ of the probability $p_i(t)$ that a protein sequence $i$ is fixed in a population by the time $t$, through mutation and selection.

Before considering the dynamics, we note that the equilibrium distribution of such probabilities will be a Boltzmann-like exponential, as shown previously [31–34]. Here, we give an alternative derivation, applying the principle of Maximum Entropy to sequence space, because it gives $p_i^*$ directly, collects together some results not made explicit elsewhere, such as the sequence entropy, and gives the meaning of *selective pressure* directly and without the metaphor of a bath temperature.

For matters of evolution, we are interested in the space of all possible amino-acid sequences. Therefore, we derive a general relationship between the probability $p_i$ of a sequence $i$ as a function of a quantity $V_i$ that we call the *fitness potential* (which Sella et. al. call the *additive fitness* [31]). The concept of fitness has been center of study of the field of evolution since Darwin's original work [35]; the mathematical formulation of fitness in terms of a function of the genetic composition of an organism was first introduced by Wright in 1932 [36] and since then the field has been developed extensively [37].

When considering evolution at the protein level, the degrees of freedom in sequence space are the different amino acid types, also called residues, that can occur at different positions in the chain. Our objective is to determine the

one particular distribution $\{p_i^*\}$ that maximizes the sequence entropy while also satisfying an observed constraint on the average fitness[1]

To do this, we first express a *sequence entropy* $S_{\text{seq}}$ as

$$S_{\text{seq}} = -\sum_i p_i \log(p_i) \tag{11}$$

We define the average value, over the population, of the fitness potential, as:

$$\langle V \rangle = \sum_i p_i V(i). \tag{12}$$

So, the equilibrium probability distribution $p_i^*$ we seek is that which maximizes the entropy, Eq. 11, subject to the constraints of the given average fitness, Eq. 12, and that the probabilities must sum to one. That is, using the method of Lagrange multipliers, we maximize the functional,

$$-\sum_i p_i \log \frac{p_i}{g_i} - \alpha \left( \sum_i p_i - 1 \right) - \lambda \left( \sum_i p_i V(i) - \langle V \rangle \right) \tag{13}$$

where $\lambda$ is the Lagrange multiplier that enforces the fitness constraint, $\alpha$ is the multiplier that enforces the sum to one and $g_i$ is the sequence degeneracy (the number of sequences having the given fitness potential) which acts as a prior for this problem. Differentiating with respect to $p_i$ gives a Boltzmann-like equilibrium distribution of the populations of amino-acid sequences having different fitnesses,

$$p_i^* = \frac{g_i e^{-\lambda V(i)}}{Q} \tag{14}$$

where $Q = \sum_i g(i) \exp(-\lambda V(i))$ is the sum of relative weights over all of sequence space.

Note a few points. **(i)** Eq 14 is a Boltzmann-like distribution. This is not a metaphorical similarity; both are reflections of the deeper point that maximizing entropy is a principle about drawing inferences over probability distributions [38, 39]. **(ii)** Maximizing Eq 13 is identical to minimizing the free-energy-like quantity $\mathcal{F}$ (Sella and Hirsh [31] called it the *Free Fitness*),

$$\mathcal{F} = \langle V \rangle - \frac{1}{\lambda} S_{\text{seq}}. \tag{15}$$

[1]Maximum entropy applies to a broad range probability-distribution predictions, not just to thermal physics [38, 39].

Eq 15 has an energy-like part $\langle V \rangle$ and an entropy-like part, $S_{\text{seq}}$. This means that a single sequence with very high fitness can sometimes be outcompeted (i.e. have higher equilibrium probability) by sequences having lesser fitness if there are many of them having that fitness. **(iii)** The Lagrange multiplier $\lambda$, which describes the force, or selection pressure, for changing sequence fitness, resembles $\beta = 1/(kT)$, the thermal driving force in material equilibria, where $T$ is temperature and $k$ is Boltzmann's constant. **(iv)** When there is no constraint that fixes the value of $\langle V \rangle$, Maximum Entropy predicts a flat distribution: all sequences will be equally likely. **(v)** Whenever two independent factors give *multiplicative* contributions to a probability distribution, they give *additive* contributions to the fitness potential [31], so

$$V(i) \equiv -\log f(i) \tag{16}$$

where $f(i)$ is the absolute fitness [31, 36].

## 1.6 A ZSB-like model of protein adaptation rates

We model a protein's evolutionary kinetics by adapting Zwanzig-Szabo-Bagchi (ZSB) theory applied to the different problem of protein folding speeds [40, 41]. On the one hand, protein folding dynamics is quite a different process than protein evolution. In folding, a particular protein explores its conformational degrees of freedom changing its shape, whereas in evolution, a protein undergoes changes of sequence through mutations and selection. But, the dynamics can be modeled by a similar formalism. We define the transition rate from an ancestor sequence $i$ to descendant sequence $j$ as $W_{ji}$; the transition takes place through a process of mutations and selection steps. Then, the change in population of sequence $j$ in a given time interval is given by the master equation expressing the "flow" from different sequences into sequence $j$, minus the flows out from $j$ to other sequences,

$$\frac{dp_j(t)}{dt} = \sum_i \left( W_{ji} p_i(t) - W_{ij} p_j(t) \right). \tag{17}$$

To solve the dynamics, we need to know the transition rates $W_{ij}$; these are dictated by the shape of the fitness potential $V_i$ since the rates are related to the equilibrium probabilities $p_i^*$ which is given by Eq. (14). Then, we can solve for two key dynamical quantities: (1) the *adaptation time*, $\tau_{\mathcal{A}}$, or *peak time*, which is the minimum time required for changes in a sequence $i$, through mutation and selection, to reach the sequence that is optimally adapted to its environment, or (2) the *substitution time*, $\tau_{\mathcal{S}}$, also called the *exit time*, which

is the average time required for a sequence $i$ to change and become any other sequence. The inverse of each of these times is a corresponding rate. The substitution rate is also called the *evolution rate*. The adaptation rate and substitution rate are measured differently, and give different insights.

### 1.6.1 Solving for the adaptation time

In real systems, the matrix $W_{ji}$ is very sparse, since not every two sequences can be connected with a single mutation. We can safely assume that only those sequences which differ by a single amino acid have a non-zero transition rate

$$W_{ij} \begin{cases} \neq 0 & i \text{ and } j \text{ differ by a single mutation} \\ = 0 & \text{otherwise} \end{cases} \tag{18}$$

Equation (17) can be further simplified if we introduce a reference sequence, the perfect adapted sequence, relative to which we count the number of mutations. In this way sequences can be binned into classes, each of which is a given number of mutations away from the perfect sequence. While this simple mutation count is not always a useful measure, it is sufficient for present purposes.

We write the transition matrix as $W_{ij} = \omega_j^- \delta_{i+1,j} + \omega_j^+ \delta_{i-1,j}$, where $\omega_i^\pm$ are the up/down transition rates from the sequence $i$. The problem is now equivalent to a death/birth process, a well-studied problem in non-equilibrium statistical mechanics. Calling $m$ the number of mutations with respect to the perfect sequence, Eq. (17) becomes

$$\frac{dP_m(t)}{dt} = \omega_{m+1}^- P_{m+1}(t) + \omega_{m-1}^+ P_{m-1}(t) - (\omega_m^- + \omega_m^+) P_m(t)$$

where $\omega_m^\pm$ is the transition rate from sequence $m$ to $m \pm 1$

The average time for a system which starts at some distance $M$ from the optimum to reach the optimum at distance 0, for a sequence with length $L$. Such mean time is called $\tau(M)$ *mean first passage time*, and it is derived by considering the average exit time from the interval $(1, L)$ when starting from $M$. $\tau(M)$ is derived from the master equation (19) and is given by the recursion relation [42]

$$\omega^+(M)\left[\tau(M+1) - \tau(M)\right] - \omega^-(M)\left[\tau(M) - \tau(M-1)\right] = -1 \tag{19}$$

whose solution is known to be [42]

$$\tau(M) = \sum_{k=1}^{M} R(k) \sum_{j=k}^{L} \frac{1}{\omega^+(j) R(j)} \tag{20}$$

where

$$R(n) = \prod_{\ell=2}^{n} \frac{\omega^-(\ell)}{\omega^+(\ell)} \tag{21}$$

Considering the detailed balance condition for the equilibrium probabilities and the linear fitness potential assumption it is possible to give a more explicit form of $\tau(M)$. When the fitness potential is linear the up/down rates are uniquely determined by the combinatorics of the sequences. For a sequence that is $n$ steps away from the optimal, there are $n$ ways to decrease the mutational distance and $L - n$ ways to increase it, so we have

$$\omega^-(n) = n\omega^- \tag{22}$$

$$\omega^+(n) = (L-n)\omega^+ \tag{23}$$

$$\frac{\omega^+}{\omega^-} = z e^{-\lambda V_0} \tag{24}$$

which gives, after some label redefinition

$$\tau(M) = \frac{1}{L\omega^+} \sum_{k=1}^{M-1} \left( \begin{array}{c} L-1 \\ k \end{array} \right)^{-1} \sum_{l=k+1}^{L} \left( \begin{array}{c} L \\ l \end{array} \right) z^{l-k} e^{-\lambda V_0 (l-k)} \tag{25}$$

The expression above can be simplified in some cases; for instance it becomes trivial when the starting sequence is at a distance $M = 1$. However, in general, sequence lengths are typically $L \gg 1$. In that case, we can approximate Eq 25 by the ZSB result [40]:

$$\tau(M) \simeq \frac{\left(1 + z e^{-\lambda V_0}\right)^L}{\omega_0 L} \tag{26}$$

where $z$ is the number of possible mutations a residue in the protein can have relative to its starting sequence ($z = 19$); $L$ is the total number of residues in the protein; and $\omega_0$ is the average fixation rate for a single point mutation. (If $L$ is large, the adaptation time is independent of the number of mutations; it becomes equally hard to find the peak, no matter what the starting sequence is.)

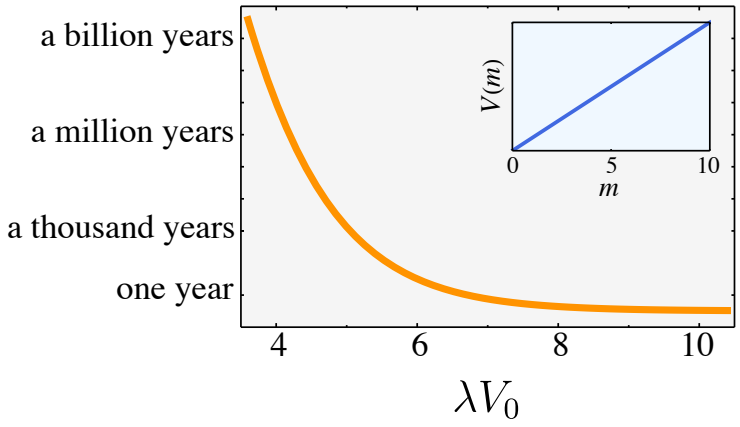


**Figure 2. The adaptation time $\tau_{\mathcal{A}}$ of a protein depends strongly on the selection pressure $\lambda$.** The time it takes for a protein to evolve to its optimally adapted sequence, assuming a linear model fitness potential (inset), if an average random mutation is fixed once every 100 years in the absence of selection pressure [43]. We assume the protein has $L = 50$ amino acids, and that each residue can be any of the 20 amino acids ($z = 19$).

For large values of $L$, the first passage time does not depend upon $M$, giving the adaptation time $\tau_{\mathcal{A}} = \tau(M)$ in Eq. 26.

### 1.6.2 A protein's adaptation rate depends strongly on the selection pressure

First, we ask how protein adaptation can sometimes be very fast. For this exploration of principle, it is sufficient to adopt the very simplest model of a fitness landscape that has a single peak. We assume the *fitness potential is linear* in the number of mutations $m$ in a single protein (meaning that the *fitness landscape* is exponential), with slope $V_0$ and minimum $-V^*$ (which is the landscape point of the optimal sequence)[2]:

$$V(m) = -V^* + mV_0. \tag{27}$$

The virtue of the linear landscape here is in allowing for a closed-form expression for the adaptation time given in Eqs. 25 and 26.

Fig.2 shows a key conclusion: a protein's adaptation speed can vary over 9 orders of magnitude as a result of only a two-fold change in selection pressure $\lambda$. This huge magnification in Eq. (26) is because the adaptation rate is nearly

[2]Both $V_0$ and $V^*$ are taken to be positive quantities

an exponential function of an exponential ($k_{\mathcal{A}} = 1/\tau_{\mathcal{A}} \sim \left(e^{\lambda V_0}\right)^L / z$). So, even though evolution 'would take forever' if fitness landscapes were flat, even a very slight tilt of a fitness landscape gets amplified into very fast adaptation for protein sequence evolution.[3] This general conclusion holds also if instead we had used other hypothetical functional forms of fitness. Here, we have considered just a single isolated protein. Below, we consider situations where mutations happen in multiple proteins.

### 1.6.3 Proteins having the steepest fitness landscapes adapt the fastest

Eq. (26) shows another key point, namely that the adaptation rate $k_{\mathcal{A}}$ increases strongly with the steepness, $V_0$ of the fitness potential. Metaphorically, a ball rolls faster down a steeper hill than down a shallower hill.[4]

## 1.7 The fitness landscape for protein stability and temperature

Above, we asked how external pressure affects adaptation speed. Here, we ask how the properties of the protein itself affect its adaptation speed. So, first, we need a model for how fitness depends on protein properties. Ever since the pioneering work of Drummond et al [12, 14, 17, 32, 45], a major idea has been the *misfolding avoidance hypothesis*; namely, that a protein's fitness is substantially due to its folding - unfolding equilibrium. What is new here is to give a model of the evolution rates. Consider a protein $i$ having folding stability, $\Delta G_i = G^{(i)}_{\rm native} - G^{(i)}_{\rm unfolded}$ ($< 0$ for a folded protein), and abundance $A_i$. Let the number of different types of proteins in the cell be $m_{\rm tot}$.

A well-known result is how the cell's fitness potential $V$ is the following nonlinear function of its folding stability [17]:

$$V(T, m_{\rm tot}, \{\Delta G\}) = -c \sum_{i=1}^{m_{tot}} A_i \left( \frac{\exp(-\Delta G_i/RT)}{1 + \exp(-\Delta G_i/RT)} \right) \tag{28}$$

Eq. 28 simply states that each protein's fitness potential is proportional to

[3] The treatment is valid in the limit of strong selection and weak mutations, for which populations are monomorphic and mutations do not interact with each other. Other contexts require different methods [44].

[4] In the limit of a small slope, adaptation will follow a random walk in a large space, requiring an exponentially long time.

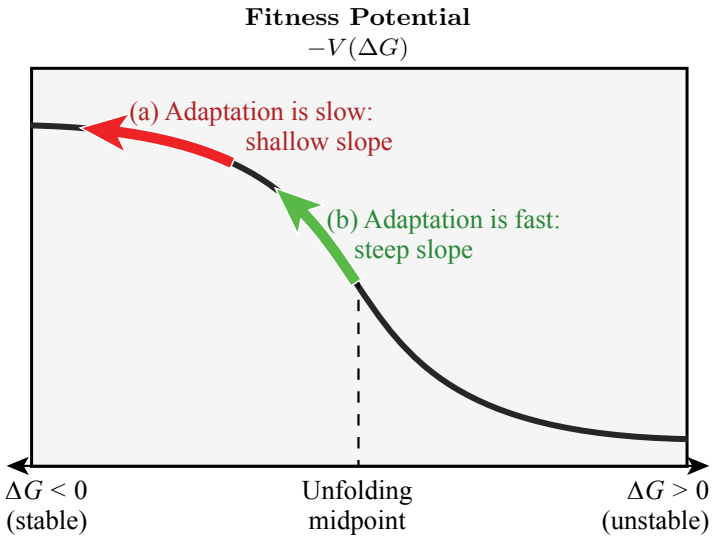


**Figure 3. The fitness potential for a protein-folding stability sequence space.** Having greater folding stability means higher fitness. The green and red arrows indicate that where the slope is steepest on this potential, adaption is fastest. And, it is fastest where proteins are least stable.

the product of (its abundance, $A_i$, in the proteome)[5] $\times$ (its fractional degree of folding, [native/(native + unfolded)]) $\times$ (the total number of protein types in the cell). (Folding stability and aggregation are not the only physical contributors to evolution rates; conformational flexibility, which we don't study here, can also affect evolvability, particularly in virus proteins [46–48]). We can picture the effect on evolution of such a fitness lanscape by looking at Fig. 3.

First, compare two proteins: one protein is more stable than the other. The logic above says that the less stable protein will accumulate adaptive mutations faster than the more stable protein. Second, compare a 'fit' protein, which is stably folded and well-adapted to its environment, to a mutated version of that same protein, which is less stably folded and less fit. The mutant protein will acquire adaptive mutations faster than the well-adapted protein.

Figure 3 illustrates that fast adaptation happens where the fitness potential is steep, which is where protein stability is marginal (near $\Delta G_i = 0$, neither stably folded, nor substantially unfolded), for a given abundance $A_i$.

The curve in Fig. 3 is general and applicable when both stabilizing and

[5]Fitness potential is assumed to be linearly proportional to the number of folded copies of the protein, but only up to the point of overexpression.

destabilizing directions are accessible to the protein. But we note that adaptation requires mutations in multiple proteins, therefore in the next section we make a binary simplification of this landscape, but it doesn't alter the slope-speed principle.

Also, it is important to notice that the complete dependence of the fitness on temperature needs to reflect the fact that at very low temperature, when proteins are extremely stable, the cell is not functioning properly. In order to account for this, we assume that the complete fitness is given by the growth rates of simple cells, which are well-known functions of temperature, and are predictable from the folding stabilities of the proteins in their proteomes [49–52]. Here, we combine that relationship with the misfolding avoidance hypothesis (given in Eq. 28) so that we are able to to consider mutational changes. So, the fitness function equals the growth-rate function,

$$r(T) = r_0 \exp\left(-\frac{\Delta H}{kT}\right) \exp\left[c \sum_{i=1}^{m_{\rm tot}} \frac{A_i \exp(-\Delta G_i/RT)}{1+\exp(-\Delta G_i/RT)}\right] \tag{29}$$

where $r_0$ is an in intrinsic growth-rate speed limit, $\Delta H$ is the activation barrier, $m_{\rm tot}$ is the number of different type of proteins that are important for growth, $A_i$ is the abundance of protein type $i$, $T$ the temperature of the environment and $k$ is Boltzmann's constant. $\Delta G_i$ is the folding free energy, whose functional form is given in detail in [53], but taken here, to good approximation, to be independent of temperature.

In this work, we consider an evolutionary process in which a cell can be represented by integer $m$, which is the number of proteins that have one mutation away from the wildtype exact sequence. We assume that every protein can mutate to increase its stability $\Delta G_{\rm f} \to \Delta G_{\rm f} + \Delta\Delta G$ (we are using the average of the change in the free energy as a first approximation). A given organism will have a certain number of these proteins mutated in the new, more stable, sequence. The more mutated proteins, the higher the optimal growth temperature; therefore, adaptation to higher or lower temperature can be achieved by mutating to a more or less stable proteome respectively.

For an $m$-mutant protein organism, the normalized growth law 29, and therefore the relative fitness, now becomes:

$$r(T,m) = r_0 k_{\rm act}(m,T) K_{\rm fold}(m,T) \tag{30}$$

$m$ is the *genotype variable*, which counts the number of protein kinds which have mutated to a more stable sequence, hence a quantity which refers to the entire proteome. $k_{\rm act}(m,T)$ is exponentially increasing with the temperature, and takes into account the *activation energy* for the cellular processes,

$$k_{\rm act}(m,T) = \exp\left(-\frac{\Delta H + m\delta h}{kT}\right) \tag{31}$$

$K_{\rm fold}(m,T)$ accounts for the decrease in the fitness due to misfolding.

$$K_{\rm fold}(m,T) = \exp\left[-c\left(\frac{mA}{1+\exp((\Delta G_{\rm f}(T)+\Delta\Delta G)/RT)}\right)\right.$$
$$\left. -c\left(\frac{(m_{\rm tot}-m)A}{1+\exp(\Delta G_{\rm f}(T)/RT)}\right)\right] \tag{32}$$

In Fig. 4 we show how the fitness depends on the two main variables: genotype $m$ and environment $T$, and show what the paths for adaptation would look like.

For simple cells, the growth rate is a direct measure of fitness, so $f(m,T) \propto r(m,T)$. So, the relation to the fitness potential 16 is

$$V(m,T) = A(T) + mB(T) \tag{33}$$

where $A$ and $B$ are functions of temperature determined by Eq. 32 and parametrized so that the peak of the landscape is at $m = 0$ when the environmental temperature is $\sim 40°C$ and at $m = m_{tot}$ when $T \sim 70°C$. We imagine that ideally evolution happens at a fixed environmental temperature; either a mesophile is kept at high temperature and evolves towards a more stable proteome or a thermophile is put in a cold environment and it undergoes the opposite process.

In this simple model, the landscape potential is linear along the $m$ axis, and the slope is determined by the environmental temperature, other than the organism-specific growth parameters, which can be obtained by fitting real data [49].

### 1.7.1 So, cells should adapt faster to a warmer environment than to a colder one

How fast can proteins adapt if cells are put in climates of different temperatures? Some unicellular organisms (*mesophiles*) live in moderate-temperature environments (around 40℃ for *E. coli*), while others (*thermophiles*) live in hotter environments. Cells grow the fastest at the temperature of their natural environment [49, 53, 54], but moved to different environments having different temperatures, they can adapt [55]. We compute the speed of adaptation of a cell that is transferred from its normal environment to a new environment having either a higher or lower temperature. We compute rates from Eq 25,

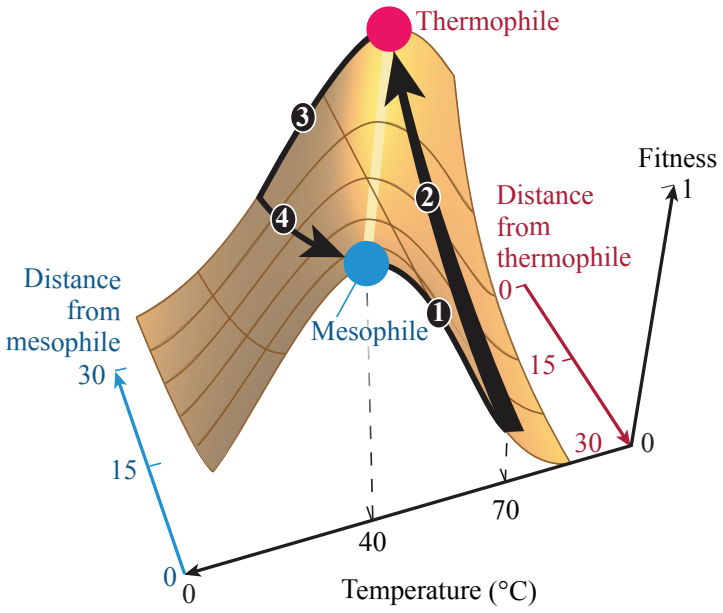


**Figure 4. Fitness trajectories for explaining why cells adapt faster to warmer environments than to cooler ones.** Paths 1 and 2 show how cell fitness changes upon heating. Path 1: start with a mesophile pre-adapted at 40℃, at the peak of its landscape. Increase the temperature. Path 2: mutations occur to bring the cell to the peak fitness for 70℃. This is fast because the proteins are destabilized by heating, so the fitness landscape is steep along path 2. Paths 3 and 4 show changes upon cooling. Path 3: cooling reduces the fitness of a pre-adapted thermophile. Path 4: he cell now undergoes mutations to bring it to the peak of adaptation for 40℃. But path 4 is much slower than path 2 because cooling pre-adapted proteins does not affect their stabilities much. So adaptation to heat is faster than to cold.

with a fitness potential given by the thermal folding Eq 28, and using Eq. 29 to find its slope along the mutation axis. In this example, we consider a given number of proteins in the cell with either zero or one adaptive mutations to each protein (assuming no epistasis).

Figure 5 shows the prediction that cells should be able to adapt much faster to a warmer environment than to a cooler environment. (We are unaware of experiments that bear on this.) Fig 4 illustrates the reason for this, using a fitness landscape. Start with a healthy mesophilic cell in its normal environment, say at $T = 40$℃, where it is maximally fit. Its proteins are stably folded. Now upshift its environment to $T = 70$℃ (path 1) (slowly in small steps, to avoid killing the cell). Initially, the cell is unfit for its new warmer environ-

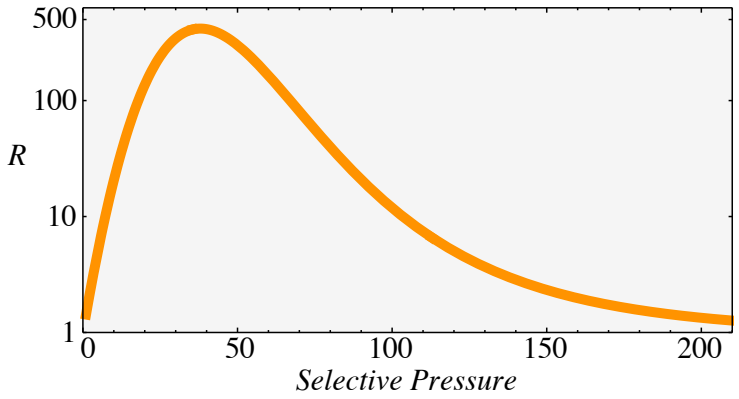


**Figure 5. Proteins adapt faster to a warmer than cooler climate.** $R = k_{\text{high}}/k_{\text{low}}$ is the ratio of adaptation rates: (a mesophile adapting to a higher temperature) / (a thermophile adapting to a colder temperature). Heat destabilizes folded proteins, putting them onto the steep slopes of fitness landscapes so cells adapt faster to warmer environments. x-axis: the selection pressure per misfolded protein, $\lambda \times c$.

ment because its proteins are less stable at this higher temperature, $T = 70$℃. Now, mutations accumulate rapidly (30 total, in the model example) because the fitness landscape is steep for proteins that are unstable, leading to fast adaption to the new peak (path 2).

Now, contrast this with cooling. Now, a thermophilic cell starts at $T = 70$℃, maximally fit, with its proteins stably folded. Cooling causes this cell to be less fit for its new environment at $T = 40$℃ (path 3). But this is not due to protein stability; cooling proteins that are already stable does not change their native populations. Rather, the reduced fitness upon cooling is because of the Arrhenius temperature factor: cells naturally grow slower in colder temperatures (see Eq 29). Overall, for this cooling situation, the cell's fitness landscape has a shallow slope (along path 4), and adaptation to the cold through mutations is slow. In summary, cells should adapt to warm climates faster than to colder ones.

## 1.8 The *substitution rate* vs. *adaptation rate*: they reflect different features of fitness terrains.

We now switch attention from the *adaptation rate* (how fast an arbitrary sequence evolves to become the sequence that has the maximal fitness) to the *substitution rate* (also called the *evolution rate*: how fast, on average, an arbi-

trary sequence changes to become fixed as a different arbitrary sequence). This switch allows us to test predictions against experimental data for the properties studied below. Substitution rates are properties of individual proteins, meaning that the accumulation of multiple mutations can take a long time. In contrast, adaptation involves mutations that can occur in parallel throughout the entire proteome, and therefore those changes can happen much faster. For this reason, for the remaining of this section we will be counting the number of mutations in a single protein, as opposed to what done in the previous part.

More importantly, these two rate properties reflect different features of fitness landscapes. Whereas our model shows that adaptation rates are *positively correlated to the slope of a fitness landscape* (see above), substitution rates, instead, are *proportional to the average mutational distance of a given protein to its fitness peak* (at equilibrium) (see below):

$$\langle W \rangle \approx \mu_0 \sum_{m>0} m \frac{e^{-\lambda V(m)}}{Q} = \mu_0 \langle m \rangle \tag{34}$$

where $\mu_0$ is a rate quantity used as fitting parameter and $\langle m \rangle$ is the average number of sequence mutations from the optimum in a single protein, hence the average mutational distance from an hypothetical optimal sequence at equilibrium.

### 1.8.1 The amino-acid substitution rate can be determined from the equilibrium probabilities

Here is how we compute the average amino-acid substitution rate $\langle W \rangle$ for accepted mutations as a function of the probability distribution, Eq. 34. For a given protein, the average rate can be written as [32]:

$$\langle W \rangle = \frac{1}{2} \sum_i \sum_j W_{ij} p_j(t), \tag{35}$$

where now the indexes $i$ and $j$ refer to different sequences of a given protein, as it can appear in two different organisms which are related in evolution.

The left side of Eq (35) depends upon time, but the average rate is constant according to molecular clock data. So, we take the long time limit, so that the expression of the probability will be determined by its Max Ent distribution $p(t) \to p^*$. Considering a death/birth process, which means assuming that we can just count the number of mutations from a reference state and including the fitness degeneracy, the rates take the form $W_{ij} = \omega_j^- \delta_{i+1,j} + \omega_j^+ \delta_{i-1,j}$, and the average substitution rate becomes

$$\langle W \rangle = \frac{1}{2} \sum_{i}^{i_{max}} \left( \omega_{i+1}^{-} p_{i+1}^{*} + \omega_{i-1}^{+} p_{i-1}^{*} \right) \tag{36}$$

Using detailed balance, we can replace $\omega_{i-1}^{+} = \omega_{i}^{-} p_{i}^{*} / p_{i-1}^{*}$, which leads, after some steps to

$$\langle W \rangle = \sum_{m>0} \omega_{m}^{-} p_{m}^{*} \tag{37}$$

The detailed balance condition is correct in this case, because we are considering the fitness to be dependent on the protein's property alone, so detailed balance is the only steady state solution of Eq. 17 as it is obvious from the theory of linear systems of equations; it is interesting to note that when the fitness depends on the frequency of a given allele, as it happens for phenomena of co-evolution, like predator-prey dynamics, detailed balance is broken, and a different approach needs to be taken [56].

Next, we express the transition rate $\omega_{m}^{-}$, the fixation rate from the sequence $m$ to the sequence $m-1$, which is a higher fitness one by construction. Based on the combinatorics, the transition rate will be proportional to the number of mutations in the protein $m$, simply because there are $m$ possible ways of reducing the number of "defects". This quantity will be multiplied by the mutation rate $\mu$ and the *probability of fixation* $\pi_{m}^{-}$. Assuming a constant probability of fixation (which is a good approximation when the selective advantage relatively small per single mutation), $\pi_{m}^{-} \to \pi_{0}$, so we can write

$$\omega_{m}^{-} \simeq \mu m \pi_{0} = m \mu_{0} \tag{38}$$

where $\mu_{0} = \mu \pi_{0}$ is a rescaled rate quantity which can be used as fit parameter. We obtain

$$\langle W \rangle \approx \mu_{0} \sum_{m>0} m P_{m}^{*} = \mu_{0} \langle m \rangle \tag{39}$$

Eq. 39 says that the average substitution rate is proportional to the average distance from the optimum at equilibrium (in the example of the main text it is the average number of mutations away from the optimum). Such distance is lower when the optimum has a high probability of being populated, then the total number of mutations per unit time tend to be smaller, and this is because there is less doubt on which direction evolution will continue; on the other hand, when there are a lot of alternatives with a relatively similar fitness potential, the system, here intended as all the possible lineages that

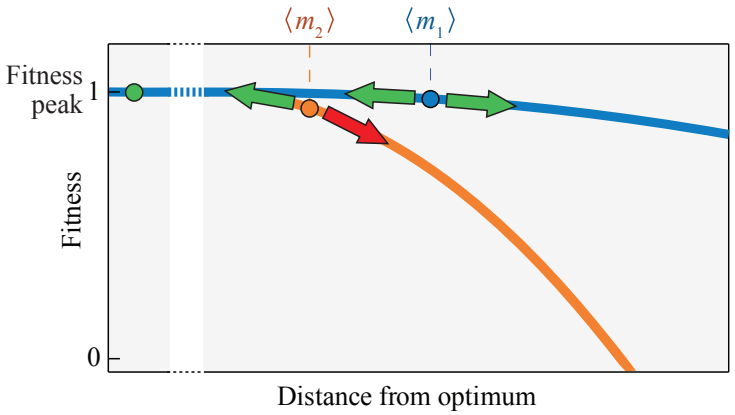


**Figure 6. Substitution rates are higher on 'high-shouldered' fitness landscapes.** The bluescape has more directions in which mutations are fit and adaptive than the orangescape has, $\langle m_1 \rangle > \langle m_2 \rangle$. On the bluescape, mutations can be fixed in either direction (green arrows). On the orangescape, mutations downhill (red arrow) are too unfit to be fixed. Eq 34 shows that the bluescape has the higher substitution rate than the orangescape.

can develop from one given individual, tends to explore more possibilities in the genotype space and the substitution rate, as a consequence, is higher.

Figure 6 shows the interpretation of $\langle m \rangle$. It measures the weight under the curve, so substitution rates are highest on fitness landscape contours that are 'high-shouldered': plateaus of high fitness where slopes are shallow. The bluescape Figure 6 is high-shouldered, with larger $\langle m \rangle$: a mutation in either direction (green arrow) is fit enough, so substitution is fast. The orangescape is not a high plateau or flat. It has smaller $\langle m \rangle$: a mutation downhill (red arrow) is too unfit to be fixed. Because of greater access to allowed directions, Eq 34 says that substitutions happen faster on the bluescape than the orangescape. Moving away from the peak on the bluescape still leads to adaptive mutations, hence to substitution; moving away on the orangescape leads to non-adaptive mutations. So the net substitution speed is greater on the bluescape. This high-shouldering principle is valid beyond the simple model used here to illustrate it.

Substitution rates of amino acids are measurable, and have been the basis for the *molecular clock* idea [57–59] that substitution rates differ among proteins, but are approximately constant for a given protein. Recent work shows that the average substitution rate is determined not by functional constraints, but by physical ones. Proteins that are more abundant are observed to evolve

more slowly than proteins that are less abundant [60]. The *E-R anticorrelation* is the observation that increasing Expression levels (protein abundances) lead to reduced Rates of their evolution. It has been hypothesized that this is a result of either protein misfolding or protein-protein interaction [32, 45, 61].

## 1.9 Abundant proteins evolve slowly

We model the mechanism of the ER anticorrelation. In a population of cells, many proteins are not peak-fitness sequences. Increasing the abundance of these imperfect proteins reduces the cell's fitness relative to a perfectly adapted cell. We consider two mechanisms: *(i) Misfolding*, where fitness, $V^{\text{core}}(n)$ depends on how perfectly a protein sequence folds in its lowest energy state to maximize HH contacts in the core of its native structure. The deviation from the fitness peak is a count of the number of *defects*, $n = 0, 1, ..., N_c$. *(ii) Aggregation and misinteraction*, where fitness, $V^{\text{surf}}(m)$ depends on how perfectly the protein surface is covered with P residues, to avoid protein-protein sticking through HH contacts. The deviation from perfect fitness is $m = 0, 1, ..., N_s$ the number of H residues on the surface. Now, to get these fitness landscapes, we use the HP lattice model, in which a protein is assumed to have only hydrophobic (H) or polar (P) residues, and different native and mutated protein sequences are enumerated on a 2D square lattice [62]. Random mutations over different proteins can reduce either form of 'perfectness'. In the next sections we will explore the two assumptions. The main distinction between these mechanisms is their dependence on abundance $A$: $V^{\text{core}}(n) \propto A$ and $V^{\text{surf}}(n) \propto A^2$. We calculate the substitution rates for these two different mechanisms using Eq 34.

### 1.9.1 Is misfolding a driving force for evolution?

In this HP model, the noncovalent folding free energy of the native protein is calculated by adding the contribution of each pair of H residues that are in contact by assuming that each pair contributes at the same way. The total folding free energy for a single protein can be written in general as

$$\Delta G_c = -pN_H\delta g \tag{40}$$

where $N_H$ is the number of H residues in the core and $p$ is the average number of HH contacts that a single H residue makes and $\delta g$ is the free energy associated with it. Considering that removing a single H residues will remove its contacts, it is better to write $N_H$ in terms of the total core residues and the number $n$ of P residues in the core: $N_H = N_c - n$. Eq. 40 now becomes

$$\Delta G_c(n) = -N_c \delta G + n \delta\delta G \tag{41}$$

where $\delta G = p\delta g$. In this case we also have $\delta\delta G = \delta G$ but in general they can also differ, in the case in which the effect of removing a H does not change $\delta G$ of the exact same quantity, so we prefer to keep them distinct.

With all these assumptions, we can write that the fitness contribution due to misfolding is

$$f_n^{\text{core}} = \exp\left(c_c \frac{A \exp(-\beta \Delta G_c(n))}{1 + \exp(-\beta \Delta G_c(n))}\right) \tag{42}$$

### 1.9.2 Is aggregation a driving force for evolution?

As the stability contribution to fitness comes from the residues in the core, aggregation, which is the basic form of misinteraction when considering a single type of protein, as we are doing in this model, is mainly due to the residues on the surface, which is the reason why the misinteraction avoidance hypothesis was proposed: E-R anticorrelation is observed also for residues on the surface, which contribute too little to the stability of the protein [18, 19]. A functional form for the additive fitness due to mutation on the surface is still lacking: results have been obtained either by analyzing known data on the basis of the interaction propensity of a protein [19] or computationally [18].

Since we need a functional form for the additive fitness we will guess a function by relying on basic principles only. We assume that the additive fitness is a decreasing function of the probability that two proteins will come in contact in the cell and of the average number of "wrong" residues (H) that can come in contact. Indeed we assume that a misinteraction takes place when two hydrophobic residues of two different proteins interact. Our guess is therefore

$$f_m^{\text{surf}} \propto \exp\left[-\Pi(A) \times M(m)\right] \tag{43}$$

where $m$ is the number of H residues on the surface and

- $\Pi(A)$ is the probability that two proteins out of $A$ have a face in contact.
- $M(m)$ is the average number of mutants on a face when there are $m$ in total.

In the lattice model it is simple to derive such probability from geometrical point of view: $\Pi(A) \simeq \left(\frac{v}{V}\right) A^2$. Where $v$ is the volume of a protein and $V$ is the volume of the cell.

In 2D we simply have $M(m) = \frac{m}{4}$ if we assume that the mutations can appear with equal probability in each side of the lattice.

In this way our guess for the additive fitness due to surface residues mutations in a single protein type is the one given in Eq. (44)

$$f_m^{\text{surf}} = \exp\left[-c_s \rho A^2 m\right] \tag{44}$$

where $c_s$ describes the degree of fitness harm there is to a cell due to a misinteraction, and $\rho = (\frac{v}{V})^2$ is the relative size of the protein with respect to the cell, which is a number that varies in the range $10^{-12} - 10^{-9}$ for bacteria.

## 1.10 The ER anticorrelation is explained by either misfolding or aggregation or both

In Figure 7 we compare the misfolding and aggregation models we discussed in the previous section to experiments. Both models predict a general ER anticorrelation. And, both are consistent with the (not very precise) data [45]. So, we have no basis for favoring one mechanism over the other. Previous modeling has also observed the ER anticorrelation, but based on assuming an anticorrelation between $\Delta G$ and mutational $\Delta\Delta G$'s taken from the PDB [17, 18]. Our more microscopic mechanism here of the full evolutionary landscape allows us also to study aggregation and chaperone effects at a single protein level.

Table 1 gives the parameters we use for the fits in Fig. 7. Defined in Eqs. 28 and 44, they are the folding energy per residue $\delta G$, the change in the folding energy per residue due to a single mutation $\delta\delta G$, the length of the protein, the protein-to-cell volume ratio $\rho$ and the two fitness parameters $c_c$ and $c_s$, multiplied by the selective pressure $\lambda$. The model focuses on a single protein, whereas the experimental data shows multiple proteins under different conditions.

The model explains the ER anticorrelation as follows. Fig. 8 (yellow surface) shows the substitution rate as functions of both protein stability and abundance. In a very stable protein, a mutation that removes a hydrophobe from the core is usually acceptable (a high-shouldered terrain), so it has a high substitution rate. In contrast, in a weakly stable protein, removing a hydrophobe from the core can unfold the protein, so it is not adaptive (not a high-shouldered terrain), so fewer possible substitutions are acceptable and the substitution rate is slower. The abundance effect is as follows. This is an integration over all the proteins in the cell, and most of them are imperfect

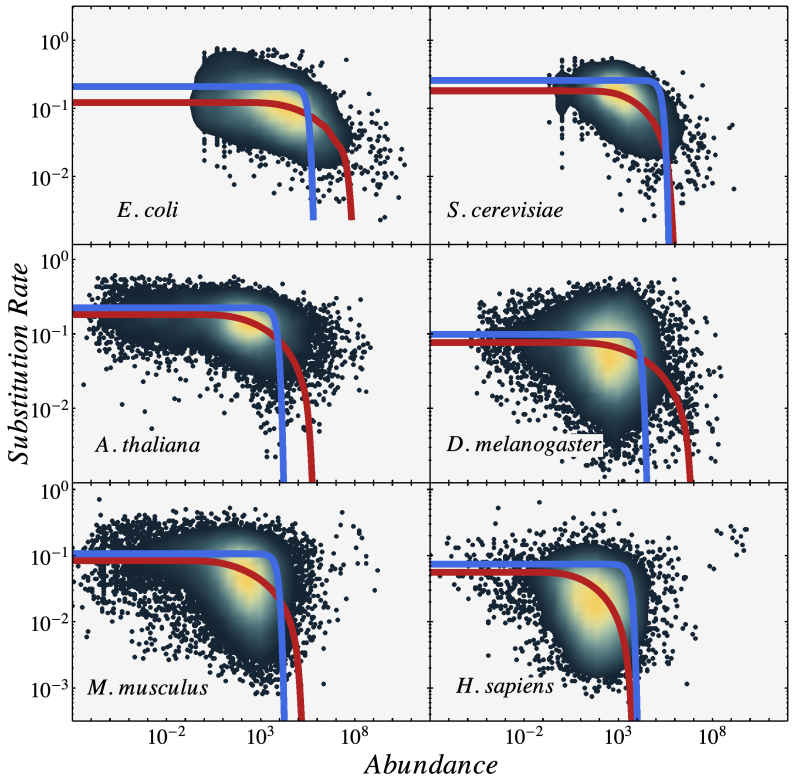


**Figure 7. Expression-Rate anti-correlation: abundant proteins evolve more slowly.** Experiments (dots and density plot) on different proteins in 6 organisms, from [45]. (Red) Misfolding model, $V \sim A$. (Blue) Aggregation model, $V \sim A^2$. The curve parameters are given in Table 1. Both misfolding and aggregation models are consistent with the data.

and not maximally stable. So, increasing the abundance manifests as increasing the concentration of imperfect proteins, which are not high-shouldered, leading to slower average substitution.

Fig. 8 explains the ER anticorrelation in terms of substitution rates. Here, we illustrate it, instead, on the fitness landscape. (1) The shape of the fitness landscape (see Fig 9) is given by Eq 42, where the mutation axis indicates proteins becoming increasingly unstable to folding due to increasing mutations, and the abundance axis indicates that the cell's overall fitness diminishes in proportion to the concentration of these unfit proteins. (2) For the same reason shown in Fig 6, evolution is faster along the bluescape than the orangescape contour in Fig 9. (3) Therefore, increasing abundance (i.e. moving from the bluescape line to the orangescape line in Fig 9) leads to slower substitution

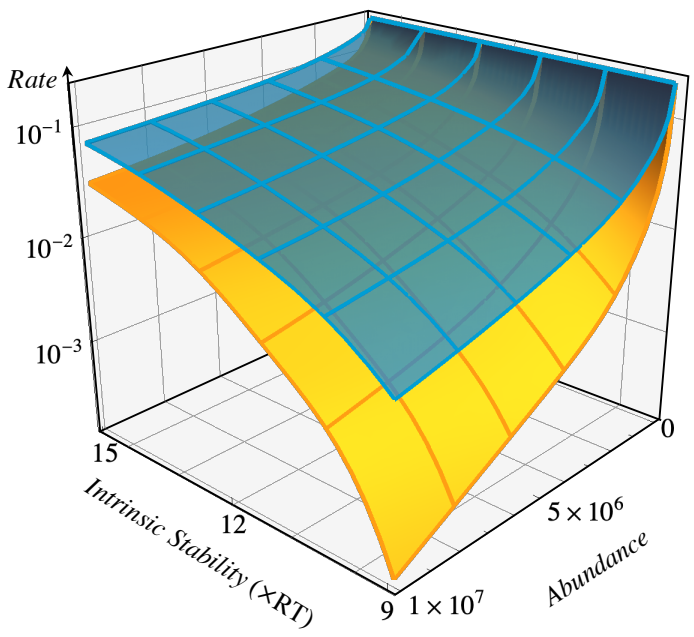


**Figure 8. (Yellow) Substitution is slower for proteins that are unstable or abundant. (Blue) Chaperones increase all the evolution rates.** (Yellow surface, proteins alone) Mutating a stable protein is usually adaptive because the protein can tolerate it. Less-stable proteins are less tolerant of mutations, so their substitution rates are lower. Since most proteins are imperfect, increasing the average abundance decreases cell fitness, leading to a lower substitution rates. (Blue surface, with chaperones). Chaperones raise the evolution rates of client proteins overall because they raise their tolerance to mutations.

rates. (The example in this figure is for the misfolding mechanism, but the same general features apply to the aggregation mechanism.) One general point is that because folding rate is so universally anticorrelated with abundance, across a broad range of proteins, it suggests that the physical misfolding and aggregation properties may be more generally relevant to sequence evolution than the biological mechanisms, that differ from one protein to another.

## 1.11 Chaperones are evolutionary accelerators

The speed of cell evolution is modulated by chaperones in the cell. Chaperones are biomolecular complexes that help other proteins (their *clients*) to fold.

| Organism | $\delta G/kT$ | $\delta\delta G/kT$ | Length | Vol ratio | $\lambda c_c$ | $\lambda c_s$ |
|---|---|---|---|---|---|---|
| *E. coli* | 1.8 | 1.8 | 20 | $2 \times 10^{-7}$ | 0.0008 | 0.000065 |
| *S. cerevisiae* | 1.1 | 1.1 | 22 | $3 \times 10^{-8}$ | 0.01 | 0.0009 |
| *A. thaliana* | 1.1 | 1.1 | 30 | $2 \times 10^{-8}$ | 1.1 | 1.1 |
| *D. melanogaster* | 0.9 | 0.9 | 35 | $1 \times 10^{-8}$ | 0.5 | 0.5 |
| *M. musculus* | 0.7 | 0.7 | 40 | $1 \times 10^{-7}$ | 20 | 20 |
| *H. sapiens* | 0.5 | 0.5 | 40 | $3 \times 10^{-7}$ | 20 | 20 |

**Table 1.** Parameters used for the curves in Fig. 7. Volume ratio and free energy per residue are not used as fitting parameters but taken from known experimental averages.

Experiments show that chaperones are generally evolution accelerators (they have been called *evolutionary capacitors*). That is, increasing a cell's chaperone concentrations can speed up the cell's evolution [20, 21, 23, 25, 26, 63].

What is the mechanism of evolutionary acceleration by chaperones? In the next section we develop a model for calculating the fitness landscape for proteins whose folding mechanism is mediated by interaction with two different type of chaperones.

### 1.11.1 How to account for the different effects of the different chaperones, DnaK and GroEl, on a client protein's evolution rate?

The misfolding avoidance hypothesis [14, 17, 45] can also be used to include the effect of chaperones in this model. Accordingly, the fitness is determined by the total number of unfolded proteins, assuming a 2 states dynamics for protein folding. However, a more realistic mechanism of protein folding has to be more complex [64]; the first modification which is needed to make the model more realistic is to consider the possibility that the protein will transition into a *misfolded* state (M), a local minimum of the free energy landscape which would make the protein non-functional and prone to aggregation. We therefore have 3 possible states M, U, N (misfolded, unfolded, native); a protein is synthesized in the unfolded state, but it does not stay for long in this state, given the energy minimum is away from this state. It either misfolds or folds correctly. When it is misfolded there is much more chance of aggregation, because many hydrophobic residues are exposed. We therefore modify the misfolding avoidance hypothesis considering this 3-states model, and the

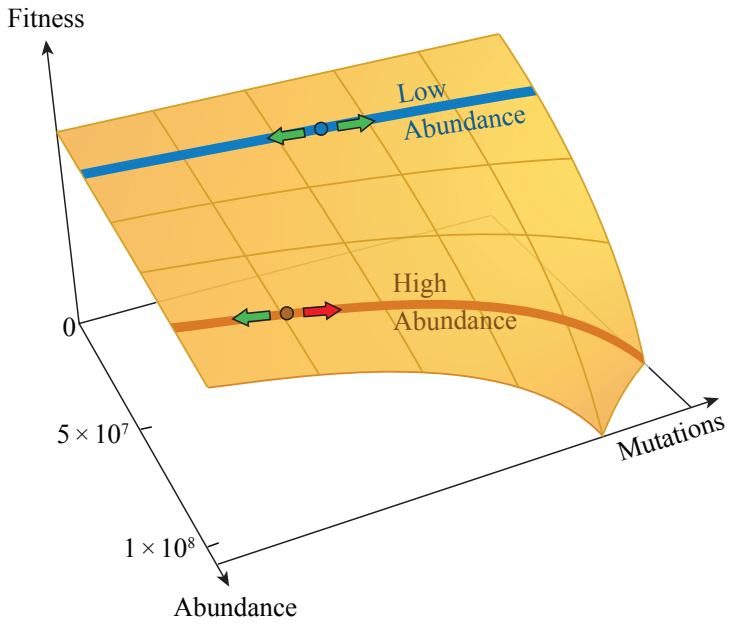


**Figure 9. Fitness landscape assuming stability only**. Increasing protein abundance changes the shape of the fitness landscape from big-shouldered (blue) to small-shouldered (orange), reducing the substitution rate for the reason explained above and expressed in Eq. 39.

fitness is taken to be proportional to the number of misfolded proteins M

$$f(\Delta G, \mathrm{C}) = e^{-c\,\mathrm{M}(\Delta G, \mathrm{C})} \tag{45}$$

where M is the number of misfolded proteins at steady state, $c$ the usual parameter for the misfolding avoidance hypothesis (see Eq. 28) and C is the chaperone concentration.

The role of chaperones in the cell is to prevent aggregation by binding to the misfolded proteins; the number of misfolded proteins at steady state is negatively correlated to the chaperones' concentration. Here we consider two models for protein-chaperone interaction, one for GroEl (G) and the other for DnaK (D). The main difference between the two chaperones is that after binding to the misfolded state, GroEl can release the protein either in the unfolded U state or in the native N state, whereas DnaK can only release in the U state, giving the protein a new chance to fold independently; they indeed belong to two different classes of chaperones called foldase (because it direcly helps folding) and holdase (because it just delays aggregation by "holding" the protein). Although this is a very minimal approximation of the

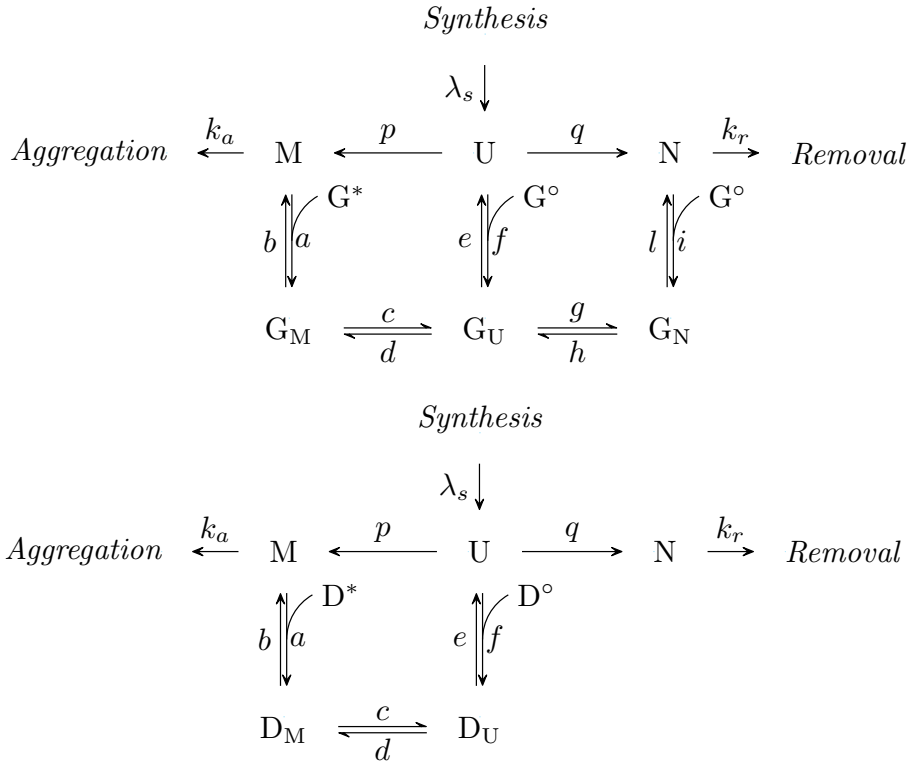


**Figure 10. The chaperone assisted protein folding model for GroEl (top) and DnaK (bottom).** The constants $a, b, c...$ are the folding/unfolding/binding rate constants and they can be expressed in terms of an activation energy. $C_X$ is the chaperone-protein complex (C can be G or D, X can be $M, U, N$).

true mechanism, it is able to capture the basic difference between the two form of chaperone-mediated folding.

Fig. 10 depicts the two models. Both models consider ATP aided folding: the chaperone-ATP complex ($G^*$ or $D^*$) binds to the M protein, ATP is used to unfold the protein and then the complex chaperone-ADP ($G^\circ$ or $D^\circ$) releases the protein in the new state (U or N).

We first consider GroEl. In order to find the number of misfolded proteins at steady state we need to solve the ODEs associated to the mechanism in Fig. 10 (top). First we consider the equations for $G_X$, where $X = M, U, N$ and solve them at steady state:

$$\begin{aligned}
\frac{d\mathrm{G_M}}{dt} &= a\mathrm{G^*M} - (b+c)\mathrm{G_M} + d\mathrm{G_U} = 0 \\
\frac{d\mathrm{G_U}}{dt} &= c\mathrm{G_M} - (d+e+g)\mathrm{G_U} + f\mathrm{G^\circ U} + h\mathrm{G_N} = 0 \\
\frac{d\mathrm{G_N}}{dt} &= g\mathrm{G_U} - (h+l)\mathrm{G_N} + i\mathrm{G^\circ N} = 0
\end{aligned} \tag{46}$$

Solving these equations at steady state, we can use the result to calculate M, U and N. For instance, the equation for M is given by

$$\frac{d\mathrm{M}}{dt} = p\mathrm{U} + b\mathrm{G_M} - a\mathrm{G^*M} - k_a\mathrm{M} \tag{47}$$

where $k_a$ is the aggregation rate. Replacing $\mathrm{G_M}$ with the solutions we found from the previous equations, we can write the latter equation in terms of some *effective rate constants* $\alpha_{\mathrm{XY}}$, which take into account the chaperone route for folding – unfolding (See Fig. 11):

$$\frac{d\mathrm{M}}{dt} = p\mathrm{U} - k_a\mathrm{M} - (\alpha_{\mathrm{MU}} + \alpha_{\mathrm{MN}})\mathrm{M} + \alpha_{\mathrm{UM}}\mathrm{U} + \alpha_{\mathrm{NM}}\mathrm{N} \tag{48}$$

Now we solve at steady state the equations for M,U and N and find all the constants

$$\begin{aligned}
\alpha_{\mathrm{UM}} &= \frac{bdf(h+l)\mathrm{G^\circ}}{ceh + b(d+e)h + c(e+g)l + b(d+e+g)l} \\
\alpha_{\mathrm{NM}} &= \frac{bdhin\mathrm{G^\circ}}{ceh + b(d+e)h + c(e+g)l + b(d+e+g)l} \\
\alpha_{\mathrm{MU}} &= \frac{eac(h+l)\mathrm{G^*}}{ceh + b(d+e)h + c(e+g)l + b(d+e+g)l} \\
\alpha_{\mathrm{NU}} &= \frac{ehi(b+c)\mathrm{G^\circ}}{ceh + b(d+e)h + c(e+g)l + b(d+e+g)l} \\
\alpha_{\mathrm{UN}} &= \frac{lfg(b+c)\mathrm{G^\circ}}{ceh + b(d+e)h + c(e+g)l + b(d+e+g)l} \\
\alpha_{\mathrm{MN}} &= \frac{lacg\mathrm{G^*}}{ceh + b(d+e)h + c(e+g)l + b(d+e+g)l}
\end{aligned} \tag{49}$$

to simplify the model we make 2 assumptions (see Fig. 11):

1. GroEl is extremely selective, it only binds to M: $i = 0$ and $f = 0$

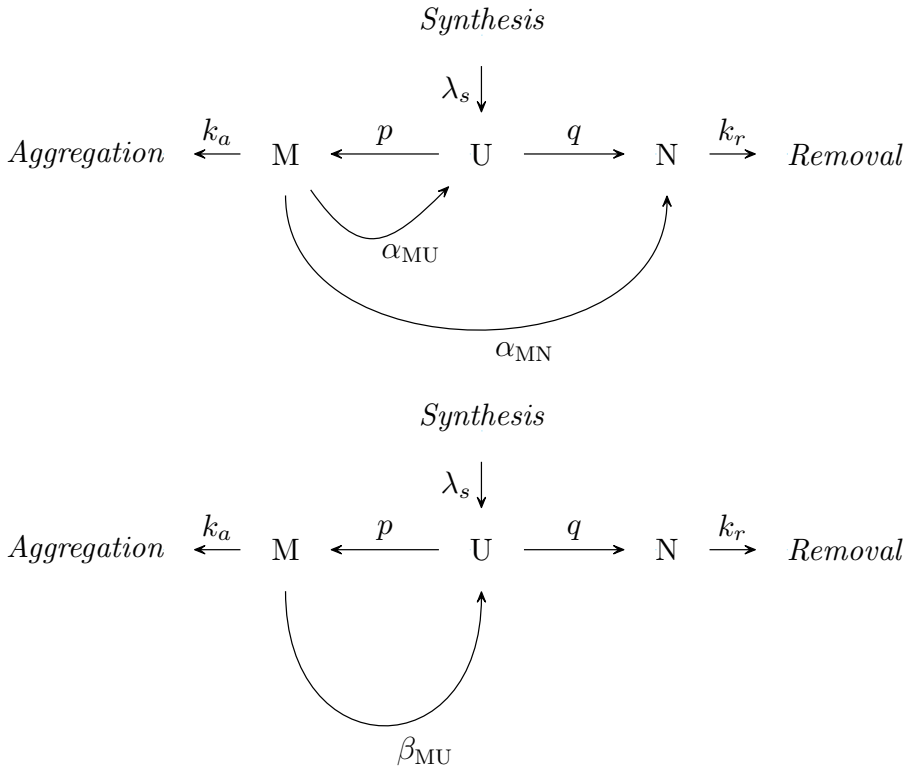


**Figure 11. Effective mechanism of protein chaperone interaction in term of the rate constants, for GroEl (top) and DnaK (bottom)**. The main difference between the two models is in the folding paths: GroEl can release the protein either in the U state or in the N state, whereas DnaK can only unfold it, giving it a second chance to fold independently.

2. GroEl is perfectly efficient, it never releases the protein in the M-state

in this way only 2 rate constants are non-zero (see Fig.11), and their expression is simplified

$$\begin{aligned} \alpha_{\mathrm{MU}} &= \frac{\sigma}{1+\sigma} a\mathrm{G}^* \\ \alpha_{\mathrm{MN}} &= \frac{1}{1+\sigma} a\mathrm{G}^* \end{aligned} \tag{50}$$

where

$$\sigma = \frac{e}{g}\left(1+\frac{h}{l}\right) \tag{51}$$

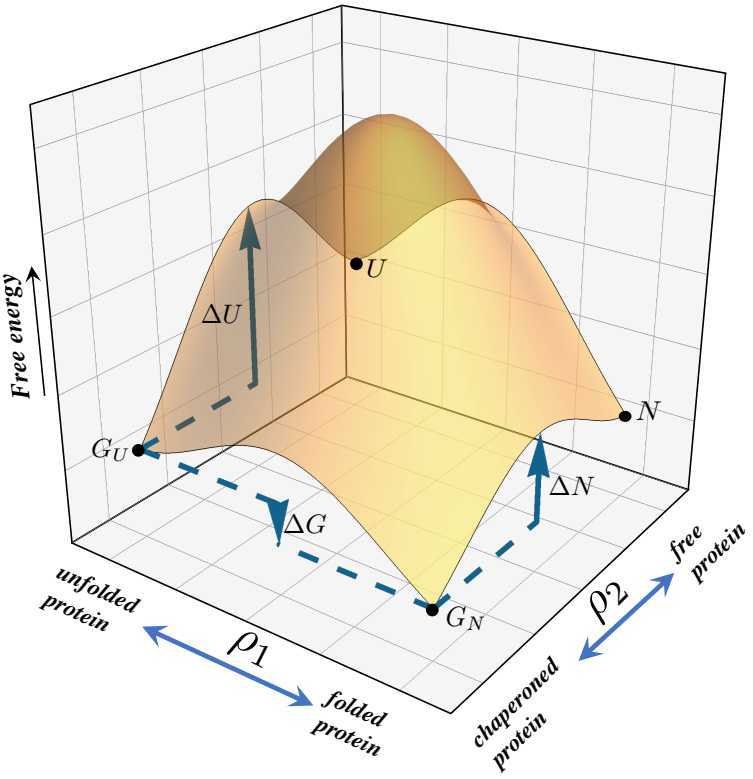


**Figure 12. A qualitative free energy landscape for the chaperone mediated protein folding.** Folding for a free protein vs a chaperoned protein follows different routes on the energy landscape, so the latter is more favorable than the former. $\rho_1$ and $\rho_2$ are reaction coordinates identifying folding and chaperone binding, respectively.

The ratios $e/g$ and $h/l$ can be expressed in terms of the activation energies. For the first, we can assume that folding inside the chaperone is much more convenient than releasing the protein in the unfolded state, therefore

$$\begin{aligned} \frac{e}{g} &\approx \exp\left[\frac{\Delta UN - \Delta U}{RT}\right] \\ \frac{h}{l} &\approx \exp\left[\frac{\Delta N - \Delta NU}{RT}\right] \end{aligned} \tag{52}$$

where $\Delta U$ and $\Delta N$ are the barriers for release of the protein in the U and N states, respectively, and $\Delta UN - \Delta NU = \Delta G < 0$ is the folding energy. Fig 12 qualitatively depicts how these energy differences are defined.

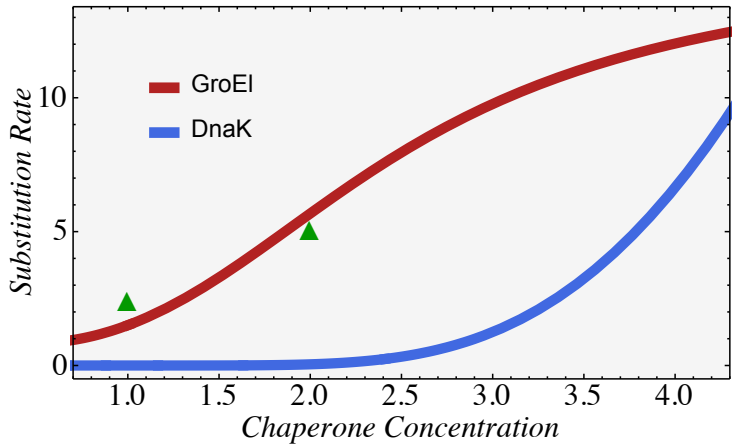


**Figure 13. Increasing chaperone concentration increases a client protein's evolution rate.** Model calculations are given in SI, based on slightly different mechanisms for GroEl and DnaK; see Fig 10. The GroEl curve is computed from Eq. 55), with a 2X overexpression level, compared to experimental data of [21], shown with green triangles. Increases from DnaK are also observed in experiments [26].

We can assume that there is no preference in the release of the protein, whether in the U or in the N state, therefore $\Delta U \approx \Delta N$. We also assume that $\exp(\Delta U/RT)$ is of order 1, so that

$$\sigma \approx \exp\left[\frac{\Delta UN}{RT}\right] + \exp\left[\frac{\Delta G}{RT}\right] \approx 1 + \exp\left[\frac{\Delta G}{RT}\right] \tag{53}$$

if we also assume that folding inside the chaperone is extremely favorable. In this way Eq. (50) becomes

$$\begin{aligned} \alpha_{\mathrm{MU}} &= \frac{1+\exp\left[\Delta G/RT\right]}{2+\exp\left[\Delta G/RT\right]} a\mathrm{G}^* \\ \alpha_{\mathrm{MN}} &= \frac{1}{2+\exp\left[\Delta G/RT\right]} a\mathrm{G}^* \end{aligned} \tag{54}$$

Now the entire model depends upon 3 measurable parameters: the GroEl–misfolded protein binding rate $a$, the GroEl concentration $\mathrm{G}^*$ and the chaperone assisted folding energy (naturally smaller than the free one) $\Delta G$. We can proceed now to calculate the fitness by solving the steady state equation for M and using Eq. (45). We therefore solve the system of linear equations

derived from Eq. (48) and the correspondent ones for U and N at steady state, leading, after some further approximations, to

$$\mathrm{M_{GroEl}} \approx \frac{A}{1+\gamma \mathrm{G}/(\mathrm{G_0}(1+\sigma))} \tag{55}$$

where we introduced the protein abundance $A$ by enforcing mass conservation $\mathrm{M+U+N} = A$ and introduced a chaperone's concentration parameter $\mathrm{G_0}$ (corresponding to the concentration in normal conditions) and $\gamma = a\mathrm{G_0}/k_r$, is the ratio between the protein-GroEl binding rate in normal conditions (i.e. at $\mathrm{G} = \mathrm{G_0}$) and the protein removal rate $k_r$, which is proportional to the overall growth rate of the cell.

At this point we have all we need to calculate the average amino-acid substitution rate with the same method used in the main text, using Eq. (39), calculating the folding energy $\Delta G$ using a lattice model (see Eq. 40). A similar analysis can be done to determine the effective rate constant $\beta_{\mathrm{MU}}$ for the DnaK assisted folding. We get

$$\mathrm{M_{DnaK}} \approx \frac{A}{1+\gamma \mathrm{D}\rho/\mathrm{D_0}} \tag{56}$$

where $\rho = \exp\left[-\Delta G/RT\right]$. We now use the two expressions (55) and (56) to calculate the average substitution rate as a function of the protein abundance A and the chaperone concentration (see Fig. 13, bottom row).

### 1.11.2 Results of the chaperone's mediation

The blue surface in Fig. 8 shows the effect of adding chaperones within the present model. Chaperones are active ATP-driven devices that shift the balance from misfolded and unfolded states to native states of client proteins, resulting in stabilizing the client proteins. And, according to theory above, more-stable proteins have terrains that are more high-shouldered, leading to faster amino acid substitution. Hence, chaperones accelerate evolution.[6]

Figure 13 shows the prediction that evolutionary acceleration can be different for different types of chaperones. The model predicts that GroEl is effective at lower concentrations, and on a different set of client proteins, than DnaK. Why the difference in chaperone concentrations? In short, clients of GroEl see only an unstable U and stable N state, so those clients mostly fold. In contrast, clients of DnaK mostly see an M state that is almost as stable as

[6] A subtle point is that while chaperones accelerate *substitution,* they can slow down *adaptation,* since chaperones can make 'near-perfect' proteins appear perfect to the cell. Such near-perfect proteins have no selective disadvantage in cells with chaperones.

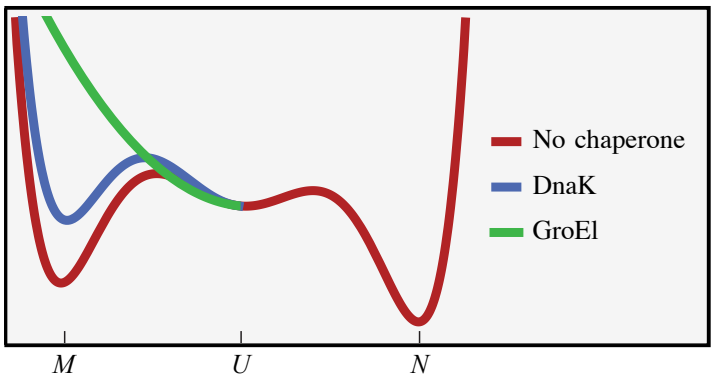


**Figure 14. How client protein folding energy landscapes are affected by different chaperones.** With no chaperone (red), native (N) and misfolded (M) states of the client are populated. Chaperones serve different client proteins, but they also act differently. GroEl (green) stabilizes and populates N. DnaK is less effective at promoting N relative to M than GroEl is, so Dnak is less effective at increasing substitution rates.

N, so more chaperone is needed to produce more N. This is reflected in the way the free energy landscape is modified when a protein interacts with different types of chaperones [64], as showed in Fig. 14. That's why GroEl and DnaK should have different values of 'evolutionary capacitance'.

## 1.12 Conclusions

We model here how rates of protein evolution depend on folding and aggregation properties. The present model gives a single framework for understanding disparate observations. (1) *Adaptation speed* depends on the slope of a fitness landscape. This depends strongly on selection pressures. It is fastest for the least-stably folded proteins. Cells that are shifted to warm climates become unstable, so they adapt rapidly. (2) *Substitution speed* depends on how "high-shouldered" is the terrain of a fitness potential. Abundant proteins evolve slowly. This is because most proteins are not perfectly stable, so increasing their abundance, shifts the cell to non-high-shouldered terrains of fitness, leading to slow substitution. (3) This effect is mitigated by chaperones, which increase protein stabilities, increasing their substitution rates. This modeling describes how protein evolution rates depend on their folding and aggregation properties.

# Chapter 2

# Maximum Caliber for Dissipative Systems

In this chapter we switch our attention to the dynamical version of the Maximum Entropy Principle, hence Max Cal.

As we mentioned in the introductory section, Max Cal begins with a model of the accessible trajectories, $X = \{\xi(t_0), \xi(t_1), \xi(t_2)...\}$ of values $\xi$ at different times $t$. Max Cal infers the probability $P(X)$ of observing trajectory $X$ within trajectory space $\{X\}$ by maximizing the path entropy, which for a continuous set of trajectories would be written as

$$S_{\text{path}} = -\int dX\ P(X) \log \frac{P(X)}{g(X)}, \tag{57}$$

where the function $g(X)$ is some reference/prior distribution in the absence of constraints. Now, in the simple situation of non-dissipative dynamics of a single dynamical quantity $J(X)$, for which the average,

$$\langle J \rangle = \int dX\ P(X) J(X) \tag{58}$$

is known, the trajectory populations are obtained using the method of Lagrange Multipliers [10, 11].

Here we want to address some potential controversies which might arise when Max Cal is applied to dissipative systems whose currents have specific symmetries under time reversal and space reflection and show that, contrarily to what it might be argued, the results are consistent with the physics of the problem when the right set of constraints are applied.

## 2.1 Dissipative dynamics requires more constraints

Two recent papers [65, 66] assert that Max Cal will fail in some cases. Jack and Evans (JE) [65] assert that Max Cal does not deal with dissipative systems, and Maes (M) [66] asserts that Max Cal does not handle cases of a time-asymmetric component in one of the constraints. Here we make use of the reasonable concerns that these argument arise to show that these are not problems of the principle of Maximum Caliber; these result from an application of the wrong constraints. When proper constraints are applied, Maximum Caliber handles these situations properly.

We first address the JE situation. Consider a dissipative system where a current $J(X)$ flows in conjunction with some finite amount of heat flow $\delta q(X)$ out of the system. Assume that the statistical ensemble of all trajectories contains also those trajectories that are related to each other through a time-reversal transformation $\mathbb{T}$ and a space-reflection transformation $\mathbb{P}$ (it can also refer to reflection along only one of the physical coordinates [65]). For the right choice of current-generating force, the resulting current will always be antisymmetric under both time reversal and space-reflection transformations, so we assume that the forces acting on the system are of this type (an example is a shear stress, which generates a current with such property). As a consequence, under a combined $\mathbb{PT}$ transformation, the current will be identical to the untransformed current [65].

Now consider the heat and work transferrence between the system and the external bath. This will be antisymmetric under time reversal: running time backwards would reverse all three: the flow, the work, and the heat along the trajectory. But, it will be invariant under space reflection. No matter whether a force drives a current in a forward or backward direction along a trajectory, an identical amount of heat will be dissipated. This is not an assertion of reversibility of heat transfer; that would violate the Second Law of thermodynamics. We are considering only a single non-equilibrium trajectory here, not a Second Law average over all trajectories. Rather, it just means that if a trajectory entails heat flowing into the system, its time-reversed trajectory entails heat flowing out. As an example, consider a particle with mass $m$ sliding on a surface with friction coefficient $\phi$ and initial velocity $v$. The total energy dissipated through the process of slowing down until stopping is equal to the total kinetic energy $E_k = 1/2mv^2$ of the particle, which will increase the temperature of the surface by $\Delta T = E_k/C$, where $C$ is the surface's heat capacity. The time-reversed process would be the following: heating up the surface by exactly $\Delta T$ and wait for the thermal energy to spontaneously transform back into kinetic energy, accelerating the particle back to velocity

$v$. This reverse process is extremely unlikely. We illustrate a calculation of this probability in Max Cal below, and at the end of this chapter we will show its relevance in the context of molecular motors.

In general, for a dissipative system, a trajectory $X$ will have some current flow $J(X)$, in which some work $\delta w(X)$ is done on the system and the system dissipates some heat $\delta q(X)$. The $\mathbb{PT}$-reversed trajectory, $\mathbb{PT}X$, would have heat $\delta q(\mathbb{PT}X) = -\delta q(X)$ going into the system and work $\delta w(\mathbb{PT}X) = -\delta w(X)$ done on the external environment, because a space reflection transformation does not change the heat/work flow, but time reversal does. The probability of the trajectory $\mathbb{PT}X$ should be much lower than of $X$ for macroscopic currents, although we know from fluctuation theorems that for very small currents they can become comparable [67, 68]. The result below agrees with such predictions.

For a dissipative steady state (DSS) the internal energy is unchanging, $\Delta U = \delta w + \delta q$, because in steady state, the heat out must equal the work in[7].

The argument of Jack and Evans is straightforward [65]. First, they correctly note that if the only constraint is on $\langle J(X)\rangle$

$$\langle J(X)\rangle = \int dX\, P(X) J(X) \tag{59}$$

then maximizing the Caliber (i.e. the path entropy subject to the constraint) gives the following probability of trajectory $X$:

$$P(X) = \frac{e^{\mu J(X)}}{Z(\mu)}, \tag{60}$$

where $Z(\mu) = \int dX e^{\mu J(X)}$ is the sum of weights over all paths. Second, since the flux is $\mathbb{PT}$ invariant, substitution of $J(X) = J(\mathbb{PT}X)$ into Eq 60 gives the result that the probabilities must be $\mathbb{PT}$ invariant,

$$P(\mathbb{PT}X) = P(X). \tag{61}$$

JE argue that such systems are not dissipative, because $\langle \delta q\rangle = 0$, which they show as follows:

$$\begin{aligned} \langle \delta q\rangle &= \int dX P(X)\delta q(X) \\ &= 1/2 \int dX\, (P(X)\delta q(X) + P(\mathbb{PT}X)\delta q(\mathbb{PT}X)) \\ &= 1/2 \int dX P(X)(\delta q(X) - \delta q(X)) = 0, \end{aligned} \tag{62}$$

[7]Note, in our convention energy going into the system is positively defined.

where the second line is obtained by considering that the Jacobian of a $\mathbb{PT}$ transformation equals 1.

JE conclude from this, incorrectly, that Maximum Caliber cannot handle systems, such as a sheared fluid, that are dissipative. On the contrary, we show here that the problem above is the use of only a single constraint, namely $\langle J(X)\rangle$. This misses the essentiality of the coupling of the flow $J$ to the heat and work exchange into the process, which require additional constraints.

## 2.2 The number of constraints must at least equal the number of independent flow variables

To illuminate the problem, consider the corresponding situation in equilibrium thermodynamics. The equilibrium entropy can be expressed as a function $S = S(U, V, N)$ of three independent extensive variables – energy, volume and particle number. If all three independent variables are free to change in a process, you cannot adequately specify the state of the system with only a single Lagrange multiplier, say the pressure $p$; you must also specify the temperature $T$ and chemical potential $\mu$. You need a Lagrange multiplier for every independent variable.

In dissipative dynamical systems too, there are multiple independent variables. You can specify an average flow rate $\langle J\rangle$, but dissipative systems also entail heat and work flows in and out, and those can affect the trajectory distribution. For example, you can achieve a given average particle flow rate in multiple ways, such as increasing the work done on the particle in a medium of increasing viscosity that dissipates more heat. Predicting the trajectory distribution in dissipative systems requires knowing the heat and work rates, not just the particle flow rate.[8]

For example, consider particles flowing along the axis of a tube, with an average current of $\langle J(X)\rangle = J$. That particle flow can be independent of the rate of work flow $\langle J_w(X)\rangle$ and heat flow $\langle J_q(X)\rangle$ into and out of the tube; for instance, if the viscosity is free to change the relation between the flow and the applied work would change as well. Some situations will reduce these 3 variables to fewer; other situations will not.

First, consider any steady-state flow, dissipative or not. By definition, the total internal energy will be unchanging with time, $\Delta U = 0$. So, it follows from the First Law that

[8]Note, however, that while $(U, V, N)$ are conserved quantities in the equilibrium metaphor, $J_q$ and $J_w$ are not necessarily conserved in flow situations. In the next chapter we will consider cases in which flows are conserved quantities.

$$\delta q = -\delta w. \tag{63}$$

Thus, in steady-state flows, the heat current must equal the work current,

$$\langle J_q(X)\rangle = -\langle J_w(X)\rangle \tag{64}$$

where our convention is that current flows into the system are defined as positive.

Now, in a non-dissipative steady state (nDSS), we have $\langle J_q(X)\rangle = -\langle J_w(X)\rangle = 0$, leaving us only one independent variable, $J$. However, in a dissipative steady state (DSS), energy must continuously enter the system in order to sustain the current $J$, so now we have 3 constraints,

$$\begin{aligned} \langle J(X)\rangle &= J & (65)\\ \langle J_w(X) + J_q(X)\rangle &= 0 & (66)\\ \tfrac{1}{2}\langle J_w(X) - J_q(X)\rangle &= J_{\rm E} & (67) \end{aligned}$$

where $J_{\rm E}$ is the energy influx rate.

Specifying a dissipative steady-state system requires specifying three independent currents. The flaw in the JE argument is their assumption that a dissipative system can be modeled by specifying only $\langle J\rangle$, which carries the implicit assumption that $J_{\rm E} = 0$. At steady state, only non-dissipative systems can be described when only a single constraint, $\langle J\rangle$, is specified.

## 2.3 For dissipative steady-states, Maximum Caliber requires at least 3 constraints.

For DSS situations with the 3 constraints above, the expression for Caliber is:

$$\begin{aligned} \mathcal{C} = & - \int dX P(X)\ln P(X) - \alpha\left(\int dX P(X) - 1\right) & (68)\\ & - \mu\left(\int dX P(X) J(X) - J\right) & (69)\\ & - \nu\left(\int dX P(X) J_w(X) - J_{\rm E}\right) & (70)\\ & - \lambda\left(\int dX P(X) J_q(X) + J_{\rm E}\right) & (71) \end{aligned}$$

where we chose here, for simplicity, to define each current individually instead of constraining the sum and the difference. Maximizing Caliber gives the trajectory probabilities as

$$P(X) = \frac{e^{\mu J(X)+\nu J_w(X)+\lambda J_q(X)}}{Z(\mu,\nu,\lambda)} \tag{72}$$

where $Z = \int dX\, e^{\mu J(X)+\nu J_w(X)+\lambda J_q(X)}$.

This Max Cal formulation shows that reverse trajectories in dissipative processes are unlikely for large currents. Using the $\mathbb{PT}$ transformation, we can calculate the relative probability that a system would absorb heat from the environment (and produce work):

$$\frac{P(\mathbb{PT}X)}{P(X)} = e^{-2(\nu J_w(X)+\lambda J_q(X))}. \tag{73}$$

This fluctuation relation shows that 'wrong-way' paths, which take up heat in dissipative flows, become exponentially improbable with increasing current, as they should. If the only constraint here were on $\langle J\rangle$, as in JE, then $\langle J_q\rangle = \langle J_w\rangle = 0$ and wrong-way flows would be predicted to be much more probable.

The Max Cal procedure gives the distribution of all the trajectories. On the one hand, it uses as an input constraint, the heat uptake $J_q(X)$ averaged over all the trajectories:

$$\langle \delta q\rangle = \langle J_q\rangle\, \Delta t = \Delta t \int dX\, P(X) J_q(X). \tag{74}$$

On the other hand, Max Cal then gives as a prediction the higher moments, such as the mean-square fluctuations of the heat:

$$\left\langle \delta q^2\right\rangle = \Delta t^2 \int dX\, J_q^2(X) P(X). \tag{75}$$

This reflects a deeper aspect of statistical mechanics which applies to equilibrium systems as well. When a macroscopic quantity is used to define a system, temperature for the Canonical Ensemble, there is no predicting power for the related measurable, hence average energy: Determining the first or the second is equivalent. In fact, Max Ent shows this from a mathematical perspective; the Lagrange multiplier (inverse temperature) is just a fictitious quantity used to constrain the actual measurable (average energy), so in a way is just an alternative way of expressing the measurable itself. On the contrary, fluctuations of the average energy are predictable quantities.

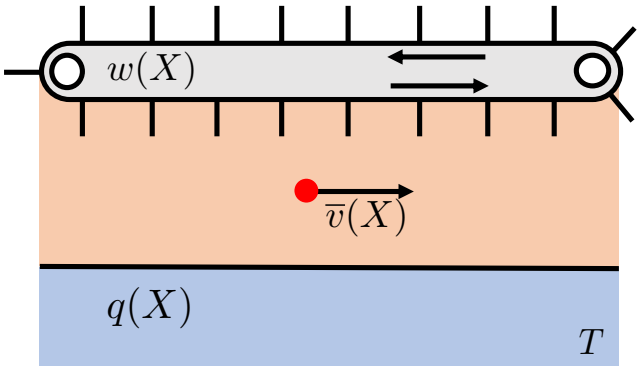


**Figure 15. A particle in a dissipative system.** The particle can receive energy from the belt or from the thermal bath, but it can also transmit energy to the belt by hitting it or to the thermal bath, by friction on the walls of the conduit.

## 2.4 A solvable model of a dissipative system: a particle in 1-dimensional flow, with heat and work.

In this section, we illustrate with a concrete model. Consider one particle moving along inside a 1D conduit. The particle is in contact with a thermal bath with which it can exchange heat. The particle can also interact with a conveyor belt that performs work to boost the particle's velocity; see Fig. 15.

A trajectory $X$ is a series of $N$ steps, each one of which takes time $\Delta t$. In each time step, the particle experiences one of three possibilities: (i) it increases or decreases its velocity by $\Delta v$, by collision with the belt, (ii) it increases or decreases its velocity by $\Delta u$ by exchanging heat with the bath, or (iii) it undergoes no change in velocity in that time step. A full trajectory is a string of such states: up, up, stay, up, down, up, .... for example. The quantities $\Delta v$ and $\Delta u$ are not limited to a fixed value, but can be anything within a given range.

The trajectory for a given particle has three identifying quantities. The average velocity of the particle along the trajectory $\overline{v}(X)$, the work done on the particle by the belt $w(X)$ and the heat absorbed by the particle from the thermal bath $q(X)$. As a convenient convention, we take both $w(X)$ and $q(X)$ to be positive when the energy flows from the external environment to the particle, so for the work, this convention is the opposite with respect to the one used in thermodynamics. Note that for the average velocity of a given trajectory $\overline{v}(X)$ we have used the overbar symbol to distinguish it from a trajectory-ensemble average; $\overline{v}(X)$ is just the average velocity maintained by

the particle in a specific trajectory, whereas we would use the symbol $\langle \overline{v}(X) \rangle \equiv \sum P(X)\overline{v}(X)$ to refer to the trajectory-ensemble average, hence averaged over all the possible trajectories.

This allows us to enforce some minimal constraints which identify a DSS without ambiguity. The constraints are the following:

$$\langle w(X) \rangle = E_{\text{in}} \tag{76}$$
$$\langle q(X) \rangle = -E_{\text{in}} \tag{77}$$
$$\langle \overline{v}(X) \rangle = V \tag{78}$$

where $E_{\text{in}}$ is the average work input (or negative heat output).

The particle starts at time $t = 0$ with velocity $v_0$. So, a given trajectory $X$ can be specified by an initial velocity and a sequence of changes in velocities:

$$X = \{v_0, \xi_1, \xi_2, ..., \xi_{N-1}\} \tag{79}$$

where $\xi_j = \Delta v_j$ or $\Delta u_j$, where $j$ is an index of the time step, depending on which processes occurred along the given trajectory. Now, Maximum Caliber gives the probability of a given DSS trajectory as

$$P(X) = P(v_0, \xi_1, \xi_2, ..., \xi_{N-1}) = \frac{e^{\nu w(X) + \lambda q(X) + \mu \overline{v}(X)}}{Z} \tag{80}$$

All the functions $w(X)$, $q(X)$ and $\overline{v}(X)$ can be expressed in terms of the particular sequence of velocity changes in trajectory $X$.

Now, under a $\mathbb{PT}$ transformation, each trajectory function is transformed as follows:

$$w(\mathbb{PT}X) = -w(X) \tag{81}$$
$$q(\mathbb{PT}X) = -q(X) \tag{82}$$
$$\overline{v}(\mathbb{PT}X) = \overline{v}(X). \tag{83}$$

This is because both heat and work are invariant under space reflection, but are anti-symmetric under time reversal. Therefore, the ratio between the $\mathbb{PT}$-transformed and untransformed trajectory is

$$\frac{P(\mathbb{PT}X)}{P(X)} = e^{-2[\nu w(X) + \lambda q(X)]} \tag{84}$$

which does not equal 1, except in the non-dissipative case that the trajectory does not involve any energy exchange[9].

For a general $N$-step process, the functional form is too complex for analytical solution, due to the non-linear relation between velocity and kinetic energy: the change in velocity at time step $n$ will depend upon all the changes in velocity at time steps $n-1$, $n-2$, ..., 0.

The partition function can be calculated numerically in that case, and the values of the Lagrange multipliers can be tuned to make sure that constraint averages are satisfied. In the next section we will show how to solve the problem analytically in an even simpler case.

### 2.4.1 Simplified trajectories with only 3 time steps

It is interesting to further simplify the model above to just 3 total time steps so that we can obtain a closed form expression. A trajectory is described by the vector

$$X = \{v_0, \xi_1, \xi_2\} \tag{85}$$

where $v_0$ is the initial velocity of the particle (first step), $\xi_1$ is the change in velocity in the second step and $\xi_2$ is the change in velocity in the third step. At steps 2 and 3, the velocity can either remain the same ($\xi_i = 0$) or change by interaction with the moving belt ($\xi_i = \Delta v_i$) or change by heat exchange ($\xi_i = \Delta u_i$); see Fig. 16. Again, the functional form of the probability is given by Eq. 80, but now just for the short-trajectories of Eq. 85.

The Max Cal dynamical partition function is obtained by computing the following sum over all the small number of trajectories $X$:

$$Z = \sum_X e^{\nu w(X) + \lambda q(X) + \mu \overline{v}(X)} \tag{86}$$

In order to correctly express the form of the sum in Eq. 86 we take into account the fact that at every step we are assuming that only one type of velocity change is possible, either heat driven or work driven.

The expression for the functions of the trajectory at the exponent for the

[9] In this case, the $\mathbb{PT}$-reversed trajectory must have identical probability, because it is the identical trajectory.

3-steps trajectory are

$$\overline{v}(X) = v_0 + \frac{2}{3}\xi_1 + \frac{1}{3}\xi_2 \tag{87}$$

$$\begin{aligned} w(X) &= m\xi_1 \left( v_0 + \frac{\xi_1}{2} \right) \delta(\xi_1 - \Delta v_1) \\ &+ m\xi_2 \left( v_0 + \xi_1 + \frac{\xi_2}{2} \right) \delta(\xi_2 - \Delta v_2) \end{aligned} \tag{88}$$

$$\begin{aligned} q(X) &= m\xi_1 \left( v_0 + \frac{\xi_1}{2} \right) \delta(\xi_1 - \Delta u_1) \\ &+ m\xi_2 \left( v_0 + \xi_1 + \frac{\xi_2}{2} \right) \delta(\xi_2 - \Delta u_2) \end{aligned} \tag{89}$$

where the Dirac delta functions assign the correct values to the specific process of energy transfer, whether it is heat or work exchange.

The partition function is therefore

$$Z = \int_{-V_{\max}}^{V_{\max}} dv_0 \int d\xi_1 d\xi_2 \times \tag{90}$$

$$\times \left( \int_{\Delta V_W}^{\Delta V_W} d\Delta v_1 \int_{\Delta V_W}^{\Delta V_W} d\Delta v_2 \; e^{\nu w(X) + \lambda q(X) + \mu \overline{v}(X)} \right. \tag{91}$$

$$+ \int_{\Delta V_W}^{\Delta V_W} d\Delta v_1 \int_{\Delta V_Q}^{\Delta V_Q} d\Delta u_2 \; e^{\nu w(X) + \lambda q(X) + \mu \overline{v}(X)} \tag{92}$$

$$+ \int_{\Delta V_Q}^{\Delta V_Q} d\Delta u_1 \int_{\Delta V_W}^{\Delta V_W} d\Delta v_2 \; e^{\nu w(X) + \lambda q(X) + \mu \overline{v}(X)} \tag{93}$$

$$\left. + \int_{\Delta V_Q}^{\Delta V_Q} d\Delta u_1 \int_{\Delta V_Q}^{\Delta V_Q} d\Delta u_2 \; e^{\nu w(X) + \lambda q(X) + \mu \overline{v}(X)} \right) \tag{94}$$

where the integrals over $\xi_i$ are only used to make use of the delta functions. The limits of integration correspond to the maximum velocities which are allowed by the physics of the system (for example, beyond such values the conduit will break down).

In the MaxCal procedure, the values of the three Lagrange multipliers $\mu, \nu, \lambda$ are unknown until measurements of the average velocity, work and heat are provided, and the following equations are then solved:

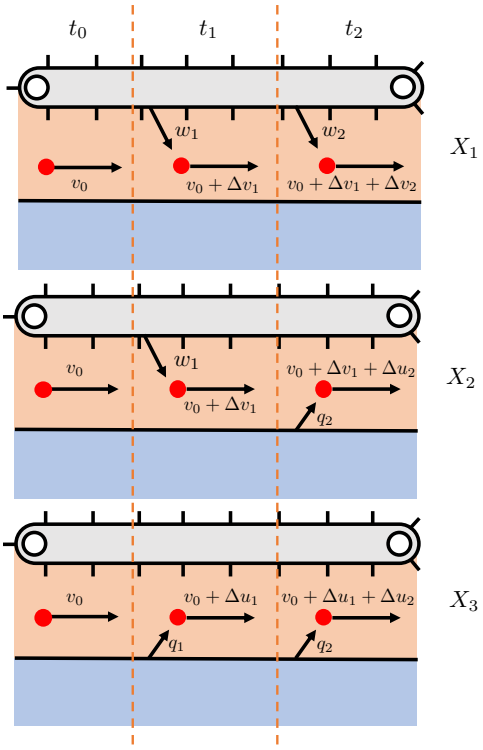


**Figure 16. Possible trajectories for the 3-step toy model.** $X_1 = \{v_0, \Delta v_1, \Delta v_2\}$ is a trajectory in which all the changes in velocity are due to work exchange (the sign of the change determines the direction of the work flow); $X_2 = \{v_0, \Delta v_1, \Delta u_2\}$ is the trajectory in which first there is exchange of work then heat; $X_3 = \{v_0, \Delta u_1, \Delta u_2\}$ is the trajectory in which there is only heat exchange. Other possible cases include a trajectory without changes and trajectory with more mixed exchanges.

$$V = \frac{\partial \ln Z}{\partial \mu} \tag{95}$$

$$E_{\text{in}} = \frac{\partial \ln Z}{\partial \nu} \tag{96}$$

$$-E_{\text{in}} = \frac{\partial \ln Z}{\partial \lambda}. \tag{97}$$

which are the same as Eqs. 76-78 but expressed in terms of the partition function.

From these, and after some approximations, we obtain the values of the Lagrange multipliers

$$\mu \simeq \frac{3\eta}{V} \tag{98}$$

$$\nu \simeq \frac{\epsilon}{2E_{\text{in}}} \tag{99}$$

$$\lambda \simeq -\frac{\epsilon}{2E_{\text{in}}} \tag{100}$$

where we have introduced the dimensionless parameters $\eta = V^2/V_{\text{max}}^2$ and $\epsilon = \Delta V_Q/\Delta V_W$ for convenience. $V_{\text{max}}$ is the maximum velocity that the conduit can withstand, $\Delta V_Q$ is the maximum change in velocity due to heat exchange and $\Delta V_W$ the one due to heat exchange.

In order to obtain this result, we have assumed that the measured velocity $V$ is much smaller than the maximum rate $V_{\text{max}}$, so $\eta << 1$; also we assumed that the maximum change in velocity due to work is much larger than the one due to heat, because work is always directed in a specific direction, so this means $\epsilon << 1$. Such assumptions, although not necessary to solve the problem, make it easier to obtain an analytical expression for the Lagrange multipliers.

The trajectory probabilities in this 3-step model is

$$P(X) = \frac{1}{Z} \exp\left\{ \epsilon \frac{w(X) - q(X)}{2E_{\text{in}}} + 3\eta \frac{\overline{v}(X)}{V} \right\} \tag{101}$$

Eq 101 computes the probability of any pathway $X$ in terms of the two observables, $E_{\text{in}}$ and $V$. Fig 17 shows an example of populations as a function of the trajectory functions $\overline{v}(X)$, $w(X)$ and $q(X)$ for fixed values of $V$, the particle flow velocity, and energy input $E_{\text{in}}$. The Max Cal result (blue plane) shows how the probability of a given trajectory is increasing when the average speed increases in the same direction of the measured velocity $V$. Also, it predicts that the probability is larger for the processes which have working going into the system and heat out ($w(X) - q(X) > 0$), and lower for the reverse processes ($w(X) - q(X) < 0$).

The orange plane is based on supposing that the only constraint in Max Cal derives from the observed particle flux alone, without knowing energy flux in or out, therefore it predicts the same probability for each process with different energy input/output.

From Eq 101, we can readily compute the ratio of probabilities for $\mathbb{PT}$-reversal:

$$\frac{P(\mathbb{PT}X)}{P(X)} \simeq e^{-2\epsilon \frac{w(X) - q(X)}{E_{\text{in}}}} \tag{102}$$

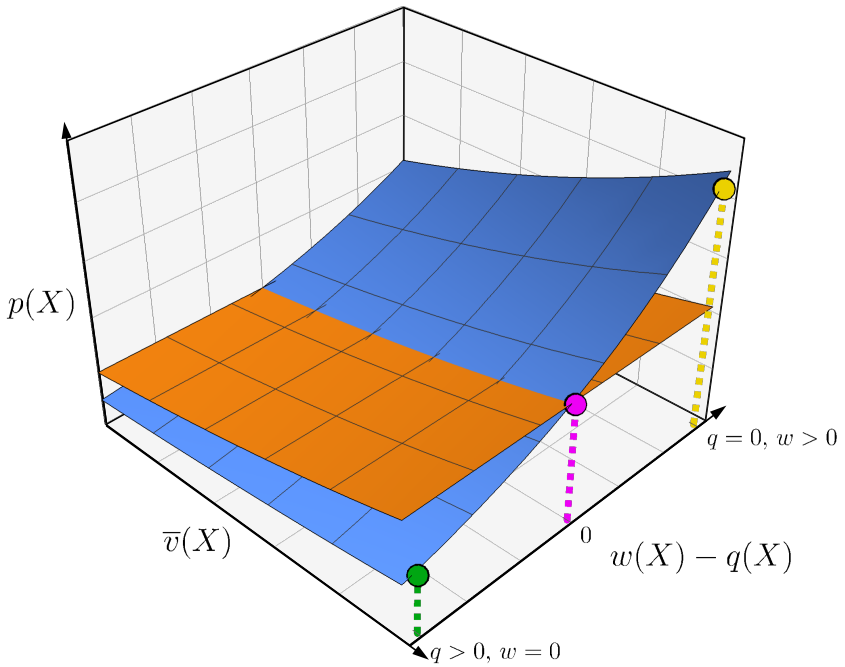


**Figure 17. The Max Cal probability distribution vs JE.** Using 3 constraints (blue plane) it is able to capture the difference between trajectories with different energy sources, which is not possible when only one constraint is used (orange plane). The coloured dots show the difference of the probability of three trajectory with the same average velocity but different energy source, as depicted in Fig. 18.

Eq 102 shows that for a given amount of energy that is put into the system, a trajectory with a large dissipative current is more likely than the $\mathbb{PT}$-reversed, non-dissipative one; at the same time, it correctly predicts that for small energy currents, the probability of a 2nd law-violating process is comparable to the opposite process.

In this way, Max Cal captures the difference between trajectories having the same average velocity but caused by very different processes. In Fig 18 we show three examples of trajectories, each with the same average velocity $v$ but with different values of $w$ and $q$. The first trajectory corresponds to the process in which the particle is hit twice by the belt; in the second the particle is hit first by the belt and then it receives energy from the thermal bath; in the third, the particle receives energy from the bath twice. If the process were non-dissipative, the three trajectories would have the same probability, but in this dissipative case, Max Cal shows how the probabilities are different

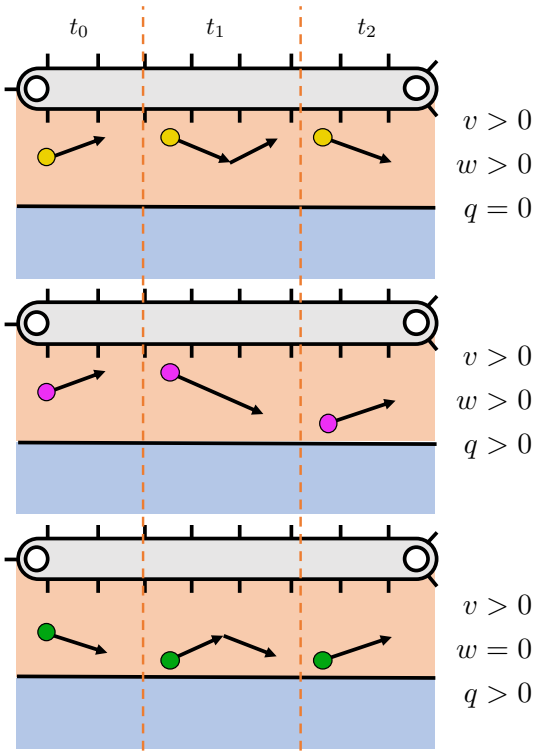


**Figure 18. Three possible trajectories for a single particle**. **Top:** The particle interacts in both steps with the conveyor belt, receiving energy as work; **Center:** The particle first receives work then heat from the thermal bath; **Bottom:** The particle only receives energy as heat from the thermal bath. In Fig. 17 the corresponding coloured dots with the respective probabilities.

(Fig 17).

## 2.5 The Maes Argument and the proper number of constraints

Maes argument [66] is a bit more subtle, because it points out the fact that when the only chosen constraints are time symmetric currents, the only possible outcome is a system without any dissipation. We agree in principle that this is the case, but with the caveat that this would be a problem with a poor choice of constraints, and not with Max Cal itself: when there is an extra knowledge of the system which is ignored, like work or heat transfer, (or in general what Maes calls a *frenetic* contribution [66]) it should not be surprising

that Max Cal will lead to inexact results. Once again, the criticism should be directed to a poor choice of constraints.

The example that seems to be of concern when we try to apply Max Cal is a system that exhibit some symmetry in a given regime and then such symmetry is broken in another regime.

Imagine a dynamical system at steady state which is macroscopically defined by some average current $J$. This time we assume that $J$ has an observed dependence upon some external parameter $\ell$: $J = J(\ell)$. An example could be a current which has some non-linear dependence upon an external stimulus, like an electric field, arbitrary far from equilibrium, so no linear approximation is allowed.

We also assume that there is some transformation in the system $\mathbb{R}$ for which the current has the same symmetry as the parameter, but only in a very specific regime of the parameter $\ell < L$:

$$\mathbb{R}\ell = \alpha\ell \tag{103}$$

$$\mathbb{R}J(\ell) = \alpha J(\ell)\theta(L-\ell) + J'(\ell)\theta(\ell - L) \tag{104}$$

$$j_\ell[\mathbb{R}\Gamma] = \alpha j_\ell[\Gamma]\theta(L-\ell) + j'_\ell[\Gamma]\theta(\ell - L) \tag{105}$$

Where $j_\ell[\Gamma]$ is the specific current for the trajectory $\Gamma$, which is itself parameter dependent, obviously, $\alpha = \pm$ for symmetric/anti-symmetric systems; $j'_\ell[\Gamma]$ and $J'(\ell)$ are the transformed microscopic and average currents outside the symmetry region $\ell < L$. $\theta(x)$ is the Heaviside step function.

We can imagine a current that increases with an electric field in a given range and then it starts decreasing when turbulence arises. With the proper choice of symmetries and at steady state this would correspond to the Maes' ideal system.

How do we apply Max Cal in this scenario? First of all, if the parameter is not allowed to change during the measurement the answer is simple: the caliber is calculated at a fixed value of the parameter and the inferred probability distribution is valid only at that specific value of the parameter. On the other hand, if the value of the parameter can arbitrarily change during the measurement, the Caliber cannot be parameter-dependent, because we need to account for all the possible trajectories and normalize the probability accordingly, irrespective of the value of the parameter. So we consider the system at steady state in this second scenario, so the caliber is

$$\mathcal{C} = \int d\Gamma p[\Gamma] \log \frac{p[\Gamma]}{q[\Gamma]} - \alpha \left( \int d\Gamma p[\Gamma] - 1 \right) - \int d\ell \beta(\ell) \left( \int d\Gamma p[\Gamma] j_\ell[\Gamma] - J(\ell) \right) \tag{106}$$

which is similar to what we obtain when the constraint is time-dependent, but this time we have a generic parameter $\ell$. So in a very similar way as for time-dependent systems we have

$$p[\Gamma] = \frac{q[\Gamma]}{Z} \exp\left[\int d\ell \beta(\ell) j_\ell[\Gamma]\right] \tag{107}$$

Now we can actually calculate the PT transformed current probability

$$\begin{aligned} p[\mathbb{P}\mathbb{T}\Gamma] &= \frac{q[\Gamma]}{Z} \exp\left[\int d\ell \beta(\ell) j_\ell[\mathbb{P}\mathbb{T}\Gamma]\right] & (108)\\ &= \frac{q[\Gamma]}{Z} \exp\left[\int d\ell \beta(\ell) \left(\alpha j_\ell[\Gamma]\theta(L-\ell) + j'_\ell[\Gamma]\theta(\ell - L)\right)\right] & (109)\\ &= \frac{q[\Gamma]}{Z} \exp\left[\alpha \int_{\ell<L} d\ell \beta(\ell) j_\ell[\Gamma] + \int_{\ell>L} d\ell \beta(\ell) j'_\ell[\Gamma]\right] & (110) \end{aligned}$$

Now we take the ratio

$$\frac{p[\mathbb{P}\mathbb{T}\Gamma]}{p[\Gamma]} = \exp\left[(\alpha - 1)\int_{\ell<L} d\ell \beta(\ell) j_\ell[\Gamma]\right] \exp\left[\int_{\ell>L} d\ell \beta(\ell)(j'_\ell[\Gamma] - j_\ell[\Gamma])\right] \tag{111}$$

If the current is symmetric $\alpha = 1$ in the entire allowed regime (basically $L \to \infty$) the system is non-dissipative, as we expected since we are assuming there is no dissipation (same argument as for Jack and Evans). However, if we observe that the current $J(\ell)$ is symmetric only in a very specific regime, the fluctuation relation has a non-trivial component due to the difference $j'_\ell[\Gamma] - j_\ell[\Gamma]$. In addition to this, for systems that we know to be dissipative, a single constraint is not sufficient, as we have seen in the previous section; as a consequence, the fluctuation relation would always contain some non-zero component which include the non-symmetric part of the current and the work/dissipation currents as well.

In the case of a simple DSS, we showed how adding two constraints on the total work and heat exchanged between the system and the external environment can give a more correct result. However, this does not mean that any non-equilibrium dissipative system can be sufficiently described with only 3 constraints, because it is possible that some other system can be designed for which some additional constraints are needed. Failure to account for that won't make Max Cal invalid as a whole, but only the particular choice of constraints.

## 2.6 Conclusions

We show here that dynamical pathways for dissipative steady-state flows are given correctly by the method of Maximum Caliber when supplied with appropriate restraints. You need to know not only the mean rate of flow, but also the work put in and the heat that is dissipated. Leaving out the latter types of energy flows is shown to be the flaw in previous arguments [65, 66]. We show this on general grounds, but in addition, we give a specific solvable model of a single particle flow subject to heat and work input and output. This toy model is a useful conceptual way to capture the relationship between flow velocities and dissipative quantities in a 1-dimensional toy case.

Current and future application of this results are shown for biologically relevant systems like molecular motors, which are actively driven system often at steady state, which require a constant energy input and consequent dissipation. Preliminary results reported in the appendix of this chapter show that the relative probability that a rotation is fully determined by thermal fluctuations depends only upon the enzymatic activity of the phosphorylation process. In the future we plan to extend the method by including the correct information about molecular motors, hence rotation rate and ATP consumption rate, in order to determine the probability distribution over trajectories as well as predict the fluctuations of dissipation and revolution rates.

# Chapter 3

# Maximum Caliber and conservation laws

In this concluding chapter we want to address this specific question: is there any physical system for which the necessary constraints can be known a priori, and are related to the physics of the problem? One of the possible limitations of the use of Max Cal is indeed the fact that there is not a general rule to determine which constraints to use; in the previous chapter we have shown a minimal condition in the case of DSS systems, here we consider cases in which the constraints can be determined from conservation laws.

We argue that when some dynamical currents are conserved they should be used as Max Cal constraints: in that case, in a similar way as or the Boltzmann distribution for systems which conserve energy, Max Cal can give insights on the probability distribution of the microtrajectories for non equilibrium systems.

## 3.1 Non equilibrium momentum ensemble

We consider a system with $\mathcal{N} \gg 1$ particles with mass $m$ which can exchange energy and momentum with each other. The total energy $E_{\text{tot}}$ is conserved, as is the momentum $\mathbf{P}_{\text{tot}}$, so there is no external forces acting on the system or dissipation to an external environment. Now we consider all the possible trajectories of one of such particles over a period of time $\tau$. A given single-particle trajectory can be represented by a velocity function $\mathbf{v}(t)$ over the time domain $(0, \tau)$. Within this period the particle can increase or decrease its velocity by interacting with the rest of $\mathcal{N} - 1$ particles, which act as an

external environment, but the average value of its energy and momentum is imposed by the overall conservation laws.

For a system like this, we can use Max Cal to determine the probability distribution over the trajectory ensemble $P([\mathbf{v}(t)])$ by maximizing the caliber

$$\begin{aligned}
\mathcal{C} = & - \int \mathcal{D}\mathbf{v}\ P([\mathbf{v}(t)]) \ln P([\mathbf{v}(t)]) - l_n \left( \int \mathcal{D}\mathbf{v}\ P([\mathbf{v}(t)]) - 1 \right) && (112) \\
& - l_E \left( \int \mathcal{D}\mathbf{v}\ \overline{E[\mathbf{v}(t)]} P([\mathbf{v}(t)]) - \frac{E_{\text{tot}}}{\mathcal{N}} \right) && (113) \\
& - \mathbf{l}_P \cdot \left( \int \mathcal{D}\mathbf{v}\ \overline{\mathbf{p}[\mathbf{v}(t)]} P([\mathbf{v}(t)]) - \frac{\mathbf{P}_{\text{tot}}}{\mathcal{N}} \right) && (114)
\end{aligned}$$

where $\mathcal{D}\mathbf{v}$ represents the functional integration over the trajectory space, and the overline represents the time average of a given quantity over the period $\tau$ (to be distinguished from the ensemble average we will introduce later in the text). The Lagrange multipliers are $l_n$, $l_E$ and $\mathbf{l}_P$ are needed to enforce normalization, average energy and average momentum, respectively.

To start, we consider the total energy and momentum fixed quantities, but we will show how to deal with systems for which they slowly change with time.

Maximizing the caliber with respect to the probability $P([\mathbf{v}(t)])$ we obtain the expression for the probability distribution

$$P([\mathbf{v}(t)]) = \frac{1}{\mathcal{Z}} \exp\left[ -l_E \overline{E[\mathbf{v}(t)]} - \mathbf{l}_P \cdot \overline{\mathbf{p}[\mathbf{v}(t)]} \right] \tag{115}$$

where $\mathcal{Z}$ is the partition function, which is the quantity we need to express as a function of the Lagrange multiplier in order to fully determine the problem:

$$\begin{aligned}
\mathcal{Z} &= \int \mathcal{D}\mathbf{v}\ \exp\left[ -l_E \overline{E[\mathbf{v}(t)]} - \mathbf{l}_P \cdot \overline{\mathbf{p}[\mathbf{v}(t)]} \right] && (116) \\
&= \int \mathcal{D}\mathbf{v}\ \exp\left[ -\int \frac{dt}{\tau} \left( l_E \frac{m}{2} v^2(t) + m \mathbf{l}_P \cdot \mathbf{v}(t) \right) \right] && (117)
\end{aligned}$$

In order to solve this integral we discretize the time interval $\tau$ in $N$ steps of size $\delta t \ll \tau$, so that we can express the functional integral in a simpler form:

$$\begin{aligned}
\mathcal{Z} &= \frac{1}{B(N)} \int d\mathbf{v}_1 d\mathbf{v}_2 ... d\mathbf{v}_N \exp\left[ -\sum_{i=1}^{N} \frac{\delta t}{\tau} \left( l_E \frac{m}{2} v_i^2 + m \mathbf{l}_P \cdot \mathbf{v}_i \right) \right] \\
&= \frac{1}{B(N)} \prod_{i=1}^{N} \left( \int d\mathbf{v}_i \exp\left[ -\frac{1}{N} \left( l_E \frac{m}{2} v_i^2 + m \mathbf{l}_P \cdot \mathbf{v}_i \right) \right] \right) && (118)
\end{aligned}$$

where we have used $N = \tau/\delta t$ and defined $\mathbf{v}_i \equiv \mathbf{v}(t_i)$; $B(N)$ is a combinatory factor needed to ensure that the correct counting is performed (for instance, if two trajectory with the same energy and momentum averages are considered indistinguishable, $B(N) = N!$, like Boltzmann correct counting). The last integral in Eq. 118 is a standard Gaussian integral with a known solution of the form

$$\mathcal{I} = \int d^3\mathbf{x} \exp\left[-\frac{1}{2}\mathbf{x}\cdot\mathrm{A}\cdot\mathbf{x} - \mathbf{J}\cdot\mathbf{x}\right] \tag{119}$$

$$= \sqrt{\frac{(2\pi)^3}{\det \mathrm{A}}} \exp\left(\frac{1}{2}\mathbf{J}\cdot\mathrm{A}^{-1}\cdot\mathbf{J}\right) \tag{120}$$

where A is a $3\times3$ matrix and $\mathbf{J}$ a 3-vector. The integral in Eq. 118 is equivalent to this with the following identifications

$$\mathrm{A} \equiv \frac{l_E m}{N} I_3 \tag{121}$$

$$\mathbf{J} = \frac{m}{N}\mathbf{l}_P \tag{122}$$

where $I_3$ is the identity, $3 \times 3$ matrix.

From this, we obtain for Eq. 118

$$\mathcal{Z} = \frac{1}{N!}\left(\frac{2\pi N}{m}\right)^{3N/2} \exp\left[\frac{m}{2}\frac{l_P^2}{l_E} - \frac{3N}{2}\ln l_E\right] \tag{123}$$

here we have introduced the following notation which we will use throughout this chapter for the norm of a vector quantity: $\|\mathbf{u}\| \equiv u$.

Now we can use the constraint equations to find the relation between the Lagrange multipliers $l_E$ and $\mathbf{l}_P$ and the physical measurements done on the system. Given the conservation laws we can assume that the path average value of each of the variables (energy and momentum) is just the overall value divided by the number of particles, so the constraint equations are

$$\frac{E_{\mathrm{tot}}}{\mathcal{N}} = -\frac{\partial \ln \mathcal{Z}}{\partial l_E} \tag{124}$$

$$\frac{\mathbf{P}_{\mathrm{tot}}}{\mathcal{N}} = -\nabla_{l_P} \ln \mathcal{Z} \tag{125}$$

which can be solved to find the Lagrange multipliers. For simplicity, we define the single particle average energy and momentum as $\epsilon \equiv E_{\mathrm{tot}}/\mathcal{N}$ and $\mathbf{p} \equiv \mathbf{P}_{\mathrm{tot}}/\mathcal{N}$, to obtain

$$l_E = \frac{3N/2}{\epsilon - \mathbf{p}^2/2m} \equiv \frac{N}{k_B\Theta} \tag{126}$$

$$\mathbf{l}_P = \frac{N}{k_B\Theta}\frac{\mathbf{p}}{m} \tag{127}$$

where $k_B$ is the Boltzmann constant and we have introduced the non-equilibrium temperature

$$\Theta \equiv \frac{\epsilon - \mathbf{p}^2/2m}{3k_B/2} \tag{128}$$

With these results we have the complete expression for the partition function

$$\mathcal{Z} = \frac{1}{N!}\left[\frac{2\pi k_B\Theta}{m}\exp\left(\frac{\mathbf{p}^2/2m}{k_B\Theta}\right)\right]^N \tag{129}$$

and the probability of a given trajectory with $N = \tau/\delta t$ steps

$$P([\mathbf{v}(t)|\tau]) = \frac{1}{\mathcal{Z}}\exp\left[-\frac{N}{k_B\Theta}\left(\overline{E[\mathbf{v}(t)]} - \mathbf{p}\cdot\overline{\mathbf{v}(t)}\right)\right] \tag{130}$$

This result is a correction to what is known as the Gibbs momentum ensemble, and it is valid arbitrary far from equilibrium for arbitrary long trajectories.

### 3.1.1 The equilibrium limit

It is interesting to observe what happens when we take the limit to equilibrium. Considering the number of steps in the trajectory $N$, we write the probability as single step probability:

$$P([\mathbf{v}(t)|\tau]) = P_1^N(\mathbf{v}(t)) \tag{131}$$

where

$$\begin{aligned} P_1(\mathbf{v}(t)) &= \frac{1}{\mathcal{Z}_1}\exp\left[-\frac{1}{k_B\Theta}\left(\overline{E[\mathbf{v}(t)]} - \mathbf{p}\cdot\overline{\mathbf{v}(t)}\right)\right] \\ \mathcal{Z}_1 &= \frac{2\pi k_B\Theta}{m}\exp\left(\frac{\mathbf{p}^2/2m}{k_B\Theta}\right) \end{aligned} \tag{132}$$

When the system reaches equilibrium, the measured single-particle average momentum goes to zero $\mathbf{p} \to 0$, so the non-equilibrium temperature becomes the actual temperature:

$$\Theta = \frac{\epsilon - \mathbf{p}^2/2m}{3k_B/2} \to \frac{\epsilon}{3k_B/2} = T \tag{133}$$

where the last step is obtained by using equipartition theorem in a 3D system. The single step partition function becomes the single-particle canonical partition function:

$$\mathcal{Z}_1 \to \frac{2\pi k_B T}{m} \equiv Q_1 \tag{134}$$

And finally, the trajectory average energy is simply the microstate energy, so the single step probability is equivalent to the Boltzmann distribution:

$$P_1(\mathbf{v}(t)) \to \frac{e^{-E_1/k_B T}}{Q_1} \tag{135}$$

## 3.2 Non-equilibrium Einstein Relation

In the context of equilibrium statistical physics, an important result is the relation between the diffusion constant entering the Fokker-Planck equation and the temperature of the system, known as *Einstein's relation* [69]; the relation states that the diffusion constant is directly proportional to the temperature:

$$D_{\text{eq}} = \mu k_B T \tag{136}$$

where $\mu$ is the mobility of the particles, namely the ratio of the terminal velocity of such particles to the applied force. It has been argued that in order for such relation to hold for non-equilibrium processes it is necessary to replace the temperature in this equation with an effective temperature [70–72]. However, the proposed replacement for such effective temperature is usually obtained from a re-definition of the diffusion constant, rather than from some independent measurable. On the contrary, we can show that, under the assumptions we mentioned above, our definition of effective temperature $\Theta$ is the right replacement to re-define the diffusion constant, giving an expression which is valid arbitrarily far from equilibrium:

$$D_{\text{non-eq}} = \mu k_B \Theta \tag{137}$$

We have already proved that $\Theta$ reduces to the absolute temperature if the system approaches equilibrium, so we just need to show that the diffusion constant can be written as in Eq. 137 when the system is not at equilibrium, hence when $\mathbf{p} \neq 0$.

The general expression for the diffusion constant is the following [70]

$$D = \lim_{\tau \to \infty} \frac{\langle \mathbf{x}^2(\tau) \rangle - \langle \mathbf{x}(\tau) \rangle^2}{2\tau} \tag{138}$$

We can calculate the path averages of $\mathbf{x}$ and $\mathbf{x}^2$ rather easily. First of all we consider a given trajectory of length $\tau = N\delta t$, $[\mathbf{v}] \equiv \{\mathbf{v}_1, \mathbf{v}_2, ..., \mathbf{v}_N\}$. The total displacement $\mathbf{x}(\tau)$ is therefore

$$\mathbf{x}(\tau) = \delta t(\mathbf{v}_1 + ... + \mathbf{v}_N) \tag{139}$$

where, without loss of generality, we have assumed that the starting position of the trajectory is the origin. It is straightforward to show that $\langle \mathbf{x} \rangle = \tau \frac{\mathbf{p}}{m}$, which is nothing but another form of the constraint equation. The quadratic term can be written as

$$\begin{aligned} \mathbf{x}^2(\tau) &= \delta t^2 \left(\mathbf{v}_1^2 + ... + \mathbf{v}_N^2\right) + 2\mathbf{v}_1 \cdot (\mathbf{v}_2 + ... + \mathbf{v}_N) + ... + 2\mathbf{v}_{N-1} \cdot \mathbf{v}_N \\ &= \delta t^2 \sum_{i=1}^{N} v_i^2 + 2 \sum_{i=1}^{N-1} \sum_{j=i+1}^{N} \mathcal{R}_{i,j} \end{aligned} \tag{140}$$

When calculating the average, the probability contains an exponential with the sum of $\mathbf{v}_i$-dependent quantities, so it factorizes in the product as in equation 118; for each of the element of the sum in equation (140) $\mathbf{v}_i \cdot \mathbf{v}_j$, there are $N - 2$ terms which can be taken out of the specific integral and they cancel out with the correspond term in the partition function at the denominator; therefore, we are left with the integrals in $\mathbf{v}_i$ and $\mathbf{v}_j$, and the average of the ratio is ratio

$$\langle \mathcal{R}_{i,j} \rangle = \frac{\int d^3\mathbf{v}_i d^3\mathbf{v}_j \mathbf{v}_i \cdot \mathbf{v}_j \exp\left[-\frac{1}{k_B\Theta}\left(\frac{m}{2}(\mathbf{v}_i^2 + \mathbf{v}_j^2) - \mathbf{p} \cdot (\mathbf{v}_i + \mathbf{v}_j)\right)\right]}{\int d^3\mathbf{v}_i d^3\mathbf{v}_j \exp\left[-\frac{1}{k_B\Theta}\left(\frac{m}{2}(\mathbf{v}_i^2 + \mathbf{v}_j^2) - \mathbf{p} \cdot (\mathbf{v}_i + \mathbf{v}_j)\right)\right]} \tag{141}$$

Since $\mathbf{v}_i$ and $\mathbf{v}_j$ are integrated variables, they can be arbitrarily renamed, so $\langle \mathcal{R}_{i,j} \rangle$ can be taken out of the summation symbols in equation 140. The summations then yield

$$\sum_{i=1}^{N-1} \sum_{j=i+1}^{N} 1 = \frac{N^2 - N}{2}. \tag{142}$$

The denominator is a simple Gaussian integral, which we have already solved in the first part of this chapter (see Eq. 120). For the numerator we write the

integrals in spherical coordinates, by taking $\mathbf{p}$ along the $z$ direction:

$$\begin{aligned}
\mathbf{v}_i &\equiv v(\sin\theta\cos\phi, \sin\theta\sin\phi, \cos\theta) && (143)\\
\mathbf{v}_j &\equiv u(\sin\alpha\cos\beta, \sin\alpha\sin\beta, \cos\alpha) && (144)\\
d^3\mathbf{v}_i &\equiv v^2 dv d\phi d\cos\theta && (145)\\
d^3\mathbf{v}_j &\equiv u^2 du d\beta d\cos\alpha && (146)
\end{aligned}$$

The internal product $\mathbf{v}_i \cdot \mathbf{v}_j$ gives the sum of three terms, but when integrated over the azimuthal angle $\phi$ the first two disappear because of the symmetry property of sin and cos functions. So the numerator factorizes in the product of two identical integrals $\mathcal{I}$, which are standard Gaussian integrals. The final result is therefore

$$\mathcal{R} = \left(\frac{\mathcal{I}}{\mathcal{Z}_1}\right)^2 = \frac{\mathbf{p}^2}{m^2} \tag{147}$$

Now we can input all these results into the expression for the mean square to obtain obtain

$$\begin{aligned}
\left\langle \mathbf{x}^2(\tau) \right\rangle &= \frac{2\epsilon}{m}\delta t^2 N + \frac{2}{\mathcal{Z}_1^2}\sum_{i=1}^{N-1}\sum_{j=i+1}^{N}\int d^3\mathbf{v}_i d^3\mathbf{v}_j \mathbf{v}_i\cdot\mathbf{v}_j && (148)\\
&\times \exp\left[-\frac{1}{k_B\Theta}\left(\frac{m}{2}(\mathbf{v}_i^2+\mathbf{v}_j^2) - \mathbf{p}\cdot(\mathbf{v}_i+\mathbf{v}_j)\right)\right] && (149)\\
&= \frac{2\epsilon}{m}\delta t^2 N + 2\delta t^2 \frac{N^2-N}{2}\frac{\mathbf{p}^2}{m^2} && (150)
\end{aligned}$$

we also have

$$\langle \mathbf{x}(\tau)\rangle^2 = \delta t^2 N^2 \frac{\mathbf{p}^2}{m^2} \tag{151}$$

which leads to the very important result

$$D_{\text{non-eq}} = \frac{3}{2}k_B\frac{\delta t}{m}\left(\frac{\epsilon - \mathbf{p}^2/2m}{3k_B/2}\right) = \mu k_B\Theta \tag{152}$$

The term within the parentheses is the non-equilibrium temperature we have introduced in Eq. 128, so we just need to identify the mobility $\mu \equiv \frac{3}{2}\delta t/m$ to obtain the expected result in Eq. 137.

This equation can be rewritten with the use of the equilibrium temperature $T = \epsilon/(3k_B/2)$ and the non-equilibrium deviation $\delta T(\mathbf{p}) \equiv (\mathbf{p}^2/2m)/(3k_B/2)$:

$$D_{\text{non-eq}} = \mu k_B (T - \delta T(\mathbf{p})) = D_{\text{eq}} - \delta D_{\text{corr}}(\mathbf{p}) \tag{153}$$

So for non-equilibrum processes with conserved momentum, the diffusion constant needs to be corrected with a term which is proportional to the average momentum squared, or equivalently introducing an effective temperature in the form obtained in Eq. 128. It is interesting to notice how the correction to the diffusion constant is always negative, which means that far from equilibrium diffusion is opposed by the non equilibrium flow, which pushes the particles towards the direction of the average momentum $\mathbf{p}$.

## 3.3 Electrophoresis: a near equilibrium result

The simplest direct application of this result is in the process of free flow electrophoresis. Electrophoresis is the process of charge migration in a solution under the action of an applied electric field. Because of the interaction between molecules flowing in opposite directions (with opposite charges), the terminal velocity of a charged molecule is linearly related to the applied electric field, yet the total momentum is conserved and always zero, because the total charge of the system is null.

There is a broad availability of measurements of the electrophoretic mobility in the literature, however, there is also a lot of confusion which we need to clarify.

Electrophoretic mobility, $\mu_E$, is defined as the ratio between the terminal velocity $\mathbf{v}_\infty(\mathbf{E})$ and the applied field $\mathbf{E}$. Often this is simply identified with the mobility $\mu$ which enters Einstein's relation and, for this reason, the diffusion constant in the case of electrophoresis is often ill defined [73, 74], because it is assumed that Einstein relation would apply. However, $\mu$ and $\mu_E$ are quantities which are conceptually different, because the first is relative to the thermal (brownian) motion of the particles in a solution, while the second is relative to a process which entails an external driving force. At low fields, it is obviuous that $\mu_E \simeq \mu$, because brownian motions become dominant, and Einstein's relation would hold in the simple form given in Eq. 136, but for arbitrary fields a non-equilibrium correction is required.

Our model allows us to find the correct relationship between $D(\mathbf{E})$ and $\mu_E$. Indeed when a charged particle is in a solution under the action of an electric field, it's average momentum is

$$\mathbf{p}(\mathbf{E}) = m\mathbf{v}_\infty(\mathbf{E}) = m\mu_E\mathbf{E} \tag{154}$$

Since the total solution is neutral in charge, the total force acting on the system is null, and the momentum is conserved. However, the field will deliver

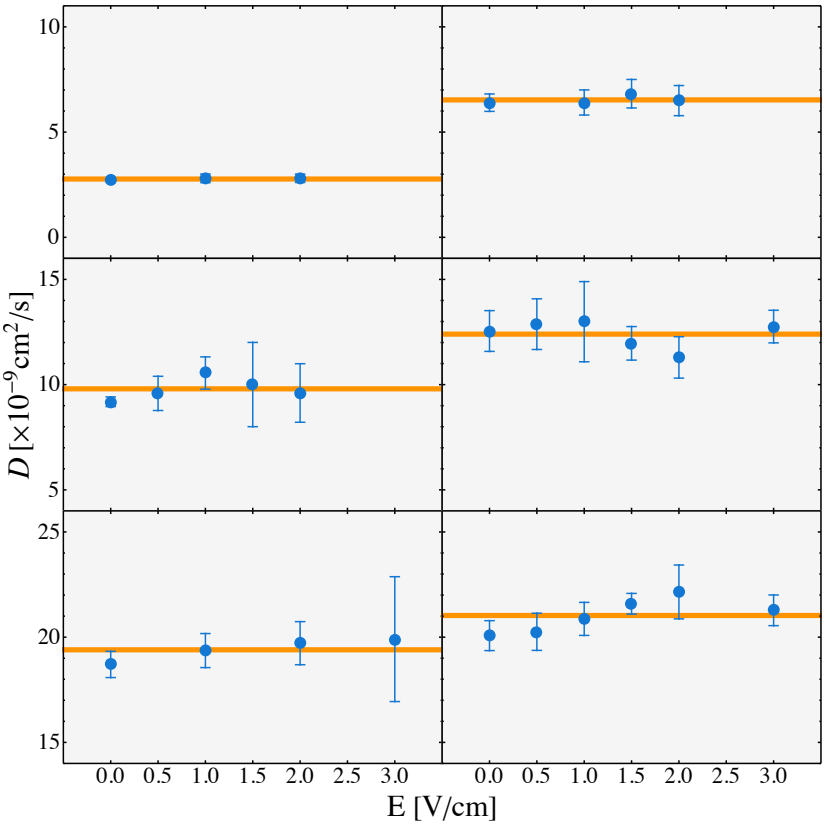


**Figure 19. Comparison of the present model with data from [73].** The error in the data points is too large for this effect to be visible in the current range of applied field.

energy to the system, which can ultimately result in an increase of the total energy of the system. In order for our assumption to hold we need to limit this to the near equilibrium case.

Under these assumptions, Eq. 153 can be written as

$$D(\mathbf{E}) = D_0 \left(1 - \frac{\mathbf{p}^2(\mathbf{E})}{3mk_BT}\right) = D_0 \left(1 - \frac{m\mu_E^2}{3k_BT}\mathbf{E}^2\right) \tag{155}$$

where $D_0$ is the zero-field, equilibrium diffusion constant.

Unfortunately, the coefficient of the $\mathbf{E}^2$ term is extremely small for the available data [73, 74], so any non-equilibrium effect can only be seen for strong fields, whereas all available data are in the range of few V/cm, as it can be seen in Fig. 19. Considering a single stranded DNA molecule, using the experimental parameters given in [73], the minimum field required to see

any non-equilibrium effects is $\mathbf{E} \gtrsim 100$ V/cm, which is far from the available range, but still within the range of near-equilibrium assumption for such small systems, because it is shown that no Joule heating is present for fields up to $\sim 250$ V/cm [73], where the discussed correction would certainly be visible.

Note that in the case of gel electrophoresis, the electrical mobility would become dependent on the applied field, because the field would stretch long, charged molecules, changing their ability to flow through the gel's pores. Our result in Eq. 155 would still be valid, once the dependence $\mu_E(\mathbf{E})$ is taken into account. However, there are not available data for the diffusion constant in such cases; many papers report a dispersion coefficient, which is believed to be equivalent to the diffusion constant, when this is measured in the same direction of the applied field. However, such quantity is obtained assuming that Einstein's relation is still valid, which is certainly not true when the mobility depends upon the applied field, so the dispersion coefficient measurement is just equivalent to a mobility one.

## 3.4 Angular Momentum Conservation

A similar argument can be applied for systems in which the angular momentum is conserved, which are very common for astrophysical objects, that are naturally isolated from external influence.

Imagine a system of $\mathcal{N}$ particles constrained to move at a distance $R$ from some arbitrary axis, hence in a cylindrical manifold. As in the original case the particles can collide and change direction, as long as they maintain the distance from the axis of rotation. Since all the forces acting on the particles are radial with respect to the axis of the cylinder, the total angular momentum along $\hat{z}$, $\mathbf{M}_{\text{tot}} = \hat{z} M_{\text{tot}}$, is conserved. We can therefore follow the same logic as before and write the probability distribution as

$$P([\mathbf{v}(t)]) = \frac{1}{\mathcal{Z}} \exp\left[-l_E \overline{E[\mathbf{v}(t)]} - \mathbf{l}_M \cdot \overline{\mathbf{M}[\mathbf{v}(t)]}\right] \tag{156}$$

Where $\overline{\mathbf{M}\left[\mathbf{v}(t)\right]]}$ is the time average of the path dependent angular momentum of a single particle $\mathbf{r}(t) \times \mathbf{v}(t)$.

In order to determine the Lagrange Multipliers we need to calculate, once

again, the partition function, which in this case is.

$$\begin{aligned}\mathcal{Z} &= \frac{1}{N!}\int \mathcal{D}\mathbf{v}\mathcal{D}\mathbf{r}\exp\left[-\sum_{i=1}^{N}\frac{\delta t}{\tau}\left(l_E\frac{m}{2}v^2(t)+m\mathbf{l}_M\cdot\mathbf{r}_i\times\mathbf{v}_i\right)\right] \\ &= \frac{1}{N!}\prod_{i=1}^{N}\left(\int d\mathbf{v}_i d\mathbf{r}_i\delta(\rho_i-R)\exp\left[-\frac{1}{N}\left(l_E\frac{m}{2}v_i^2+m\mathbf{l}_M\cdot\mathbf{r}_i\times\mathbf{v}_i\right)\right]\right)\end{aligned} \tag{157}$$

where $\mathcal{D}\mathbf{v}\mathcal{D}\mathbf{r} = d\mathbf{v}_1...d\mathbf{v}_N d\mathbf{r}_1...d\mathbf{r}_N\delta(\rho_1-R)...\delta(\rho_N-R)$; here $\rho_i=\sqrt{x_i^2+y_i^2}$ and the Dirac delta functions are used to enforce the integration over the correct trajectory space. Because of the rotational symmetry we can choose $\mathbf{l}_M$ to be along the $\hat{z}$ axis as well: $\mathbf{l}_M = l_M\hat{z}$ so that we need to solve the integral

$$\int d\mathbf{v}_i d\mathbf{r}_i\delta(\rho_i-R)\exp\left[-\frac{1}{N}\left(l_E\frac{m}{2}v_i^2+ml_M(x_iv_i^y-y_iv_i^x)\right)\right] \tag{158}$$

The integral over the velocity is once again a Gaussian integral, so we can solve it again using equation 120, but with the new associations

$$\mathrm{A} = \frac{l_E m}{N}I_3 \tag{159}$$

$$\mathbf{J} = \frac{m}{N}l_M\begin{pmatrix}-y_i\\ x_i\\ 0\end{pmatrix} \tag{160}$$

so that Eq. 158 gives

$$\int d\mathbf{r}_i\delta(\rho_i-R)\left(\frac{2\pi N}{ml_E}\right)^{3/2}\exp\left[\frac{ml_M^2}{2Nl_E}\left(x_i^2+y_i^2\right)\right] \tag{161}$$

$$= \int dz_i\rho_i d\rho_i d\phi_i\delta(\rho_i-R)\left(\frac{2\pi N}{ml_E}\right)^{3/2}\exp\left[\frac{ml_M^2}{2Nl_E}\rho_i^2\right] \tag{162}$$

$$= 2\pi hR\left(\frac{2\pi N}{ml_E}\right)^{3/2}\exp\left[\frac{ml_M^2}{2Nl_E}R^2\right] \tag{163}$$

At this point it must be clear that the result we obtain is analogous to the same we obtained in the case of linear momentum conservation with the standard associations $\mathbf{p}\to\mathbf{M}$ and $m\to mR^2$. The effective temperature in this case is

$$\Theta = \frac{\epsilon - \mathbf{M}^2/2mR^2}{3k_B/2} \tag{164}$$

where $\mathbf{M} = \mathbf{M}_{\text{tot}}/\mathcal{N}$.

From this we have the full probability distribution

$$P([\mathbf{v}(t)|\tau]) = \frac{1}{\mathcal{Z}} \exp\left[-\frac{N}{k_B\Theta}\left(\overline{E[\mathbf{v}(t)]} - \frac{1}{I}\mathbf{M}\cdot\overline{\mathbf{r}(t)\times\mathbf{p}[\mathbf{v}(t)]}\right)\right] \tag{165}$$

where $\mathbf{r}(t) = R\hat{\rho}(t)$ is the radial vector of fixed length $R$. $I$ is the moment of inertia of the particle.

This result has an interesting range of applicability to a lot of rotating object, common in astrophysics: every time it can be reasonably assumed that the trajectories of the particles are limited to the surface of the object (for instance, what happens for rotating black holes) this result can be applied to determine the probability of each trajectory. $\Theta$ represents, once again, the deviation of the system from the equilibrium. The extension to spherical symmetric object generated by a central potential $V(\mathbf{r})$ needs to be done by enforcing the fact that each trajectory respects the proper dynamical equations, hence Hamilton's equations.

## 3.5 Discussion

We have shown how Max Cal can obtain an exact expression for the path probabilities of a single particle in a medium of $\mathcal{N}$ particles moving with total energy $E_{\text{tot}}$ and momentum $\mathbf{P}_{\text{tot}}$. In this case, Max Cal gives an exact result because the constraints are enforced by physics conservation laws, rather than physical measurements. Max Cal is therefore the natural extension to dynamical systems out of equilibrium. This is also confirmed by the fact that when the equilibrium limit is taken the single particle distribution is the same as in Boltzmann theory.

It is also interesting to observe how a generalized definition of temperature was found, which we call non-equilibrium temperature, which deviates from the equilibrium temperature the more a system is taken away from equilibrium, but never reaching negative values, and reduces to the thermodynamics temperature if the equilibrium limit is taken.

The non-equilibrium temperature might be the long-sought measurable marker for deviation from equilibrium: maximum deviation from equilibrium is achieved when $\Theta \ll T$, whereas near equilibrium condition is simply $\Theta \lesssim T$.

A very important result obtained here is the non-equilibrium correction to Einstein's relation, which relate the diffusion constant to the mobility and

the equilibrium temperature. For non equilibrium processes, the temperature needs to be corrected, so that the effective/non-equilibrium temperature is always smaller than the equilibrium counterpart. Indeed for non equilibrium processes there is a current which opposes random diffusion and, in the case of system for which the momentum is conserved, such current is the average momentum of the system.

The form of the Diffusion constant is a testable prediction in the context of free flow electrophoresis, where the fact that the total charge of the system is zero ensures net zero force on the system and, therefore, no change in momentum. However, present experimental data are not resolved enough to observe the effect of this correction (see Fig. 19), in addition, other phenomena like Joule heating could prevent the possibility of observing this feature if the electric field range is improved.

# References


[1] J W Gibbs. *Elementary Principles in Statistical Mechanics, developed with especial reference to the rational foundation of thermodynamics.* Charles Scribner's Sons, 1902.

[2] Claude Elwood Shannon. A mathematical theory of communication. *Bell system technical journal*, 27(3):379–423, 1948.

[3] Edwin T Jaynes. Information theory and statistical mechanics. *Physical review*, 106(4):620, 1957.

[4] Edwin T Jaynes. Information theory and statistical mechanics. ii. *Physical review*, 108(2):171, 1957.

[5] John Shore and Rodney Johnson. Axiomatic derivation of the principle of maximum entropy and the principle of minimum cross-entropy. *IEEE Transactions on information theory*, 26(1):26–37, 1980.

[6] ET Jaynes et al. The maximum entropy formalism. *Ed. Levine, RD, Tribus, M., Where do we stand*, 1979.

[7] ET Jaynes and H Haken. Complex systems: Operational approaches. *Springer Series in Synergetics. Haken, H.(ed.). Berlin, Heidelberg, New York: Springer*, 1985.

[8] H Haken. A new access to path integrals and fokker planck equations via the maximum calibre principle. *Zeitschrift für Physik B Condensed Matter*, 63(4):505–510, 1986.

[9] Roderick C Dewar. Maximum entropy production and the fluctuation theorem. *Journal of Physics A: Mathematical and General*, 38(21):L371, 2005.

[10] Steve Pressé, Kingshuk Ghosh, Julian Lee, and Ken A Dill. Principles of maximum entropy and maximum caliber in statistical physics. *Reviews of Modern Physics*, 85(3):1115, 2013.

[11] Purushottam D Dixit, Jason Wagoner, Corey Weistuch, Steve Pressé, Kingshuk Ghosh, and Ken A Dill. Perspective: Maximum caliber is a general variational principle for dynamical systems. *The Journal of chemical physics*, 148(1):010901, 2018.

[12] D Allan Drummond, Jesse D Bloom, Christoph Adami, Claus O Wilke, and Frances H Arnold. Why highly expressed proteins evolve slowly. *Proceedings of the National Academy of Sciences*, 102(40):14338–14343, 2005.

[13] Konstantin B Zeldovich, Peiqiu Chen, and Eugene I Shakhnovich. Protein stability imposes limits on organism complexity and speed of molecular evolution. *Proceedings of the National Academy of Sciences of the United States of America*, 104(41):16152–7, 2007.

[14] D. Allan Drummond and Claus O. Wilke. Mistranslation-Induced Protein Misfolding as a Dominant Constraint on Coding-Sequence Evolution. *Cell*, 134(2):341–352, 2008.

[15] Jian-Rong Yang, Shi-Mei Zhuang, and Jianzhi Zhang. Impact of translational error-induced and error-free misfolding on the rate of protein evolution. *Molecular systems biology*, 6(421):421, 2010.

[16] Adrian W R Serohijos, S. Y Ryan Lee, and Eugene I. Shakhnovich. Highly abundant proteins favor more stable 3D structures in yeast. *Biophysical journal*, 104(3):L1–L3, 2013.

[17] Adrian W R Serohijos, Zilvinas Rimas, and Eugene I. Shakhnovich. Protein Biophysics Explains Why Highly Abundant Proteins Evolve Slowly. *Cell Reports*, 2(2):249–256, 2012.

[18] J R Yang, B Y Liao, S M Zhuang, and J Z Zhang. Protein misinteraction avoidance causes highly expressed proteins to evolve slowly. *Proceedings of the National Academy of Sciences of the United States of America*, 109(14):E831–E840, 2012.

[19] Emmanuel D Levy, Subhajyoti De, and Sarah a Teichmann. Cellular crowding imposes global constraints on the chemistry and evolution of proteomes. *Proceedings of the National Academy of Sciences of the United States of America*, 109(50):20461–6, 2012.

[20] S L Rutherford and S Lindquist. Hsp90 as a capacitor for morphological evolution. *Nature*, 396(6709):336–342, 1998.

[21] Nobuhiko Tokuriki and Dan S Tawfik. Chaperonin overexpression promotes genetic variation and enzyme evolution. *Nature*, 459(7247):668–73, 2009.

[22] S L Rutherford. Between genotype and phenotype: protein chaperones and evolvability. *Nature Reviews: Genetics*, 4(4):263–274, 2003.

[23] Todd A. Sangster, Susan Lindquist, and Christine Queitsch. Under cover: Causes, effects and implications of Hsp90-mediated genetic capacitance. *BioEssays*, 26(4):348–362, 2004.

[24] Amar Nath Gupta, Krishna Neupane, Negar Rezajooei, Leonardo M Cortez, Valerie L Sim, and Michael T Woodside. Pharmacological chaperone reshapes the energy landscape for folding and aggregation of the prion protein. *Nature communications*, 7(May):12058, 2016.

[25] David Bogumil, Giddy Landan, Judith Ilhan, and Tal Dagan. Chaperones divide yeast proteins into classes of expression level and evolutionary rate. *Genome Biology and Evolution*, 4(5):618–625, 2012.

[26] A Samer Kadibalban, David Bogumil, Giddy Landan, and Tal Dagan. DnaK-Dependent Accelerated Evolutionary Rate in Prokaryotes. *Genome biology and evolution*, 8(5):1590–9, 2016.

[27] José Aguilar-Rodríguez, Beatriz Sabater-Muñoz, Roser Montagud-Martínez, Víctor Berlanga, David Alvarez-Ponce, Andreas Wagner, and Mario A. Fares. The molecular chaperone DnaK is a source of mutational robustness. *Genome Biology and Evolution*, 8(9):evw176, 2016.

[28] J L Martinez and F Baquero. MINIREVIEW-Mutation Frequencies and Antibiotic Resistance. *Antimicrobial agents and chemotherapy*, 44(7):1771–1777, 2000.

[29] Michael Baym, Tami D Lieberman, Eric D Kelsic, Remy Chait, Rotem Gross, Idan Yelin, and Roy Kishony. Spatiotemporal microbial evolution on antibiotic landscapes. *Science*, 353(6304):1147 LP – 1151, 2016.

[30] Philip Greulich, Bartłomiej Waclaw, and Rosalind J. Allen. Mutational pathway determines whether drug gradients accelerate evolution of drug-resistant cells. *Physical Review Letters*, 109(8):1–5, 2012.

[31] Guy Sella and Aaron E. Hirsh. The application of statistical physics to evolutionary biology. *Proceedings of the National Academy of Sciences*, 102(40):14475–14475, oct 2005.

[32] Julian Echave and Claus O Wilke. Biophysical models of protein evolution: understanding the patterns of evolutionary sequence divergence. *Annual review of biophysics*, 46:85–103, 2017.

[33] N. H. Barton and J. B. Coe. On the application of statistical physics to evolutionary biology. *Journal of Theoretical Biology*, 259(2):317–324, 2009.

[34] Harold P. De Vladar and Nicholas H. Barton. The contribution of statistical physics to evolutionary biology. *Trends in Ecology and Evolution*, 26(8):424–432, 2011.

[35] C Darwin. *On the origins of species by means of natural selection*. John Murray, London, 1859.

[36] Sewall Wright. *The roles of mutation, inbreeding, crossbreeding, and selection in evolution*, volume 1. na, 1932.

[37] Inês Fragata, Alexandre Blanckaert, Marco António Dias Louro, David A Liberles, and Claudia Bank. Evolution in the light of fitness landscape theory. *Trends in ecology & evolution*, 34(1):69–82, 2019.

[38] Steve Pressé, Kingshuk Ghosh, Julian Lee, and Ken A Dill. Principles of maximum entropy and maximum caliber in statistical physics. *Reviews of Modern Physics*, 85(3):1115, 2013.

[39] Michael J Hazoglou, Valentin Walther, Purushottam D Dixit, and Ken A Dill. Communication : Maximum caliber is a general variational principle for nonequilibrium statistical mechanics Communication : Maximum caliber is a general variational principle for nonequilibrium statistical mechanics. *The Journal of Chemical Physics*, 143(051104), 2015.

[40] R Zwanzig, A Szabo, and B Bagchi. Levinthal's paradox. *Proceedings of the National Academy of Sciences*, 89(1):20–2, 1992.

[41] G. C. Rollins and K. A. Dill. General mechanism of two-state protein folding kinetics. *J. Am. Chem. Soc.*, 136(32):11420–11427, Aug 2014.

[42] Daniel Arovas. Lecture Notes on Nonequilibrium Statistical Physics. *arXiv*, 2014.

[43] Heewook Lee, Ellen Popodi, Haixu Tang, and Patricia L Foster. Rate and molecular spectrum of spontaneous mutations in the bacterium escherichia coli as determined by whole-genome sequencing. *Proceedings of the National Academy of Sciences*, 109(41):E2774–E2783, 2012.

[44] Igor M Rouzine, Éric Brunet, and Claus O Wilke. The traveling-wave approach to asexual evolution: Muller's ratchet and speed of adaptation. *Theoretical population biology*, 73(1):24–46, 2008.

[45] Jianzhi Zhang and Jian-Rong Yang. Determinants of the rate of protein sequence evolution. *Nature reviews. Genetics*, 16(7):409–420, 2015.

[46] Nobuhiko Tokuriki, Christopher J Oldfield, Vladimir N Uversky, Igor N Berezovsky, and Dan S Tawfik. Do viral proteins possess unique biophysical features? *Trends in biochemical sciences*, 34(2):53–59, 2009.

[47] Nobuhiko Tokuriki and Dan S Tawfik. Protein dynamism and evolvability. *Science*, 324(5924):203–207, 2009.

[48] Misha Soskine and Dan S Tawfik. Mutational effects and the evolution of new protein functions. *Nature Reviews Genetics*, 11(8):572, 2010.

[49] K. A. Dill, K. Ghosh, and J. D. Schmit. Physical limits of cells and proteomes. *Proceedings of the National Academy of Sciences*, 108(44):17876–17882, 2011.

[50] J. L. England, B. E. Shakhnovich, and E. I. Shakhnovich. Natural selection of more designable folds: A mechanism for thermophilic adaptation. *Proceedings of the National Academy of Sciences*, 100(15):8727–8731, 2003.

[51] Igor N Berezovsky, Eugene I Shakhnovich, and Alan R Fersht. Physics and evolution of thermophilic adaptation. *Pnas*, 102(36):12742–12747, 2005.

[52] Peiqiu Chen and Eugene I Shakhnovich. Thermal Adaptation of Viruses and Bacteria. *Biophysical Journal*, 98(7):1109–1118, 2010.

[53] Kingshuk Ghosh, Adam M.R. De Graff, Lucas Sawle, and Ken A. Dill. Role of Proteome Physical Chemistry in Cell Behavior. *Journal of Physical Chemistry B*, 120(36):9549–9563, 2016.

[54] Lucas Sawle and Kingshuk Ghosh. How do thermophilic proteins and proteomes withstand high temperature? *Biophysical Journal*, 101(1):217–227, 2011.

[55] Ian K. Blaby, Benjamin J. Lyons, Ewa Wroclawska-Hughes, Grier C F Phillips, Tyler P. Pyle, Stephen G. Chamberlin, Steven A. Benner,

Thomas J. Lyons, Valérie de Crécy-Lagard, and Eudes de Crécy. Experimental evolution of a facultative thermophile from a mesophilic ancestor. *Applied and Environmental Microbiology*, 78(1):144–155, 2012.

[56] Feng Zhang, Li Xu, Kun Zhang, Erkang Wang, and Jin Wang. The potential and flux landscape theory of evolution. *The Journal of chemical physics*, 137(6):065102, 2012.

[57] Emile Zuckerkandl and Linus Pauling. Molecular Disease, Evolution, and Genic Heterogeneity. *Horizons in Biochemistry*, pages 189–222, 1962.

[58] Masatoshi Nei, Yoshiyuki Suzuki, and Masafumi Nozawa. The neutral theory of molecular evolution in the genomic era. *Annual review of genomics and human genetics*, 11:265–289, 2010.

[59] David M Mccandlish and Arlin Stoltzfus. Modeling Evolution Using the Probability of Fixation: History and Implications. *Source: The Quarterly Review of Biology*, 89(3):225–252, 2014.

[60] Csaba Pal, Balazs Papp, and Laurence D. Hurst. Highly Expressed Genes in Yeast Evolve Slowly Csaba. *Genetics*, 3(2):125–126, 2001.

[61] Tobias Sikosek and Hue Sun Chan. Biophysics of protein evolution and evolutionary protein biophysics. *Journal of the Royal Society, Interface / the Royal Society*, 11(100):20140419, 2014.

[62] Kit Fun Lau and Ken A Dill. A lattice statistical mechanics model of the conformational and sequence spaces of proteins. *Macromolecules*, 22(10):3986–3997, 1989.

[63] Kirsten T. Wyganowski, Miriam Kaltenbach, and Nobuhiko Tokuriki. GroEL/ES buffering and compensatory mutations promote protein evolution by stabilizing folding intermediates. *Journal of Molecular Biology*, 425(18):3403–3414, 2013.

[64] Mantu Santra, Daniel W. Farrell, and Ken A. Dill. Bacterial proteostasis balances energy and chaperone utilization efficiently. *Proceedings of the National Academy of Sciences*, page 201620646, 2017.

[65] Robert L Jack and RML Evans. Absence of dissipation in trajectory ensembles biased by currents. *Journal of Statistical Mechanics: Theory and Experiment*, 2016(9):093305, 2016.

[66] Christian Maes. *Non-dissipative effects in nonequilibrium systems*. Springer, 2018.

[67] Christopher Jarzynski. Nonequilibrium equality for free energy differences. *Physical Review Letters*, 78(14):2690, 1997.

[68] Gavin E Crooks. Entropy production fluctuation theorem and the nonequilibrium work relation for free energy differences. *Physical Review E*, 60(3):2721, 1999.

[69] Ken Dill and Sarina Bromberg. *Molecular driving forces: statistical thermodynamics in biology, chemistry, physics, and nanoscience*. Garland Science, 2012.

[70] T Speck and U Seifert. Restoring a fluctuation-dissipation theorem in a nonequilibrium steady state. *EPL (Europhysics Letters)*, 74(3):391, 2006.

[71] Valentin Blickle, Thomas Speck, Christoph Lutz, Udo Seifert, and Clemens Bechinger. Einstein relation generalized to nonequilibrium. *Physical review letters*, 98(21):210601, 2007.

[72] Debasish Chaudhuri and Abhishek Chaudhuri. Modified fluctuation-dissipation and einstein relation at nonequilibrium steady states. *Physical Review E*, 85(2):021102, 2012.

[73] Axel E Nkodo, Jean M Garnier, Bernard Tinland, Hongji Ren, Claude Desruisseaux, Laurette C McCormick, Guy Drouin, and Gary W Slater. Diffusion coefficient of dna molecules during free solution electrophoresis. *Electrophoresis*, 22(12):2424–2432, 2001.

[74] Alexander C Johnson and Michael T Bowser. Micro free flow electrophoresis. *Lab on a Chip*, 18(1):27–40, 2018.

[75] Edwin T Jaynes. The minimum entropy production principle. *Annual Review of Physical Chemistry*, 31(1):579–601, 1980.

[76] M Adam, B Murali, N. O Glenn, and SS Potter. Epigenetic inheritance based evolution of antibiotic resistance in bacteria. *BMC Evol. Biol.*, 8:52, Feb 2008.

[77] M Stam and O Mittelsten Scheid. Paramutation: an encounter leaving a lasting impression. *Trends Plant Sci.*, 10(6):283–290, Jun 2005.

[78] G Cavalli and R Paro. The Drosophila Fab-7 chromosomal element conveys epigenetic inheritance during mitosis and meiosis. *Cell*, 93(4):505–518, May 1998.

[79] D Nevozhay, RM Adams, E Van Itallie, MR Bennett, and G Balázsi. Mapping the environmental fitness landscape of a synthetic gene circuit. *PLoS computational biology*, 8(4):e1002480, 2012.

[80] C Queitsch, TA Sangster, and S Lindquist. Hsp90 as a capacitor of phenotypic variation. *Nature*, 417(6889):618–624, Jun 2002.

[81] M Kaern, TC Elston, WJ Blake, and JJ Collins. Stochasticity in gene expression: from theories to phenotypes. *Nat. Rev. Genet.*, 6(6):451–464, Jun 2005.

[82] MS Samoilov, G Price, and AP Arkin. From fluctuations to phenotypes: the physiology of noise. *Sci. STKE*, 2006(366):re17, Dec 2006.

[83] Z Bódi, Z Farkas, D Nevozhay, D Kalapis, V Lázár, B Csörgő, Á Nyerges, B Szamecz, G Fekete, B Papp, et al. Phenotypic heterogeneity promotes adaptive evolution. *PLoS biology*, 15(5):e2000644, 2017.

[84] C González, JCJ Ray, M Manhart, RM Adams, D Nevozhay, AV Morozov, and G Balázsi. Stress-response balance drives the evolution of a network module and its host genome. *Molecular systems biology*, 11(8):827, 2015.

[85] DA Charlebois, G Balazsi, and M Kaern. Coherent feedforward transcriptional regulatory motifs enhance drug resistance. *Phys Rev E Stat Nonlin Soft Matter Phys*, 89(5):052708, May 2014.

[86] B Xue and S Leibler. Evolutionary learning of adaptation to varying environments through a transgenerational feedback. *Proc. Natl. Acad. Sci. U.S.A.*, 113(40):11266–11271, 2016.

[87] DA Charlebois, N Abdennur, and M Kaern. Gene expression noise facilitates adaptation and drug resistance independently of mutation. *Physical review letters*, 107(21):218101, 2011.

[88] DA Charlebois. Effect and evolution of gene expression noise on the fitness landscape. *Phys Rev E Stat Nonlin Soft Matter Phys*, 92(2):022713, Aug 2015.

[89] Nobutaka Hirokawa. Kinesin and dynein superfamily proteins and the mechanism of organelle transport. *Science*, 279(5350):519–526, 1998.

[90] Feng-Ching Tsai, Sophie Roth, Marileen Dogterom, and Gijsje Hendrika Koenderink. Biomimetic liposome model systems to study cell shape control by the cytoskeleton. In *Advances in Planar Lipid Bilayers and Liposomes*, volume 19, pages 139–173. Elsevier, 2014.

# Appendices

# Appendices

## Appendix A2: Caliber is maximized by non-equilibrium dynamics.

The generality of the SJ argument is extremely powerful when one wants to go beyond equilibrium statistical mechanics. Indeed, nowhere in their derivation any assumption on the type of system is made: as long as the concept of probability is well defined in the given space, Max Ent can be applied, so Max Cal is its natural extension for non-equilibriyum systems.

In the case of non-equilibrium physics, however, it is important to define the working space correctly. Indeed, the standard definition of State Entropy becomes problematic as soon as we move away from equilibrium, and the reason is simple: one of the most important properties of entropy is additivity. We know from thermodynamics that taking two sub-systems at equilibrium, the total entropy is the sum of the entropy of the two systems. This holds true naturally for Shannon's definition of entropy when applied to equilibrium states and it is in fact one of the fundamental properties that any functional $H[p]$ needs to satisfy in order to respect the SJ axioms [5].

As an example let's consider a 1D lattice model for a gas, with total $2N$ lattice sites and $n$ total particles, with $n \ll N$. Let's divide the volume into two compartments $C_1$ and $C_2$, each with $N$ lattice sites and consider the system as far from equilibrium as possible: all the particles are in subset one. Considering the particles to be all identical, the state entropy $S_1$ of the subset one would just be given by Boltzmann formula $S_1 = \log W = \log \frac{N!}{(N-n)!n!}$, whereas $S_2 = \log 1 = 0$. When one particle moves from $C_1$ to $C_2$, the state entropy in both system changes, and one can easily verify that

$$\Delta S_1 = \log \frac{n}{N-n+1} < 0 \tag{166}$$

$$\Delta S_2 = \log N > 0 \tag{167}$$

The entropy has decreased in $C_1$ and increased in $C_2$ but, as it is obvious, $|\Delta S_1| \neq |\Delta S_2|$, which means that the state entropy does not *flow*, that is a well known result, because the total entropy needs to increase when reaching

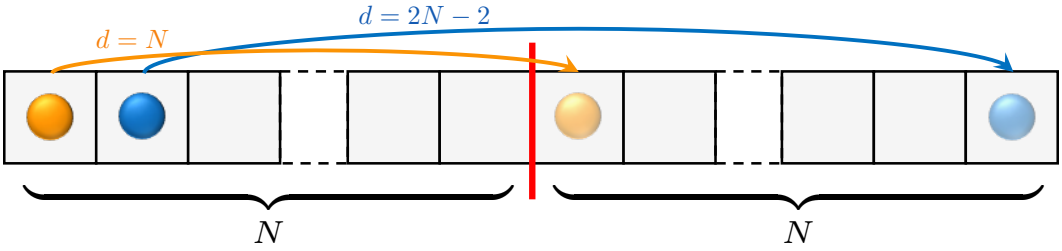


**Figure 20. Trajectories in a 1D lattice.** The possible lengths of the trajectories from the left to the right side of the lattice are $d = 1, 2, ..., 2N - 1$; the multiplicity of each trajectory is given in Eq. 168.

the new equilibrium, as the second law of thermodynamics tells us. When the system is very close to equilibrium, the behavior of entropy becomes more flow-like, as one can easily show, so it becomes possible to treat entropy with differential methods, introducing the concept of *entropy production* [75].

However, using entropy production to address non-equilibrium problems must be done carefully, because state entropy, as we said above, is meaningful only at equilibrium, when it does not depend on time. It is reasonable to expect that the mathematical entropy, which is time dependent for non-equilibrium processes, is continuous and differentiable in the neighborhood of equilibrium, but when a system is far from equilibrium we cannot maximize the state entropy anymore, hence in order to use correctly the SJ approach we need to redefine the system altogether.

We now consider all the possible *routes* that a particle can take to move from subset $C_1$ to $C_2$, we will refer to these routes with the term *path* or *trajectory*. We call $P_d$ the probability that the observed path is $d$. As an example, we can consider that $d$ is the number of lattice sites crossed in a given trajectory; for a 1D lattice, the possible lengths are $d = 1, 2, ..., 2N - 1$. Let's consider for instance the example above for a single particle; the number of possible trajectories of length $d$ can be written as

$$q(d) = \theta(N - d)d + \theta(d - N - 1)(2N - d) \tag{168}$$

where $\theta(n)$ is the step function with the convention $\theta(0) = 1$; Fig. 20 shows some examples of such trajectories. We want to determine the probability $P(d)$ of observing a trajectory of length $d$, using $q(d)$ as prior of such distribution.

The path entropy for this system is

$$S_{\text{path}} = -\sum_{d=1}^{2N-1} P(d) \log \frac{P(d)}{q(d)} \tag{169}$$

Since we have no additional information about what is driving the transition other than random mixing, we can obtain the most likely distribution by simply maximizing $S_{\text{path}}$ under the constraint that the probability sums to one. Hence the caliber, as defined in equation 8 is

$$\mathcal{C} = S_{\text{path}} - \alpha \left( \sum_{d=1}^{2N-1} P(d) - 1 \right) \tag{170}$$

with the single Lagrange multiplier $\alpha$ to enforce the constraint on the probability sum. From this we obtain that the most likely probability distribution is simply the prior $P^*(d) = q(d)/Q$, where $Q = \sum q(d)$, which is what we expected because *a priori* there is no reason why one route should be preferred with respect to another, other than simply the multiplicity of a given route.

Now we assume that some dynamical quantity is known for a system like this. For instance, let's assume that we can measure the average time $\langle \tau \rangle$ that a particle takes to complete a trajectory at steady state. If $k_0$ is the transition rate from one site to the next, the time of a specific trajectory is $\tau(d) = d/k_0$, and the average can be written as

$$\langle \tau \rangle = \sum_{d=1}^{2N-1} \frac{d}{k_0} P(d) \tag{171}$$

As a consequence, the caliber is

$$\mathcal{C} = -\sum_{d=1}^{2N-1} P(d) \log \frac{P(d)}{q(d)} - \alpha \left( \sum_{d=1}^{2N-1} P(d) - 1 \right) - \beta \left( \sum_{d=1}^{2N-1} dP(d) - k_0 \langle \tau \rangle \right) \tag{172}$$

where we have chosen to constrain the dimensionless quantity $k_0\langle \tau \rangle$ for simplicity. In the large $N$ limit we can obtain an analytical expression for the probability of observing a trajectory of length $d$

$$P(d) = \frac{g(d)}{Q} \left( 1 + \frac{2}{k_0 \langle \Delta\tau \rangle} \right)^d \tag{173}$$

where $\langle \Delta\tau \rangle = \langle \tau_{max} - \tau \rangle = 2N/k_0 - \langle \tau \rangle$ is the difference between the maximum and the average time.

Fig. 21 shows how the most likely probability distribution is modified by the knowledge of the average transition rate. This simple example shows how $S_{\text{path}}$ is the right type of entropy necessary to extract information for a dynamical process. To extend to multiple particles we only need to express the combinatorics of the multi-particle trajectories. We can also expand to

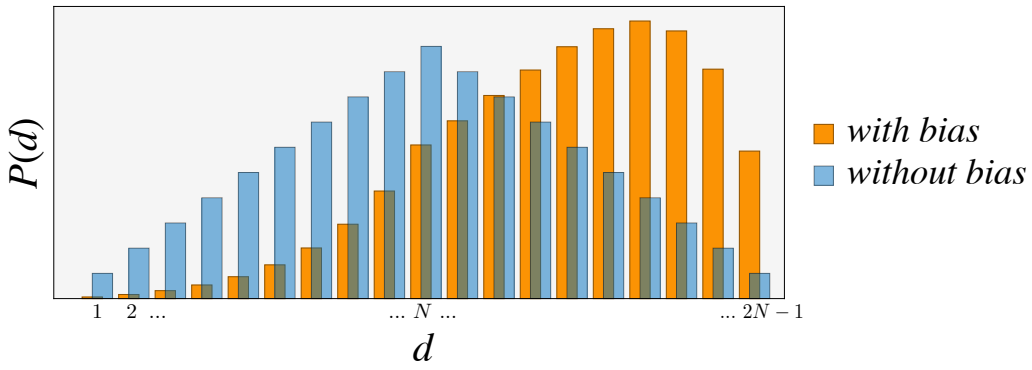


**Figure 21. Trajectory probability distribution with and without bias.** The bias given by the knowledge of the average transition time modifies the most likely probability distribution into an asymmetrically shaped one.

describe a time-dependent rate, hence by lifting the steady state hypothesis: in that case the constraint itself becomes time-dependent and so does the Lagrange multiplier $\beta(t)$. The general approach to the problem remains unchanged: $S_{\text{path}}$ is still the quantity that correctly describes the process.

It is worth noting that the SJ argument is only a method for inferring probability distribution from partially known information, and nowhere it implies that it can only be used for equilibrium probability distributions. As long as the entropy function is well defined it is possible to extend its use to non-equilibrium systems, with the important specification that the path entropy is used instead of the state entropy.

## Appendix A2: The equilibrium limit for physical systems

In order for Max Cal to correctly describe non-equilibrium systems it is required that if at any point, for a thermal system, we take the equilibrium limit, we recover the well known equilibrium results. Since we already know that Max Ent is successful to describe equilibrium system, it is sufficient that the entropy $S_{\text{path}}$ is equivalent to the traditional state entropy, that we know is maximized by the equilibrium distribution.

For this reason we consider a physical system specified by some Hamiltonian $H(\{\mathbf{q}, \mathbf{p}\})$. In general, and of course including when the system is far from equilibrium, the trajectory of every component of the system is governed by Hamilton's equations. Solving them for large systems is in general non possible, but we can imagine that there is some high dimensional function

$\mathbf{q}(t) = \{q_1(t), q_2(t), ..., q_N(t), p_1(t), p_2(t), ..., p_N(t)\}$ representing the full trajectory, or path. The path probability is therefore defined as $P_r = P[\mathbf{q}(t)]$, and the path entropy is

$$\mathcal{S} = -\sum_{\{\mathbf{q}(t)\}} P[\mathbf{q}(t)] \log P[\mathbf{q}(t)] \tag{174}$$

However, for an Hamiltonian system as this, the trajectory at any time $t$ is uniquely defined by the initial conditions (result of Liouville's theorem), therefore we have

$$\mathcal{S} = -\sum_{\{\mathbf{q}(0)\}} P[\mathbf{q}(0)] \log P[\mathbf{q}(0)] \tag{175}$$

Now we take the equilibrium limit, meaning that every initial condition is basically correspondent to an equilibrium state. Finding the system with initial condition $\mathbf{q}(0)$ is indeed equivalent to finding it in the equilibrium state $\boldsymbol{\epsilon} = \{\epsilon_1, \epsilon_2, ...\}$ (for the canonical ensemble this would be the energy configuration of the specific microstate), therefore in the equilibrium limit we can replace the path probability with the state probability $P[\mathbf{q}(0)] \to p(\boldsymbol{\epsilon})$, and

$$\mathcal{S} = -\sum_{\{\mathbf{q}(0)\}} P[\mathbf{q}(0)] \log P[\mathbf{q}(0)] \to -\sum_{\{\epsilon_0\}} p(\boldsymbol{\epsilon}) \log p(\boldsymbol{\epsilon}) \tag{176}$$

where we have used the lower case letter to indicate the state probability as opposed to the path probability upper case letter.

For example we can consider a gas of $N$ non-interacting particles in a volume $V$; the probability in this case factorizes into the product of single particle probabilities, but if the particles are identical we need to include a combinatory correction (known as Boltzmann correct counting), because if particles are identical so are their trajectories

$$P[\mathbf{q}(0)] = \frac{1}{N!} P_1[q_1(0)] P_2[q_2(0)] ... P_N[q_N(0)] \tag{177}$$

so

$$\begin{aligned}
\frac{\mathcal{S}}{k_B} &= -\frac{1}{N!}\sum_{q_1(0),\ldots} P_1[q_1(0)]...P_N[q_N(0)]\log(P_1[q_1(0)]...P_N[q_N(0)]) \\
&= -\frac{1}{N!}\sum_{q_1(0)} P_1[q_1(0)]\log P_1[q_1(0)] - ... \\
&\quad ... - \frac{1}{N!}\sum_{q_N(0)} P_N[q_N(0)]\log P_N[q_N(0)] \\
&\to -\frac{1}{N!}\sum_{\epsilon_1} p_1[\epsilon_1]\log p_1[\epsilon_1] - ... - \frac{1}{N!}\sum_{\epsilon_N} p_N[\epsilon_N]\log p_N[\epsilon_N] \quad (178)
\end{aligned}$$

In the last line we have taken the equilibrium limit and assumed that the particles are identical, so the states available to each particles are the same. If the gas is in contact with a reservoir at temperature $T$, the probability is just Boltzmann distribution for a canonical ensemble, so we obtain the well known Sackur-Tetrode formula

$$S = k_B N\left[\frac{5}{2} + \log\left(\frac{V}{N}\left(\frac{2\pi m k_B T}{h^2}\right)^{\frac{3}{2}}\right)\right] \quad (179)$$

This shows how the path entropy is well defined in any regime, arbitrary far from equilibrium, and it reduces to the state probability for physical systems (hence Hamiltonian) in the equilibrium limit.

## Appendix B: What are the mechanisms of non-genetic inheritance of stress responses?

In a population of cells that all have identical genes, there are natural cell-to-cell variations, such as in some protein concentrations. Remarkably, those non-genetic variations can ultimately become genetically inherited through mutations and selection. This is not a violation of any Darwinian precept, but is a new and important addendum to those ideas, although the mechanism is not yet understood. Our specific focus here is on how cells inherit their stress responses. Isogenic cells that happen to handle stress well can duplicate into daughter cells that are also better at handling stress. Inheriting stress responses entail chaperones, and hence protein folding and aggregation. Our question is: how do non-genetic fluctuations become genetically heritable in cellular stress responses?

Normally, phenotypic traits evolve through mutations in the genes that are passed from ancestors to descendants. But, some traits are heritable in ways that do not involve genes, at least for a few generations. A well-known example of non-genetic transmission is epigenetic changes: chemical modifications to DNA that happen inside a mother cell can result in corresponding behaviors in daughter cells [76–78]. These non-genetic fluctuations within cell populations can sometimes ultimately become encoded in the genes. Of interest here is how cell stress responses are transmitted this way [79, 80]. A population of mother cells – even isogenic ones in the same environment – will have a natural distribution of molecular concentrations, for example of chaperone complexes (the cell's main stress-response machinery [81, 82]. The mothers that best respond to stress can pass that stress advantage to the daughter cells, first non-genetically, and then that advantage can be captured in the genome of the lineage [83, 84].

We seek the mechanism(s). We believe the following hypothesis is the best initial starting point. Suppose a population of isogenic cells has a distribution of chaperone concentrations. Different cells have different concentrations of chaperone. Cell $i$ has chaperone concentration $c_i$, which does not necessarily equal the population average level, $c_{\text{avg}}$. Now, non-genetic inheritance means there is some non-genetic form of 'memory' that transmits something from mother to daughter. One source of memory is positive feedback loops. For example, such loops are like 'thermostats' that hold chaperone concentrations fixed. That is, mother cell $i$ has a biochemical regulatory circuit that holds its chaperone levels close to $c_i$. The daughter will inherit that feedback circuit, holding its own chaperone levels to around $c_i$, plus noise, and that level can survive for several generations [79, 85–87].

How does this non-genetic memory become encodable in normal evolutionary mutation and selection? We believe it is a matter of timescales (Fig. 22). If drug pulses hit the cells slowly, they will regrow back their initial population: new mutations that confer resistance don't take over. But, if drug pulses hit the cell population rapidly, it kills the regrowth of cells lacking the resistance-conferring mutation. This ultimately moves the population toward higher chaperone concentrations, in a way that is preserved in genetic memory.

Two factors determine whether the higher chaperone concentration is propagated to the next generation of cells: (1) the difference between the speed (frequency) of fluctuations of chaperone concentrations and the speed of cell duplication (doubling time) [87], and (2) the speed of the feedback mechanism that maintains the concentration of chaperone [85]. Both of these factors contribute to a cellular "memory" of how long the daughters cells remain similar to the mother cell. We can introduce these two mechanisms, and their rates, into Fokker-Planck and diffusional changes across generations. If $c$ is the concentration of chaperone in a given mother cell, the concentration in the daughter will be:

$$c' = c + (\Delta c_{\text{env}} + \Delta c_{\text{noise}}) \tag{180}$$

where $\Delta c_{\text{env}}$ is the change in chaperone concentration from one generation to the other due to the response to the environment and $\Delta c_{\text{noise}}$ is the change due to noise, hence the change due to stochastic fluctuations. Both of these quantities are encoded in the genes of the organism: the first will determine the mean value of the non-genetic distribution of $c$, the second will determine its variance. If we assume that the partitioning of cellular contents proportional to cell volume of the daughter cells, the daughters will have the same starting concentration given by the baseline of the mother, with fluctuations from the environment and noise.

We can express these dynamics in terms of the Langevin equation [87]

$$\frac{dc}{dt} = \frac{1}{t_r}[c - \mu] + DW_t \tag{181}$$

where $t_r$ and $D$ are the relaxation time and the diffusion constant, respectively; $W_t$ is Gaussian white noise. $\mu$ is the mean value of the steady-state distribution generated by this process, which will have a variance $\sigma^2 = Dt_r/2$. The value $\mu$ corresponds to the response to the environment (it determines the value of $\Delta c_{\text{env}}$) whereas $W_t$ represents the non-genetic noise (it determines the value of $\Delta c_{\text{noise}}$); both these quantities (hence mean and variance of the distribution) can be encoded in the DNA of the cell and are themselves subject to evolutionary pressures [88]. From this, we can derive a Fokker-Planck equation that determines how the population of cells will behave over time.

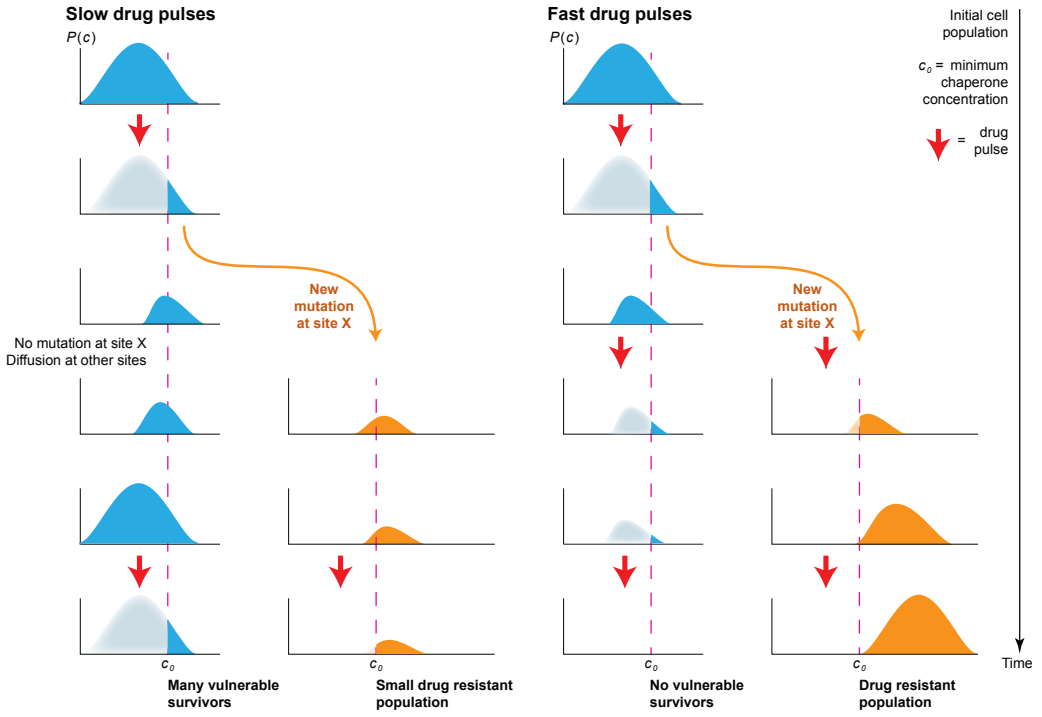


**Figure 22. Hypothesis for how non-genetic fluctuations can become subject to mutation and selection for long-term genome changes.** Depending upon the drug pulses frequency, a population with a higher mean chaperone's concentration, and hence resistant to drug, might become dominant.

If an adaptive mutation happens, it will change the value of $\mu$, and thus the direction in which the population moves, increasing the average chaperone's concentration and conferring long-term genetically heritable drug resistance to the cell. There is nothing Lamarkian here. The mutations to P* are random and Darwinian. In this way, cell-to-cell fluctuations could become subject to genetic transmission by mutation and selection.

## Appendix C:Dissipative systems in biology: Molecular motors

Proteins are biological machines that perform fundamental tasks in the cell. Often such functions need to be cyclic; for instance, some proteins are designed to drag other complexes across microtubules in the cell [89], for which they need to repeat a series of conformational changes in a very specific cyclic sequence, so the process can be repeated arbitrarily. The minimum number of conformational changes you need in a protein to be able to perform work is 3, since otherwise the entire process would be a simple transition back and forth between two states.

So we imagine that a molecular motor can be represented by 3 states $A$, $B$ and $C$. We call $G_k$ the free energy of conformation $k = a, b, c$ (see Fig. 23). In order to transition between two conformations an energy barrier needs to be overcome, so we call such energy barrier $\Delta G^{\ddagger}_{kl} = G^{\ddagger}_{kl} - G_k$ ($G^{\ddagger}_{kl}$ is the free energy of the transition state between $k$ and $l$) and the barrier for the reverse process would therefore be $\Delta G^{\ddagger}_{lk} = G^{\ddagger}_{kl} - G_l$. In order for this process to happen it is necessary to transfer energy from the surrounding to the motor itself, especially if the final energy. This happens actively in the cell through ATP binding and hydrolysis, which creates a more convenient energy balance for the process to happen. However, in general there is also the possibility that this process could happen naturally by pure thermal fluctuations. Using the same approach we described above we can calculate the probability that a molecular motor can be run by pure thermal fluctuations.

Without specifying the details of the biochemistry of the process, we consider such system and call $P(\Gamma) = P^1_{ab} \cdot P^2_{bc} \cdot P^3_{ca}$ the probability of a rotation of the motor through the transition $a \to b \to c$. Each step in the trajectory can happen through different processes: intuitively, the most probable way would be by absorbing chemical energy $\Delta\mu$ from the molecules around it (ATP hydrolysis) and dissipating it through thermal energy $\Delta q$. However, as we have seen above, the reverse process (absorbing thermal energy and synthesizing ATP) needs to be taken into account, so we define the following probabilities:

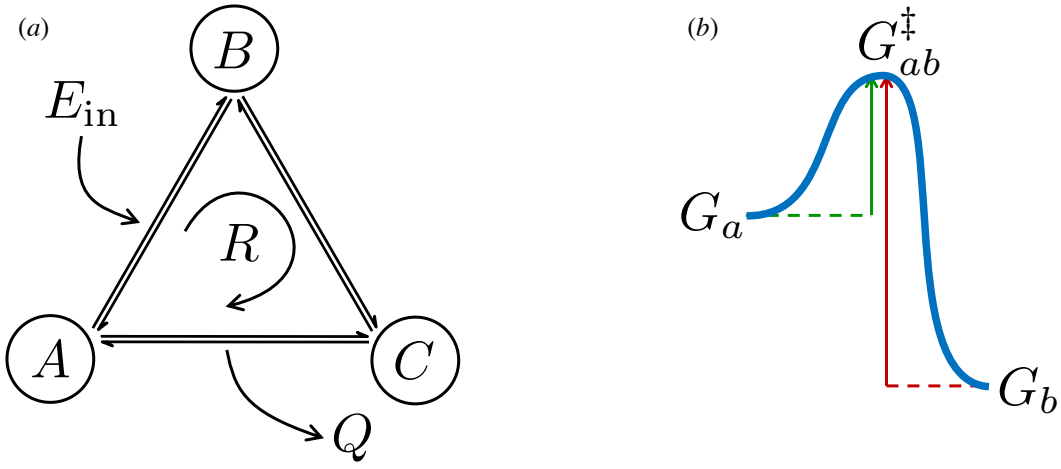


**Figure 23. Schematic representation of a molecular motor.** (a) The three states of a molecular motor which rotates with constant velocity $R$ and constant energy input/dissipation $E_{\text{in}}$. (b) The energy barrier for the transition between states $A$ and $B$.

$$K_{ij}: \begin{cases} i \to i^{\ddagger} \text{ driven by } \Delta\mu \\ i^{\ddagger} \to j \text{ driven by } \Delta q \end{cases} \tag{182}$$

$$L_{ij}: \begin{cases} i \to i^{\ddagger} \text{ driven by } \Delta\mu \\ i^{\ddagger} \to j \text{ driven by } \Delta\mu \end{cases} \tag{183}$$

$$M_{ij}: \begin{cases} i \to i^{\ddagger} \text{ driven by } \Delta q \\ i^{\ddagger} \to j \text{ driven by } \Delta\mu \end{cases} \tag{184}$$

$$N_{ij}: \begin{cases} i \to i^{\ddagger} \text{ driven by } \Delta q \\ i^{\ddagger} \to j \text{ driven by } \Delta q \end{cases} \tag{185}$$

where $i^{\ddagger}$ is the transition state between $i$ and $j$; the sign of $\Delta\mu$ and $\Delta q$ determines whether energy is being absorbed or released by the molecular motor. The path probability, normalized by the number of steps, in this case can written as

$$S_{\text{path}} = -\sum_{i \neq j} \left(K_{ij} \log K_{ij} + L_{ij} \log L_{ij} + M_{ij} \log M_{ij} + N_{ij} \log N_{ij}\right) \tag{186}$$

Now we follow the standard procedure and enforce the known constraints. Assuming that the system is at steady state, we know that the total average

chemical energy input $\langle \Delta\mu \rangle$ (e.g. ATP usage per unit time) is constant and equal and opposite to the total dissipation $\langle \Delta q \rangle$. Also the total rotational velocity $\langle r \rangle$ is constant, so we have the following constraints:

$$\langle r \rangle = \sum_{i \neq j} \left[ (K_{ij} + L_{ij})\, r_{ij} + (M_{ij} + N_{ij})\, \bar{r}_{ij} \right] \tag{187}$$

$$\langle \Delta\mu \rangle = \sum_{i \neq j} \left[ (K_{ij} + L_{ij})\, \Delta G^{\ddagger}_{ij} - (L_{ij} + M_{ij})\, \Delta G^{\ddagger}_{ji} \right] \tag{188}$$

$$\langle \Delta q \rangle = -\langle \Delta\mu \rangle = \sum_{i \neq j} \left[ (M_{ij} + N_{ij})\, \Delta G^{\ddagger}_{ij} - (K_{ij} + N_{ij})\, \Delta G^{\ddagger}_{ji} \right] \tag{189}$$

where we have distinguished the ATP-driven rotational velocity $r_{ij}$ from the thermal fluctuation-driven one $\bar{r}_{ij}$, because the latter is uniquely determined by the energy landscape, whereas in the former the effective energy landscape is modified by the enzymatic reaction which provides ATP. For instance, in the case of Kinesin, the binding of ATP to the molecular motor head causes a conformational change that catalyzes the reaction [90].

We therefore define $\bar{r}_{ij} = \pm r_0 \exp(-\Delta G^{\ddagger}_{ij}/k_B T)$ and $r_{ij} = \pm r_0 \exp(-(\Delta G^{\ddagger}_{ij} - \delta h_{ij})/k_B T)$, where the sign is positive or negative whether the transition $i \to j$ is in the same or opposite direction of the overall rotation $\langle r \rangle$. $\delta h_{ij}$ is the change in the transition barrier due to the enzymatic, ATP-driven reaction. The constraints above need to be completed by the proper normalization condition

$$\sum_j (K_{i,j} + L_{i,j} + M_{i,j} + N_{i,j}) = 1 \;\; \forall i \neq j \tag{190}$$

Maximizing the caliber subject to these constraints we obtain the following probabilities

$$K_{ij} = \frac{1}{Z_i} e^{\alpha r_{ij} + \beta \Delta G^{\ddagger}_{ij} - \gamma \Delta G^{\ddagger}_{ji}} \tag{191}$$

$$L_{ij} = \frac{1}{Z_i} e^{\alpha r_{ij} + \beta (\Delta G^{\ddagger}_{ij} - \Delta G^{\ddagger}_{ji})} \tag{192}$$

$$M_{ij} = \frac{1}{Z_i} e^{\alpha \bar{r}_{ij} - \beta \Delta G^{\ddagger}_{ij} + \gamma \Delta G^{\ddagger}_{ji}} \tag{193}$$

$$N_{ij} = \frac{1}{Z_i} e^{\alpha \bar{r}_{ij} + \gamma (\Delta G^{\ddagger}_{ij} - \Delta G^{\ddagger}_{ji})} \tag{194}$$

where $Z_i$ are normalization factors determined by the constraints in Eq. 190 and $\alpha$, $\beta$ and $\mu$ are Lagrange Multipliers to be determined by imposing the constraints 187, 188 and 189, respectively.

From this, we can determine the probability that a single transition would be completely determined by thermal fluctuations. As one can imagine, such probability is not extremely small for a microscopic system; MaxCal allows us to quantify the exact probability for an arbitrarily far-from-equilibrium system. Considering the process $K$ and its reverse $M$ the ratio of the probabilities is:

$$\frac{M_{ij}}{K_{ij}} \simeq \exp\left(-\alpha r_0 \frac{\delta h_{ij}}{kT} - 2\beta \Delta G_{ji}\right) \tag{195}$$

where we have assumed a small enzymatic barrier so that $\bar{r}_{ij} - r_{ij} \simeq -r_0 \delta h_{ij}/kT$ and the fact that the energy and dissipation constraints are equal and opposite to set $\gamma = -\beta$. We have also introduced the free energy difference $\Delta G_{ji} = G_j - G_i$. Note that without the enzymatic activity of the ATP burning reaction the ration only depends upon the free energy difference between the two states $(i, j)$, which is what we expect: For a reaction between states with very similar free energy $\Delta G \simeq 0$, thermal fluctuations and chemical energy have equal probability of causing a transition.

In general, the probability of observing phenomenon like this is exponentially suppressed for all the trajectories which rotate oppositely to the average rotation $\langle r \rangle$; If we consider a full rotation and assume that the barrier reduction is independent on the specific transition ($\delta h_{ij} = \delta h$), the relative probability that the entire process is driven by thermal fluctuations would be:

$$\frac{M_{ab}}{K_{ab}} \frac{M_{bc}}{K_{bc}} \frac{M_{ca}}{K_{ca}} \simeq \exp\left(-3\alpha r_0 \frac{\delta h}{kT}\right) \tag{196}$$

because the total free energy change is zero after a full rotation. The relative probability is completely determined by the enzymatic activity and the temperature: the smaller the activity or the larger the temperature the higher the probability that thermal fluctuation can drive the motor. A more quantitative result can be easily obtained once the motor energy landscape $G_i$ is fully specified so that the constraint equations can be solved numerically.

It is also worth noticing that this system breaks detail balance, as it should, since it is an actively driven system with a constant rotational velocity $\langle r \rangle$, so the steady state condition does not correspond to an equilibrium condition. In order to restore microscopic reversibility it would be necessary to model exactly the thermal bath in which the motor is immersed and the energy source dynamics (hence the time-dependence of ATP concentration).